Faint Relics of Violent High Energy Physics in the Early Universe

by

Jeffrey Morgan Hyde

A Dissertation Presented in Partial Fulfillment
of the Requirements for the Degree
Doctor of Philosophy

Approved May 2016 by the
Graduate Supervisory Committee:

Tanmay Vachaspati, Chair
Damien Easson
Andrei Belitsky
Joseph Comfort

ARIZONA STATE UNIVERSITY

August 2016

ABSTRACT

The work presented in this dissertation examines three different nonequilibrium particle physics processes that could play a role in answering the question "how was the particle content of today's universe produced after the big bang?" Cosmic strings produced from spontaneous breaking of a hidden sector $U(1)_{\rm X}$ symmetry could couple to Standard Model fields through Higgs Portal or Kinetic Mixing operators and radiate particles that contribute to the diffuse gamma ray background. In this work we calculate the properties of these strings, including finding effective couplings between the strings and Standard Model fields. Explosive particle production after inflation, known as preheating, would have produced a stochastic background of gravitational waves (GW). This work shows how the presence of realistic additional fields and interactions can affect this prediction dramatically. Specifically, it considers the inflaton to be coupled to a light scalar field, and shows that even a very small quartic self-interaction term will reduce the amplitude of the gravitational wave spectrum. For self-coupling $\lambda_\chi \gtrsim g^2$, where g^2 is the inflaton-scalar coupling, the peak energy density goes as $\Omega_{\rm GW}^{(\lambda_\chi)}/\Omega_{\rm GW}^{(\lambda_\chi=0)} \sim (g^2/\lambda_\chi)^2$. Finally, leptonic charge-parity (CP) violation could be an important clue to understanding the origin of our universe's matter-antimatter asymmetry, and long-baseline neutrino oscillation experiments in the coming decade may uncover this. The CP violating effects of a possible fourth "sterile" neutrino can interfere with the usual three neutrinos; this work shows how combinations of various measurements can help break those degeneracies.

To my grandmother, Jean Randt Morgan, unrelenting fan and critic:

"Darling, I don't know how you understand any of this!"

ACKNOWLEDGMENTS

I am deeply indebted to my adviser, Tanmay Vachaspati, for both teaching me so much about cosmology, particle physics and many other things, and for providing me the opportunity and guidance to become a physicist in my own right. I can't adequately express my gratitude for such patient and dedicated mentoring and enthusiastic support. Thank you!

I'd also like to thank the other members of my thesis committee – Damien Easson, Andrei Belitsky and Joseph Comfort – for serving on my committee and lending insight when I've asked. Two professors from Miami - Perry Rice and Charles Holmes - deserve many thanks for providing an enormous amount of support and opportunities (not to mention insight into physics and math).

I am also grateful to Dr.s Andrew Long, Cecilia Lunardini, Alex Kagan and Richard Lebed for going out of their way to teach me so much about particle physics and cosmology, whether in a class or in research. I'm also very grateful to Dr. Anna Zaniewski for her leadership of Sundial, and especially the mentoring program at ASU. This has been a very rewarding part of my time at ASU and I have learned a lot.

I've been lucky to be surrounded during my PhD by a tremendous group of physicists at a similar stage in their career. Alyssa Adams, Bryce Davis, David Dotson, Francis Duplessis, Varda Faghir Hagh, Yao Ji, Hank Lamm, Veronica Meeks, Jayden Newstead, Nadia Newstead, Subir Sabharwal, Seyed Mahdi Sadjadi, Russ TerBeek, Todd Van Woerkom, are top notch scientists and friends. I'm also grateful to Dana Bennewitz, Brandon King, Erik Moss, Erik Rios, and Steve, Mom and Dad for friendship, love and support along the way!

TABLE OF CONTENTS

CHAPTER Page

LIST OF FIGURES

Figure Page

Chapter 1

INTRODUCTION

"Art is anything you can get away with."

–Andy Warhol

The current understanding of fundamental physics and cosmology explains an enormous range of observed phenomena, but also embodies some unavoidable contradictions. How does the universe get away with this? The work presented in this dissertation examines three different nonequilibrium particle physics processes that could help resolve the question "how was the particle content of today's universe produced after the big bang?" In each case, the work ties the details of an observable (or potentially observable) quantity to the underlying parameters responsible for it. Studying out-of-equilibrium particle physics is difficult because it is not obvious *a priori* how the free parameters of a model will manifest themselves in the resulting physical phenomena. For this reason, it is essential to couple numerical solutions with analytic understanding of simpler situations.

The first subject will be "dark sector" cosmic strings formed when a hidden sector $U(1)_{\rm X}$ that couples to the electroweak sector is spontaneously broken before the electroweak phase transition. The interplay between the electroweak and dark sector symmetry breaking scales makes it difficult to determine which scale controls the properties of the strings that affect present-day observability. The second subject will be gravitational wave production during a period of "preheating" after inflation, and the effect of new interactions on the predicted spectrum. The third subject will be the effect of "generic" types of new interactions on the observability of CP violation in

neutrino oscillation experiments. In particular, this work develops the biprobability representation of flavor oscillation probabilities in order to provide a straightforward way to understand the effects of each new interaction parameter.

The rest of this introductory chapter will be organized in the following way. Sec. 1.1 will describe the aspects of the Standard Model of particle interactions relevant to this work, focusing on the electroweak interaction and its modification in the (now-known) case of nonzero neutrino masses. Sec. 1.2 will describe the aspects of the "ΛCDM" standard cosmological model relevant to this work. It will also review some unresolved problems and potential solutions (inflation, reheating, baryon asymmetry) that are relevant to the work in this dissertation. Sec. 1.3 will describe some specific ways that the particle interactions described above could be modified towards the goal of resolving these or other gaps our current understanding of the universe. Because the work described in the following chapters is diverse, some of these will begin with an extended introduction where some other relevant background is developed. Sec. 1.4 will summarize this chapter and specify the context for the work that is described in the remaining chapters of this dissertation.

1.1 The Standard Model of Particle Interactions

Here we will briefly review the Standard Model and certain extensions that have been studied for this dissertation, setting notation that will be used throughout this document. This mainly focuses on phenomenology of extensions to the electroweak sector.

Briefly, the Standard Model of particle interactions describes a set of quark and lepton fields charged under a $SU(3)_{\text{color}} \times SU(2)_{\text{L}} \times U(1)_{\text{Y}}$ gauge group, whose gauge bosons are responsible for the strong nuclear, weak and electromagnetic forces [1, 2]. The interaction of quarks and gluons, the $SU(3)_{\text{color}}$ gauge bosons, constitutes

Quantum Chromodynamics (QCD), the accepted theory of the strong interaction (see e.g. [3]). Interactions of quarks and leptons with the gauge bosons of $SU(2)_{\rm L} \times U(1)_{\rm Y}$ constitutes the electroweak (EW) interaction.

1.1.1 Electroweak Interactions

The electroweak interaction is the main component of the Standard Model studied in this work. The overall structure of this interaction is

$$\mathcal{L}_{\rm EW} = \mathcal{L}^{\rm gauge\,bosons} + \mathcal{L}^{\rm leptons} + \mathcal{L}^{\rm quarks} + \mathcal{L}^{\rm Higgs} + \mathcal{L}^{\rm interactions} \tag{1.1}$$

This model involves interaction of the lepton fields e, μ, τ, $\nu_{\rm e}$, ν_μ, ν_τ via the gauge bosons W^a_μ and Y_μ of $SU(2)_{\rm L}$ and $U(1)_{\rm Y}$, respectively. It is most convenient to write the Lagrangian in terms of separate left- and right-handed fields:

$$\begin{aligned} e_L &\equiv P_L e = \frac{1}{2}\left(\mathbf{1} - \gamma_5\right) e \\ e_R &\equiv P_R e = \frac{1}{2}\left(\mathbf{1} + \gamma_5\right) e \end{aligned} \tag{1.2}$$

where e is a Dirac field and similarly for the other charged fermion fields: μ_L and μ_R, etc. For convenience of notation, we'll label the charged lepton fields $(l_i)_L$ and $(l_i)_R$, with $i =$ e, μ, τ, and the neutrinos by $(\nu_i)_L$. Here in the Standard Model there is no neutrino mass term, so only the left-handed neutrino states contribute. As will be discussed later, neutrinos are now known to have small masses, but it is not known whether they are Dirac or Majorana fermions.

In terms of the $SU(2)_{\rm L}$ doublets

$$L_{{\rm e},\mu,\tau} \equiv \begin{pmatrix} (\nu_L)_{{\rm e},\mu,\tau} \\ (e_L)_{{\rm e},\mu,\tau} \end{pmatrix}, \qquad \Phi \equiv \begin{pmatrix} \Phi^+ \\ H \end{pmatrix}, \tag{1.3}$$

the kinetic term and interaction terms for leptons are together

$$\mathcal{L}_{\rm leptons} = L_i^\dagger i\overline{\sigma}^\mu D_\mu L_i - y^l_{ij} L_i^\dagger \Phi (l_R)_j - y^{l\,*}_{ij} (l_R)_j^\dagger \Phi^\dagger L_i \tag{1.4}$$

where $\overline{\sigma}^{\mu} \equiv (1, -\vec{\sigma})$ and the covariant derivative is

$$D_{\mu} = \partial_{\mu} + iQ_{\mathrm{Y}}Y_{\mu} + iQ_{\mathrm{L}}\sigma^{a}W_{\mu}^{a}. \tag{1.5}$$

When dealing with all three generations of fermions, we will frequently avoid writing sums over the generation (flavor) indices by using the "unindexed" symbols (barred symbols) to represent column (row) vectors of fields (barred fields):

$$l \equiv \begin{pmatrix} \mathrm{e} \\ \mu \\ \tau \end{pmatrix}, \quad \nu \equiv \begin{pmatrix} \nu_{\mathrm{e}} \\ \nu_{\mu} \\ \nu_{\tau} \end{pmatrix}, \quad u \equiv \begin{pmatrix} u_{\mathrm{u}} \\ u_{\mathrm{c}} \\ u_{\mathrm{t}} \end{pmatrix}, \quad d \equiv \begin{pmatrix} d_{\mathrm{d}} \\ d_{\mathrm{s}} \\ d_{\mathrm{b}} \end{pmatrix}, \tag{1.6}$$

and double brackets $[M]$ refer to a matrix in flavor space that is 3×3 in the Standard Model case.

After electroweak symmetry breaking (EWSB), the leptons have an effective mass-squared matrix M that couples left- and right-handed fields:

$$\mathcal{L}_{\text{lepton masses}} = -\bar{l}_{\mathrm{L}} \left[M^{l}\right] l_{\mathrm{R}} - \bar{l}_{\mathrm{R}} \left[M^{l}\right]^{\dagger} l_{\mathrm{L}} \tag{1.7}$$

Transforming the lepton fields by

$$l_{\mathrm{L}} \to U_{\mathrm{L}}^{l} l_{\mathrm{L}}, \quad l_{\mathrm{R}} \to U_{\mathrm{R}}^{l} l_{\mathrm{R}}, \tag{1.8}$$

and choosing $U_{\mathrm{L,\,R}}^{l}$ such that

$$U_{\mathrm{L}}^{l} \left[M^{l}\right] U_{\mathrm{R}}^{l\,\dagger} = \left[D^{l}\right] = \mathrm{diag}(m_{\mathrm{e}}, m_{\mu}, m_{\tau}), \tag{1.9}$$

$\mathcal{L}$ will be written in a basis where the charged leptons have definite masses and definite weak interactions (diagonal mass terms and diagonal weak neutral current and charged current terms).

1.1.2 Quark Mixing and Lepton Mixing

As seen above, in the Standard Model there is no problem choosing a basis where the lepton fields have definite mass (i.e. diagonal Higgs Yukawa couplings) as well as flavor (neutral and charged current). Here we will see that this is not true for quark mixing in the Standard Model as described by the Cabibbo-Kobayashi-Maskawa (CKM) matrix. We will then see that with nondegenerate nonzero neutrino masses, the exact same form of mixing occurs in the lepton sector as described by the Pontecorvo-Maki-Nakagawa-Sakata (PMNS) matrix.

Directly analogous to the charged leptons, the part of the Lagrangian covering electroweak interactions of quarks (fields $u^i = u,\ c,\ t$ and $d^i = d,\ s,\ b$) is written in terms of the $SU(2)_{\mathrm{L}}$ doublet

$$Q^i_{\mathrm{L}} \equiv \begin{pmatrix} u^i_{\mathrm{L}} \\ d^i_{\mathrm{L}} \end{pmatrix}, \tag{1.10}$$

as

$$\mathcal{L}^{\mathrm{quarks}}_{\mathrm{EW}} = \mathcal{L}^{\mathrm{quarks}}_{\mathrm{Yukawa}} + \mathcal{L}^{\mathrm{quarks}}_{\mathrm{CC}} + \mathcal{L}^{\mathrm{quarks}}_{\mathrm{NC}} + \mathcal{L}^{\mathrm{quarks}}_{\mathrm{EM}} \tag{1.11}$$

with

$$\begin{aligned}
\mathcal{L}^{\mathrm{quarks}}_{\mathrm{Yukawa}} &= -y^d_{ij}(\overline{Q}^i_{\mathrm{L}}\Phi d^j_{\mathrm{R}} + \Phi^\dagger Q^i_{\mathrm{L}}\overline{d}^j_{\mathrm{R}}) - y^u_{ij}(\overline{Q}^i_{\mathrm{L}}\overline{\Phi} u^j_{\mathrm{R}} + \overline{\Phi}^\dagger Q^i_{\mathrm{L}}\overline{u}^j_{\mathrm{R}}) \\
\mathcal{L}^{\mathrm{quarks}}_{\mathrm{CC}} &= \frac{g'}{\sqrt{2}} W^+_\mu \overline{u}^i_{\mathrm{L}}\gamma^\mu d^i_{\mathrm{L}} + \frac{g'}{\sqrt{2}} W^-_\mu \overline{d}^i_{\mathrm{L}}\gamma^\mu u^i_{\mathrm{L}} \\
\mathcal{L}^{\mathrm{quarks}}_{\mathrm{NC}} &= \frac{e}{s_w c_w} Z_\mu \left(\frac{1}{2}\overline{u}^i_{\mathrm{L}}\gamma^\mu u^i_{\mathrm{L}} - \frac{1}{2}\overline{d}^i_{\mathrm{L}}\gamma^\mu d^i_{\mathrm{L}} - s^2_w \frac{2}{3}\overline{u}^i_{\mathrm{L}}\gamma^\mu u^i_{\mathrm{L}} + s^2_w \frac{1}{3}\overline{d}^i_{\mathrm{L}}\gamma^\mu d^i_{\mathrm{L}} \right)
\end{aligned} \tag{1.12}$$

The $\mathcal{L}^{\mathrm{quarks}}_{\mathrm{Yukawa}}$ term results in mass matrices that are not diagonal as written:

$$\mathcal{L}^{\mathrm{quarks}}_{\mathrm{mass}} = -\overline{u}_{\mathrm{L}} \left[M^u\right] u_{\mathrm{R}} - \overline{d}_{\mathrm{R}} \left[M^d\right]^\dagger d_{\mathrm{L}} + \mathrm{h.c.} \tag{1.13}$$

As in the charged lepton case, field redefinitions

$$u^i_{\mathrm{L,R}} \to U^u_{\mathrm{L,R}} u^i_{\mathrm{L,R}}, \quad d^i_{\mathrm{L,R}} \to U^d_{\mathrm{L,R}} d^i_{\mathrm{L,R}} \tag{1.14}$$

allow the mass matrices to be diagonalized by

$$\begin{aligned} U_{\rm L}^{u}\,[M^{u}]\,U_{\rm R}^{u\dagger} &= [D^{u}] = {\rm diag}(m_{\rm u}, m_{\rm c}, m_{\rm t}), \\ U_{\rm L}^{d}\,\left[M^{d}\right]\,U_{\rm R}^{d\dagger} &= \left[D^{d}\right] = {\rm diag}(m_{\rm d}, m_{\rm s}, m_{\rm b}) \end{aligned} \tag{1.15}$$

The charged current part of the Lagrangian, then, involves

$$\begin{aligned} \mathcal{L}_{\rm CC}^{\rm quarks} &= \frac{g'}{\sqrt{2}} W_{\mu}^{+} \overline{u}_{\rm L} (U_{\rm L}^{u})^{\dagger} (U_{\rm L}^{d}) \gamma^{\mu} d_{\rm L} + \frac{g'}{\sqrt{2}} W_{\mu}^{-} \overline{d}_{\rm L} (U_{\rm L}^{d})^{\dagger} (U_{\rm L}^{u}) \gamma^{\mu} u_{\rm L} \\ &\equiv \frac{g'}{\sqrt{2}} W_{\mu}^{+} \overline{u}_{\rm L} V_{\rm CKM} \gamma^{\mu} d_{\rm L} + \frac{g'}{\sqrt{2}} W_{\mu}^{-} \overline{d}_{\rm L} V_{\rm CKM}^{\dagger} \gamma^{\mu} u_{\rm L} \end{aligned} \tag{1.16}$$

The neutral current interactions only involve the combinations $\overline{u}_{\rm L}\gamma^{\mu}u_{\rm L}$ and $\overline{d}_{\rm L}\gamma^{\mu}d_{\rm L}$, so there won't be factors of $V_{\rm CKM}$. However, because $V_{\rm CKM}^{\dagger}V_{\rm CKM} = \mathbf{1}$ we can generalize and say that the up-type fields that participate in the weak interaction are related to the up-type fields of definite mass by $u_{\rm L}^{\rm flavor} = V_{\rm CKM}^{\dagger} u_{\rm L}^{\rm mass}$ (since this will make the neutral current interaction end up with a factor of $\mathbf{1}$ in it). This way of expressing the result is not the usual language, but we use it here because it directly maps onto the language used in the leptonic sector. There, we say that the upper component of the $SU(2)_{\rm L}$ doublet – i.e. neutrino – fields with definite flavor content are related to the fields of definite mass by a linear transformation.

In the Standard Model, neutrinos are exactly massless left-handed fermions. The earliest evidence that the Standard Model is insufficient to account for all neutrino phenomenology was the "solar neutrino problem" – the flux of electron neutrinos from nuclear reactions in the sun was found to be much less than predicted by solar models. This suggested the phenomenon of neutrino flavor mixing that is analogous to mixing of quarks via the weak interaction; eventually it was shown that the flavor mixing probabilities follow the dependence on length and energy that would be expected if neutrinos have mass eigenstates that differ from their flavor eigenstates [4] and solve the solar neutrino problem [5]. Of particular interest is that this allows for

the possibility of CP violation in the lepton sector. Phenomenology of neutrino oscillations and CP violation will be discussed and studied further in Chapter 4.

Finally, it is useful to point out that, even though quark mixing and lepton mixing are formally described in the same way, there are very significant differences in practice. One is that the components of $V_{\rm CKM}$ are nearly diagonal with relatively small off-diagonal elements, while the analogous $U_{\rm PMNS}$ has relatively large off-diagonal elements. Their magnitudes are [6]

$$|V_{\rm CKM}| = \begin{pmatrix} 0.974 & 0.225 & 0.00413 \\ 0.225 & 0.986 & 0.0411 \\ 0.0084 & 0.040 & 1.021 \end{pmatrix}, \quad |U_{\rm PMNS}| = \begin{pmatrix} 0.82 & 0.54 & 0.15 \\ 0.35 & 0.70 & 0.62 \\ 0.44 & 0.45 & 0.77 \end{pmatrix} \tag{1.17}$$

Difficulty in measuring neutrino mixing stems from the difficulty in detecting neutrinos in general.

1.2 Cosmology

1.2.1 The Homogeneous and Isotropic Universe

Observation indicates a universe that is homogeneous and isotropic on large scales ($\gtrsim 300$ Mpc) and that is expanding (the fractional rate of change of distances is today $H_0 \approx 70\,\mathrm{km\,s^{-1}\,Mpc^{-1}}$). This universe can be described by the Einstein Equations

$$R_{\mu\nu} - \frac{1}{2}\mathcal{R} g_{\mu\nu} = 8\pi G\, T_{\mu\nu} + \Lambda g_{\mu\nu} \tag{1.18}$$

where $R_{\mu\nu}$ is the Ricci tensor, $\mathcal{R}$ is the Ricci scalar, G is Newton's constant and Λ is the cosmological constant term, with the Friedmann Lemaitre Robertson Walker (FLRW) metric, given in terms of its line element as

$$\begin{aligned} ds^2 &= dt^2 + a^2(t)\left(\frac{dr^2}{1-kr^2} - r^2 d\theta^2 - r^2 \sin^2\theta d\phi^2\right) \\ &= a^2(\eta)\left(d\eta^2 + \frac{dr^2}{1-kr^2} - r^2 d\theta^2 - r^2 \sin^2\theta d\phi^2\right), \end{aligned} \tag{1.19}$$

where the conformal time is defined by $d\eta = dt/a$. The parameter a is called the scale factor, and comparison of scale factors at different times is used to quantify the expansion of the universe. Since one effect of this is the gravitational redshift of light,

$$\frac{\lambda_f}{\lambda_i} = \frac{a_f}{a_i}, \tag{1.20}$$

another frequently useful quantity (more popular among astronomers) is the redshift, z, defined by

$$1 + z \equiv \frac{a_0}{a}. \tag{1.21}$$

Here, the subscript 0 on a or H refers to present-day quantities; therefore the redshift of a given time is the fraction by which the wavelength of a light signal emitted at that time is stretched between then and now.

The overall matter content that determines the evolution of the scale factor $a(t)$ is well described as a perfect fluid with stress-energy tensor

$$T_{\mu\nu} = \mathrm{diag}\,(\rho,\, -p,\, -p,\, -p) \tag{1.22}$$

where ρ is the energy density and p is the pressure. Then the $\mu = 0$, $\nu = 0$ component of Eq. (1.18) gives the Friedmann Equation,

$$H^2 + \frac{k}{a^2} = \frac{8\pi G}{3}\rho, \tag{1.23}$$

where $H \equiv \frac{1}{a}\frac{da}{dt}$ is the Hubble parameter. The μ, $\nu = i$ component of Eq. (1.18) gives

$$2\frac{\ddot{a}}{a} + H^2 + \frac{k}{a^2} = -8\pi G\,\rho, \tag{1.24}$$

which can be combined with Eq. (1.23) go give the acceleration equation

$$\frac{\ddot{a}}{a} = -\frac{4\pi G}{3}(\rho + 3p). \tag{1.25}$$

Each type of matter present in the universe contributes: $\rho = \rho_{\text{electrons}} + \rho_{\text{photons}} + \rho_{\text{baryons}} + \cdots$. But for many purposes, the various components of matter that contribute to the stress-energy tensor in the standard hot big bang cosmology are well approximated as either relativistic particles ("radiation"), nonrelativistic particles ("matter") or vacuum energy / cosmological constant. Then the density and pressure are related by a simple equation of state,

$$p = w\rho, \tag{1.26}$$

with $w = 1/3$ for radiation, $w = 0$ for matter, $w = -1$ for vacuum energy. A useful expression for the dynamics then comes from the stress-energy conservation,

$$\nabla_\nu T^{\mu\nu} = 0, \tag{1.27}$$

whose $\mu = 0$ component gives

$$\mathrm{d}(\rho a^3) = -w\rho\,\mathrm{d}(a^3), \tag{1.28}$$

which is integrated to give

$$\rho \propto a^{-3(1+w)}. \tag{1.29}$$

The different power-law evolution of the scale factor, $a(t)$, for different types of matter means that the universe will nearly always be dominated by one type of matter, punctuated by transitions from one form of scaling to the next as one form or another becomes the main component. In particular, the ΛCDM model fits observation very well by assuming the universe was radiation-dominated before Big Bang Nucleosynthesis (BBN) began, but $\rho_{\text{radiation}} \propto a^{-4}$ while $\rho_{\text{matter}} \propto a^{-3}$, so at some a_{eq} (equality of matter and radiation energy densities) the universe transitioned to matter-dominated evolution. In 1998, careful measurements of Type Ia supernovae

[7, 8] showed that the universe's expansion is accelerating; i.e. five billion years ago there was another transition from matter-dominated expansion to vacuum-dominated expansion governed by a small cosmological constant (or "dark energy").

The curvature constant $k = -1,\ 0,\ +1$ if the total energy density is respectively less than, equal to, or greater than the critical density, defined as

$$\rho_{\rm crit} = \frac{3H^2}{8\pi G}. \tag{1.30}$$

Frequently it is useful to express energy densities as a fraction of the critical density: for some component i of matter,

$$\Omega_i = \rho_i/\rho_{\rm crit}. \tag{1.31}$$

If one treats the curvature term $\frac{k}{a^2}$ in the Friedmann Equation Eq. (1.23) as an "energy density" that scales as $\rho_{\rm k} \propto a^{-2}$, then there will be an

$$\Omega_{\rm k} = \rho_{\rm k}/\rho_{\rm crit}. \tag{1.32}$$

Observations indicate $\Omega_{\rm k} \approx 0$, so for our universe the critical density is approximately the total energy density, and

$$\sum_i \Omega_i = 1. \tag{1.33}$$

The ΛCDM model begins with a radiation dominated era, followed by a matter dominated era, and finally a vacuum energy dominated era that we are currently in. The Planck satellite [9] has measured from cosmic microwave background (CMB) observations $H_0 = 67.3\,{\rm km\,s^{-1}\,Mpc^{-1}}$, $\Omega_\Lambda = 0.69$, $\Omega_{\rm matter} = 0.315$, $z_{\rm eq} \approx 3400$ and $|\Omega_{\rm k}| < 0.005$. The matter density is divided into baryonic matter with $\Omega_{\rm baryon} = 0.049$ and dark matter with $\Omega_{\rm DM} = 0.264$.

This basic picture is supported by computation and observation involving many other observational tests, and serves very well to describe the observed content and

evolution of the universe from BBN onward. In fact, this success demands that new questions be answered. Some of them are directly questions of matter content – the particle physics nature of dark matter and the abundance of matter over antimatter are unexplained by any Standard Model physics. However, the initial conditions setting the stage for BBN also invite explanation.

One such difficulty is the "flatness problem," which is related to the observed flatness (or very near flatness) of the universe today. Since $\Omega_{\rm k}$ evolves proportionally to $1/(aH)^2$, a quantity which has increased many times since the time of BBN ($1/(aH)$ is also known as the comoving Hubble radius), the universe must have entered the radiation-dominated era with curvature extremely fine-tuned close to zero (equivalently, with energy density fine-tuned very close to critical) [10]. If $1/(aH)$ were to instead decrease by a large amount before the beginning of the radiation-dominated era and standard big bang cosmology, a situation that will be examined in Sec. 1.2.2, this would be avoided.

Another issue is the "horizon problem," which can be stated in the following way [11]. The comoving particle horizon is defined by

$$\tau = \int_0^t \frac{dt'}{a(t')}. \tag{1.34}$$

This gives the furthest that a light ray, and thus any causal effects, could have traveled as $a(t)$ evolves. Using the definition of H in terms of a to change the integration variable, this can be expressed in terms of the comoving Hubble radius as

$$\tau = \int_0^a \left(\frac{1}{aH}\right) d\ln a. \tag{1.35}$$

With negligible curvature, $H \sim \rho^{1/2}$ or

$$\frac{1}{aH} = \frac{1}{H_0} a^{\frac{3}{2}(1+w)-1} \tag{1.36}$$

so

$$\tau = \int_0^a \left(\frac{a^{\frac{1}{2}(1+w)}}{H_0} \right) d \ln a. \tag{1.37}$$

In a universe of matter and radiation, the exponent will always be positive and therefore τ will always increase. In this case, the cosmic microwave background radiation, observed to have a very nearly thermal blackbody spectrum, would be comprised of photons carrying information from separate regions that have never been in causal contact.

Finally, many grand unified field theories predict topological defect production during early universe phase transitions, a topic that will be covered in more depth in Chapter 2. In particular, there should be many more magnetic monopoles per Hubble volume than the existing observational bounds.

1.2.2 Inflation

Sec. 1.2.1 reviewed the standard big bang cosmology that successfully describes many observations, but suffers from several "initial conditions" problems. One way to solve them is to have some era of a decreasing comoving horizon,

$$\frac{d}{dt} \left(\frac{1}{aH} \right) < 0, \tag{1.38}$$

known as inflation. A consequence of Eq. (1.38) is that $\ddot{a} > 0$, i.e. accelerated expansion. Another expression that follows from Eq. (1.38) and will be useful later is

$$1 > -\frac{\dot{H}}{H^2} \equiv \varepsilon. \tag{1.39}$$

In order to solve fine-tuning problems of many orders of magnitude, inflation has to inflate a lot. How to quantify the duration of this inflationary era? One convenient choice is the "number of e-folds" N between the initial and final scale factors a_i, a_f,

defined by

$$\frac{a_f}{a_i} = e^N, \tag{1.40}$$

or

$$\begin{aligned} N &= \ln\left(a_f/a_i\right) \\ &= \int_{a_i}^{a_f} \frac{da}{a} \\ &= \int_{a_i}^{a_f} \mathrm{d}\ln(a). \end{aligned} \tag{1.41}$$

Then since $H = a^{-1}\frac{da}{dt}$, $\frac{da}{a} = H\,dt$ so

$$N = \int_{t_i}^{t_f} H(t)\,dt, \tag{1.42}$$

where the beginning and ending times are defined following Eq. (1.39) as times when $\varepsilon = 1$.

Having described inflation in terms of its duration and effects, we now ask how it may be implemented. The simplest way is with a scalar field, $\phi(t, \vec{x})$, minimally coupled to gravity with

$$\mathcal{L} = \frac{1}{2}\nabla_\mu\phi^2 - V(\phi). \tag{1.43}$$

In the FLRW background of Eq. (1.19), it will have equation of motion

$$\Box\phi + 3H\dot{\phi} + \frac{dV}{d\phi} = 0, \tag{1.44}$$

or for a homogeneous field configuration with no spatial gradients,

$$\ddot{\phi} + 3H\dot{\phi} + \frac{dV}{d\phi} = 0. \tag{1.45}$$

Then the Friedmann Equation Eq. (1.23) gives

$$H^2 = \frac{8\pi}{3M_{\mathrm{P}}^2}\left(\frac{1}{2}\dot{\phi}^2 + V(\phi)\right). \tag{1.46}$$

Taken together with Eq. (1.39), this gives an expression for the slow roll parameter in this situation:

$$\varepsilon = \frac{3\left(\frac{1}{2}\dot{\phi}^2\right)}{\left(\frac{1}{2}\dot{\phi}^2 + V(\phi)\right)}. \tag{1.47}$$

In other words, in this case inflation ($\varepsilon < 1$) occurs when the potential energy $V(\phi)$ dominates over the kinetic energy term, $\frac{1}{2}\dot{\phi}^2$. The simplest example is a polynomial potential,

$$V(\phi) = \frac{1}{n}\lambda\phi^n. \tag{1.48}$$

The idea is that ϕ will start high up on its potential, and then execute a "slow roll" to the minimum of the potential, during which time the potential energy dominates and the universe inflates. A very flat potential, where the parameter λ is chosen to be very small (e.g. $\lambda \approx 10^{-14}$ if $n = 4$), ensures that the kinetic energy remains small for suffcient time to obtain enough e-folds of inflation as defined in Eq. (1.42). It turns out that the simple polynomial models of inflation Eq. (1.48) are observationally disfavored (this will be discussed in Sec. 1.2.3), but they are still a useful toy model for understanding how inflation might work. There is no shortage of often-baroque inflation models [12], many of which are not constrained by observation [13].

Inflation may solve the problems of flatness, super-horizon correlations, and of magnetic monopoles by exponential increase of the scale factor over 60 or so e-folds, but this would necessarily "inflate away" any other particle densities as well. "Re-heating" refers to the process after the end of inflation that would populate the universe with a thermal bath of relativistic particles prior to BBN. Interesting things can happen during this period; this is the subject of Chapter 3.

1.2.3 Cosmological Perturbations

So far, we have only discussed the dynamics of a homogeneous, isotropic universe. While this is a good approximation to our universe as a whole, the existence of galaxy clusters, solar systems, etc. means it is obviously not exact. These small deviations from homogeneity and isotropy can be very important tools for understanding cosmology, since early processes that would produce them can be constrained or detected through careful observation. In this section, we will first understand them in a formal way, and then apply this to understand observational consequences of processes such as inflation and reheating.

Perturbations to the FLRW metric can be written [14] as

$$ds^2 = a^2 \left(d\eta^2 - \gamma_{ij}(\vec{x}) dx^i dx^j - h_{\mu\nu}(\vec{x}, t) dx^\mu dx^\nu \right) \tag{1.49}$$

The physical (as opposed to gauge) perturbations may be classified as scalar, vector, or tensor according to their transformation properties. This is useful because the evolution of each type of mode is independent of the others. The tensor perturbation is the pair of h_{ij}'s physical degrees of freedom – "transverse, traceless" (TT) – that can't be expressed as the gradient of a scalar or vector; h_{ij}^{TT} is gravitational radiation with two degrees of freedom.

The perturbations described above are of tremendous importance in the early universe: quantum fluctuations during inflation are "frozen in" as the comoving horizon shrinks, and then begin to evolve as essentially classical perturbations once they reenter the horizon. This process would produce a nearly scale invariant spectrum of scalar and tensor perturbations. Scalar perturbations matching this expectation have been very precisely measured by CMB experiments and are responsible for seeding the formation of large scale structure of galaxiy clusters, while the search is ongoing for primordial tensor perturbations.

Additionally, and of importance to the work presented in Chapter 3 of this dissertation, other early universe processes such as reheating after inflation could also produce a spectrum of tensor perturbations whose detection would provide a direct window to the high energy physics of that era.

1.2.4 Baryon Asymmetry

There is one more situation evident in cosmology that poses a problem for particle physics. This is the abundance of matter compared with antimatter, or "baryon asymmetry of the universe" (BAU). It is frequently quantified by the baryon number to photon ratio [10]

$$\eta = 5 \times 10^{-10}. \tag{1.50}$$

A period of inflation would wipe out any pre-existing matter densities, requiring the baryon asymmetry to be generated dynamically rather than as an initial condition. The Sakharov conditions [15] enumerate the requirements in order for this to happen. First, there must be processes that violate baryon number, if net baryon number is to be produced from a situation with equal numbers of baryons and antibaryons. Baryon number violation is expected to be present in the Standard Model via sphaleron processes, although it has never been observed experimentally. Second, both C (charge conjugation) and CP (simultaneous charge conjugation and parity) must not be symmetries that always hold, because the presence of a baryon asymmetry violates C and CP. It is known that weak interactions satisfy this requirement. Third, there must have been processes occurring out of thermal equilibrium, because a baryon-number-violating process and its reverse would have the same rates in equilibrium.

In spite of the existence of all of these necessary elements separately, there is no

successful baryogenesis mechanism among known physics. In particular, electroweak baryogenesis would require additional CP violation beyond that present in the CKM matrix, as well as a first-order electroweak phase transition [16]. The search for new sources of CP violation leads to the question of whether the PMNS lepton mixing matrix introduced in Sec. 1.1.2 also violates CP. This is the subject of Chapter 4.

1.3 Modeling Physics Beyond Standard Model

In trying to model new physics beyond SM, one can take a "top-down" approach and write a full model such as SUSY, and work out the implications. One can also take a "bottom-up" approach, writing effective operators that could come from integrating out higher energy degrees of freedom, in a way exactly analogous to the appearance of the "effective" Fermi interaction out of the full EW Lagrangian.

1.3.1 Higgs Portal and Kinetic Mixing

There are a few such effective operators that are both renormalizable (mass dimension four) and gauge-invariant. These include a "Higgs Portal" coupling to a complex scalar field S that is a singlet of the SM gauge group:

$$\mathcal{L}_{\mathrm{HP}} = -\alpha \Phi^{\dagger}\Phi S^{*}S \tag{1.51}$$

a "kinetic mixing" between the $U(1)_{\mathrm{Y}}$ gauge boson Y_{μ} and the gauge boson X_{μ} of a spontaneously broken $U(1)_{\mathrm{X}}$:

$$\mathcal{L}_{\mathrm{KM}} = -\frac{1}{2}\sin\epsilon X_{\mu\nu}Y^{\mu\nu} \tag{1.52}$$

where $X_{\mu\nu}\,(Y_{\mu\nu})$ is the field strength tensor associated with the field $X_{\mu}\,(Y_{\mu})$. The choice of coefficient $\sin\epsilon$, instead of ϵ, is purely a choice of convention.

There are many experiments that have searched for these kinds of interactions at energies below the TeV scale. For example, kinetic mixing with a light Z' gauge

boson can significantly affect electroweak precision variables which have been tightly constrained, or show up as a dilepton resonance in a hadron collider [17]. Likewise, many constraints from colliders and direct dark matter detection experiments place stringent bounds on light scalar dark matter that interacts through a Higgs portal [18]. Constraints on interactions with new particles above the TeV scale are virually nonexistent. However, it turns out that there are cosmological consequences of these models – the hidden $U(1)$ is spontaneously broken, it can produce a network of cosmic strings whose radiation of Standard Model particles could lead to a constraint. This is the subject of Chapter 2.

1.3.2 Models of Reheating

The spirit of effective field theory is useful beyond studying minimal extensions of the Standard Model. In the case of inflation and reheating, it is not known which fields participate in the dynamics (i.e. whether they are SM fields as in Higgs inflation, new scalar fields arising through supersymmetry, other scalar fields, gauge fields, etc.). Therefore much study focuses on "generic" scenarios that aim to capture the main dynamics and hope to generalize to more realistic cases. It is typical of inflationary scenarios to end with an inflaton field $\phi(t, \vec{x})$ oscillating about a minimum of its potential. Reheating, therefore, frequently studies particle production of a "light field" $\chi(t, \vec{x})$ that is coupled weakly to ϕ in the context of "background oscillations" of ϕ. This leads to an effective Lagrangian:

$$\mathcal{L} = \mathcal{L}_{\text{inflation}}(\phi) + \mathcal{L}_{\text{interaction}}(\phi, \chi) + \mathcal{L}_{\text{reheat fields}}(\chi) \tag{1.53}$$

where typically $V_{\text{interaction}} = \frac{1}{2} g^2 \phi^2 \chi^2$ and $V_{\text{reheat fields}} = 0$. Since we don't know the fields that interact (presumably in complex ways, if the SM is any guide) with these toy model inflationary and reheating fields, the EFT framework is a motivation to

add an effective interaction potential for χ that summarizes the effects of unknown dynamics into a few parameters. Does the addition of small couplings with other fields qualitatively alter the results from a toy model? If so, is this alteration predictable – could quantitative observations directly tie back to parameters of these interactions? This subject will be addressed in Chapter 3. There has been recent work by others who are starting to consider such approaches to reheating [19, 20], but much is still not understood.

1.4 Outline of This Dissertation

The remainder of this dissertation is organized as follows. Chapter 2 introduces topological defects as unavoidable relics of some early universe phase transitions, and then presents work on "dark" cosmic strings formed when a hidden sector $U(1)$ is spontaneously broken by the vacuum expectation value of a hidden sector scalar field. In particular, the properties of these strings are studied, with the goal of possibly providing useful constraints on high energy physics models that feature dark sector – Standard Model interactions through the Higgs Portal and kinetic mixing operators.

Chapter 3 picks up where the discussion of inflation left off at the end of Sec. 1.2.2. Some models of reheating predict gravitational wave production during a brief, violent unstable resonance known as "preheating" (since it would occur before most of the period of reheating and thermalization). This chapter presents work that shows how the spectrum of gravitational waves is very sensitive to the details of the underlying particle physics model.

Chapter 4 addresses a question of particle physics phenomenology that is possibly relevant to the baryon asymmetry of the universe – namely, is there CP violation in the lepton sector? Recent work has shown that long baseline neutrino oscillation experiments can be significantly affected by a "sterile neutrino" that mixes with the

three active neutrinos. There is a degeneracy between the complex phases that would be responsible for any violation of CP symmetry in these experiments. The work presented in this chapter shows how the experimental results depend on the active-sterile mixing parameters, and how combinations of experiments can help reduce degeneracies.

Chapter 5 summarizes the results and points out interesting directions for possible future work in these areas.

Chapter 2

DARK STRINGS AND RADIATION OF STANDARD MODEL PARTICLES

2.1 Topological Defects in Cosmology

A fascinating consequence of the field theory description of particle interactions is the existence of solutions to the equations of motion that are topologically stable, extended field configurations. These topological defects are commonplace in condensed matter theory and experiment, and appear in many particle physics models relevant to the early universe [21, 22], although no cosmological relic topological defects have been found yet. For a given field theory, the collection of lowest-energy field configurations is known as the vacuum manifold. If this has a nontrivial "fundamental group" - i.e. if there are loops in this vacuum manifold that cannot be contracted to a point, then there will be topological defect solutions to the equations of motion.

Depending on the model, these topological defects could be monopoles, strings, domain walls, or textures, for example. Each of these has an analog system in the realm of condensed matter physics. For example, vortices in superfluid helium are directly analogous to cosmic strings. The standard example of such a string is the Nielsen-Olesen string, which occurs in a model where a complex scalar field ϕ's $U(1)$ symmetry is spontaneously broken:

$$\mathcal{L} = (D_\mu \phi)^* D^\mu \phi - \frac{1}{4} X_{\mu\nu} X^{\mu\nu} - \lambda \left(\phi^* \phi - \eta\right)^2 \tag{2.1}$$

where the covariant derivative is $D_\mu \phi = \partial_\mu \phi - ieX_\mu$ and $X_{\mu\nu}$ is the field strength tensor corresponding to the gauge field X_μ associated with the $U(1)$.

This potential has a "ring" of minima with nonzero vacuum expectation value for the field ϕ. At high temperatures, such as those present in the early universe,

the expectation value of ϕ will be zero, but as the temperature decreases it will be energetically favorable for the field to settle down to one of the minima. Since none are preferred, the field will randomly choose them at different locations in space. Inevitably, there will be some locations around which the phase of the field will wrap from 0 to 2π, and the field at the location in the center won't be able to settle down to one of the minima while maintaining a continuous field configuration. A string is born!

Since they are topologically stable, cosmic strings will persist throughout the subsequent evolution of the universe. The nature of the string network will change, though. When strings intersect, they can either pass through each other or reconnect in a different configuration. They can also lose energy by gravitational radiation [23] or radiation of particles that couple to the field forming the string. In particular, features such as cusps - where a point on the string instantaneously approaches the speed of light - or kinks - where the tangent vector to the string is discontinuous - will violently radiate energy as they accelerate back towards a more stable configuration. By looking for these effects, as well as others such as gravitational lensing, cosmic strings can be discovered or constrained. Strings formed from symmetry breaking far below the GUT scale, though, won't be subject to gravitational probes. The work presented in this chapter considers "light" strings formed in a specific model, and computes properties relevant to particle radiation.

2.2 "Dark" Cosmic Strings

Many compelling extensions of the Standard Model (SM) require additional gauged $\mathrm{U}(1)_X$ factors that are spontaneously broken giving rise to massive vector bosons. The high energy physics community has been studying the phenomenology of these models for years while collider experiments have been searching for the so-called Z' at

energies up to O(TeV) (see, *e.g.*, the reviews [17, 24]). Similar models have recently attracted attention in the dark matter community as well. In this context it is commonly assumed that the fields that transform under the SM gauge group are singlets under the $\mathrm{U}(1)_X$ and vice versa. Such a theory decomposes into a visible sector (SM fields) and a hidden or dark sector (fields charged under $\mathrm{U}(1)_X$). The massive vector boson may either play the role of dark matter itself [25, 26, 27, 28] [1] , or it may act as a mediator between the visible and the dark sectors [30, 31, 32, 33] [2] . In these types of models, the breaking of the $\mathrm{U}(1)_X$ during a cosmological phase transition is invariably accompanied by the formation of a unique kind of cosmic string, known as a "dark string" [36].

The presence of these dark strings in our universe has largely been overlooked. The tension, which is on the order of the symmetry breaking scale $\mu \sim$ TeV^2, is far too small for dark strings to have any detectable gravitational effect on the cosmic microwave background [37] or pulsar timing [38], which typically provide the strongest constraints on GUT-scale strings [39] . However, as we will see below, the fields that compose the dark sting have very specific couplings to the SM fields, and therefore they are able to radiate and scatter on SM particles. The presence of these cosmic dark strings in our universe can, therefore, have observable consequences and yield constraints on model building that are as yet largely unexplored.

The structure of dark strings was first studied in Refs. [36] and [40] (see also [41]). Our analysis expands upon that work in a number of ways: (i) we retain the complete electroweak gauge sector, specifically, we do not work in the semilocal limit $\sin^2\theta_w = 1$, where θ_w is the weak mixing angle as in [40]; (ii) we restrict the parameter

[1] If the gauge symmetry is non-Abelian the massive vector may still be the dark matter [29], but a topologically stable cosmic string solution is not guaranteed to exist.

[2] If the $\mathrm{U}(1)_X$ is unbroken, the massless force carrier is known as a dark photon [34, 35]. In this case the model has no string solution.

space using the measured value of the Higgs boson mass $M_H \approx 125$ GeV [42, 43], which had not been discovered at the time of the previous work; (iii) we include the interaction between the Higgs field and the scalar field responsible for the formation of the string [see Eq. (2.2.2)]; (iv) we do not necessarily assume that the gauge-kinetic mixing is small ($\sin\epsilon \ll 1$; see below); and (v) we calculate, for the first time, the effective couplings of the dark string to the SM fields. Understanding the structure of the dark string and its couplings to SM fields, in particular, are important in evaluating the cosmological signatures of dark strings.

Our analysis will focus on the smallest extension of the SM that contains a spontaneously broken, gauged Abelian symmetry. Specifically, we introduce a complex scalar field S charged under the Abelian symmetry group $\mathrm{U}(1)_X$, which has $\hat{X}^\mu$ as its vector potential; collectively, these fields will be referred to as the dark sector. After S acquires a vacuum expectation value, the mass for $\hat{X}^\mu$ is generated. This model is particularly interesting because the symmetries forbid all but two renormalizable, tree-level interactions between the SM and hidden sector fields. These are the Higgs portal (HP) operator [44]

$$\mathcal{L}_{\mathrm{HP}} = -\alpha \Phi^\dagger \Phi S^* S \tag{2.2.2}$$

where Φ is the SM Higgs doublet, and the gauge kinetic mixing (GKM) operator [45, 46, 47]

$$\mathcal{L}_{\mathrm{GKM}} = -\frac{\sin\epsilon}{2} \hat{X}_{\mu\nu} Y^{\mu\nu} \tag{2.2.3}$$

where $\hat{X}_{\mu\nu}$ and $Y_{\mu\nu}$ are the field strength tensors for the $\mathrm{U}(1)_X$ and $\mathrm{U}(1)_Y$ hypercharge. Vacuum stability considerations bound $|\alpha|$ from above [see Sec. 2.3], and the avoidance of ghosts requires $|\sin\epsilon| < 1$. For the sake of generality, we will study this model with $\alpha, \epsilon \neq 0$. However, note that in this case neither the S nor the $\hat{X}^\mu$ field is stable.

The model must be extended if it is to include a stable dark matter candidate [3] . Alternatively, imposing a discrete (reflectional) symmetry on $\hat{X}^\mu$ enforces $\sin\epsilon = 0$ [25, 26, 27, 28].

The interaction in $\mathcal{L}_{\text{HP}}$ gives rise to a mixing between the Higgs and the singlet scalar, and therefore it is constrained in light of the Higgs discovery [48]. The interaction in $\mathcal{L}_{\text{GKM}}$ is tightly constrained by a number of observables at low energies giving roughly (see [49] for a review)

$$|\sin\epsilon| < O(10^{-3}) \qquad \text{for} \qquad M_X \lesssim \text{ TeV} \ . \tag{2.2.4}$$

However, it is important to recognize that the model is yet unconstrained if the masses are large, $M_S \sim M_X > O(\text{TeV})$, where laboratory tests have not yet explored. For the sake of generality, we will not make any *a priori* assumptions about the scale of symmetry breaking in our analytic analysis, and in our numerical analysis we will focus on $M_S \sim M_X > M_H$ allowing $\sin\epsilon = O(1)$.

After setting up the model in Sec. 2.3, we diagonalize the gauge sector and derive the equations of motion relevant for a string. In Sec. 2.4 we find the dark string solution and calculate the effective couplings of the string to the SM fields in terms of the Higgs portal and gauge kinetic mixing parameters. The SM Higgs interacts with the string and thus we also take into account the possibility that it winds around the string. However the lightest string is obtained when only the dark scalar field winds and so we focus on more detailed properties of these strings, especially their three types of interactions with SM particles. Fermions of the SM can have Aharonov-Bohm couplings to the dark string if there is gauge-kinetic mixing between the hypercharge

[3] After electroweak symmetry breaking, S mixes with the Higgs and thereby acquires all of its interactions with the SM fields, which opens new decay channels. Similarly, $\hat{X}^\mu$ mixes with the Z-boson. If the mass scale in the hidden sector is very low or the couplings very small, then the dark matter can be metastable. Such models will also contain dark strings. In this paper, however, we will focus on strings with energy scales higher than the electroweak scale and arbitrary couplings.

and dark U(1)'s. The SM Higgs can have a non-trivial interaction in the presence of a "Higgs portal" coupling – a quartic interaction between the Higgs and the dark scalar field. The Z gauge field also has a non-trivial profile on the string because of the gauge-kinetic mixing. Each of these interactions is potentially relevant to the cosmological evolution of the dark string network. We summarize our findings in Sec. 2.5.

2.3 The Dark String Model

In this section we introduce the model. We focus on the gauge sector first and the role of the GKM operator, and then we turn to the scalar sector and the HP operator. In the third subsection we derive the string equations and discuss the boundary conditions.

2.3.1 Gauge Sector

We consider an extension of the SM electroweak sector that adds a complex scalar field $S(x)$ charged under a new gauge group, $\mathrm{U}(1)_X$, that has $\hat{X}^\mu(x)$ as its vector potential. In general, one can only write two renormalizable interactions between the SM and the dark sector: the Higgs portal operator, $\Phi^\dagger\Phi S^* S$, and the gauge kinetic mixing operator, $\hat{X}_{\mu\nu}Y^{\mu\nu}$. The Lagrangian that defines this model is

$$\mathcal{L} = |D_\mu\Phi|^2 + |D_\mu S|^2 - U(\Phi,S) - \frac{1}{4}\sum_{a=1,2,3}\left(W^a_{\mu\nu}\right)^2 - \frac{1}{4}\left(Y_{\mu\nu}\right)^2 - \frac{1}{4}\left(\hat{X}_{\mu\nu}\right)^2 - \frac{s_\epsilon}{2}\hat{X}_{\mu\nu}Y^{\mu\nu} \tag{2.3.1.1}$$

plus the remaining terms in the SM Lagrangian, which are unmodified and not written explicitly here. The parameter $s_\epsilon \equiv \sin\epsilon$ with $-\pi/2 \le \epsilon \le \pi/2$ controls the strength

of the gauge kinetic mixing. The covariant derivatives are given by

$$\begin{aligned} D_\mu \Phi &= \left(\partial_\mu - i\tfrac{g}{2}\,\sigma^a W_\mu^a - i\tfrac{g'}{2} Y_\mu\right)\Phi \\ D_\mu S &= \left(\partial_\mu - i\tfrac{g_{\rm X}}{2}\hat{X}_\mu\right) S \end{aligned} \tag{2.3.1.2}$$

where $\Phi = (\Phi^+\,,\, H)^T$ is the Higgs doublet. The scalar potential is

$$U(\Phi, S) = \lambda\left(\Phi^\dagger\Phi - \eta^2\right)^2 + \kappa\left(S^*S - \sigma^2\right)^2 + \alpha\left(\Phi^\dagger\Phi - \eta^2\right)\left(S^*S - \sigma^2\right) \quad , \tag{2.3.1.3}$$

and the parameter α is called the "Higgs portal coupling" as it is the gateway for interactions between the SM and dark sectors. This potential induces the vacuum expectation values

$$\langle\Phi\rangle = (0\,,\,\eta)^T \qquad \text{and} \qquad \langle S\rangle = \sigma \tag{2.3.1.4}$$

with $\eta = v/\sqrt{2} \approx 174$ GeV (see Sec. 2.3 for an extended discussion of the vacuum structure). The parameter λ can be exchanged for the Higgs boson mass, and we are left with five free parameters: α, κ, σ, $g_{\rm X}$, and s_ϵ.

The Lagrangian Eq. (2.3.1.1) gives rise to the following field equations:

$$\begin{aligned} &(D_\nu W^{\nu\mu})^a = \tfrac{1}{2} g J_\Phi^{a\,\mu} \\ &\partial_\nu Y^{\nu\mu} - s_\epsilon\,\partial_\nu \hat{X}^{\nu\mu} = \tfrac{1}{2} g' J_\Phi^\mu \\ &\partial_\nu \hat{X}^{\nu\mu} - s_\epsilon\,\partial_\nu Y^{\nu\mu} = \tfrac{1}{2} g_{\rm X} J_S^\mu \\ &D_\mu D^\mu \Phi = -2\lambda\left(\Phi^\dagger\Phi - \eta^2\right)\Phi - \alpha\left(S^*S - \sigma^2\right)\Phi \\ &D_\mu D^\mu S = -2\kappa\left(S^*S - \sigma^2\right) S - \alpha\left(\Phi^\dagger\Phi - \eta^2\right) S \end{aligned} \tag{2.3.1.5}$$

where the currents are defined as

$$\begin{aligned} J_\Phi^{a\,\mu} &\equiv i\left(\left(D^\mu\Phi\right)^\dagger \sigma^a \Phi - \Phi^\dagger \sigma^a D^\mu \Phi\right) \\ J_\Phi^\mu &\equiv i\left(\left(D^\mu\Phi\right)^\dagger \Phi - \Phi^\dagger D^\mu \Phi\right) \\ J_S^\mu &\equiv i\left(S D^\mu S^* - S^* D^\mu S\right) \end{aligned} \tag{2.3.1.6}$$

and $(D_\nu W^{\mu\nu})^a \equiv \partial_\nu W^{a\,\mu\nu} + g\epsilon^{abc} W^b_\nu W^{c\,\mu\nu}$. The presence of the $O(s_\epsilon)$ terms in Eq. (2.3.1.5) implies that both gauge fields Y^μ and $\hat{X}^\mu$ are sourced when either J^μ_Φ or J^μ_S is nonzero.

It will be convenient to move to a basis in which the GKM term is absent from the Lagrangian. This could be accomplished by merely rotating between the U(1) gauge fields, Y^μ and $\hat{X}^\mu$, as was done in previous studies of the dark string [40, 36]. However, in order to connect with the low energy observables, we would like to choose the basis that coincides with the mass eigenstates after electroweak symmetry breaking. In order to identify the appropriate basis, we insert the vacuum expectation values Eq. (2.3.1.4) into the Lagrangian Eq. (2.3.1.1) to obtain

$$\begin{aligned}\mathcal{L}\big|_{\text{vevs}} = m_W^2 \left|\frac{W^1_\mu - iW^2_\mu}{\sqrt{2}}\right|^2 + \frac{1}{2}m_Z^2\big(c_w W^3_\mu - s_w Y_\mu\big)^2 + \frac{1}{2}m_X^2\big(\hat{X}_\mu\big)^2 \\ - \frac{1}{4}\sum_{a=1,2,3} W^a_{\mu\nu}W^{a\,\mu\nu} - \frac{1}{4}Y_{\mu\nu}Y^{\mu\nu} - \frac{1}{4}\hat{X}_{\mu\nu}\hat{X}^{\mu\nu} - \frac{s_\epsilon}{2}\,\hat{X}_{\mu\nu}Y^{\mu\nu}\end{aligned} \tag{2.3.1.7}$$

where

$$m_W \equiv \frac{g\eta}{\sqrt{2}} \quad , \quad m_Z \equiv \frac{\bar{g}\eta}{\sqrt{2}} \quad , \quad m_X \equiv \frac{g_{\rm X}\sigma}{\sqrt{2}} \ , \tag{2.3.1.8}$$

and the weak mixing angle is defined as usual: $s_w \equiv \sin\theta_w = g'/\bar{g}$ and $c_w \equiv \cos\theta_w = g/\bar{g}$ with $\bar{g} \equiv \sqrt{g^2 + g'^2}$. Both the kinetic and the mass terms of the Lagrangian, Eq. (2.3.1.7), can be diagonalized by the transformation

$$\begin{pmatrix} W^1_\mu \\ W^2_\mu \end{pmatrix} = \begin{pmatrix} \frac{1}{\sqrt{2}} & \frac{1}{\sqrt{2}} \\ \frac{i}{\sqrt{2}} & -\frac{i}{\sqrt{2}} \end{pmatrix} \begin{pmatrix} W^+_\mu \\ W^-_\mu \end{pmatrix} \qquad \text{and} \qquad \begin{pmatrix} Y_\mu \\ W^3_\mu \\ \hat{X}_\mu \end{pmatrix} = \mathbf{M} \begin{pmatrix} A_\mu \\ Z_\mu \\ X_\mu \end{pmatrix} \tag{2.3.1.9}$$

where

$$\mathbf{M} = \begin{pmatrix} c_w & -s_w c_\zeta - t_\epsilon s_\zeta & s_w s_\zeta - t_\epsilon c_\zeta \\ s_w & c_w c_\zeta & -c_w s_\zeta \\ 0 & s_\zeta/c_\epsilon & c_\zeta/c_\epsilon \end{pmatrix} . \tag{2.3.1.10}$$

We continue to use the shorthand $s_\theta = \sin\theta$, $c_\theta = \cos\theta$, and $t_\theta = \tan\theta$ for $\theta = \epsilon, \zeta$. The angle ζ falls in the range $-\pi/4 < \zeta < \pi/4$, and its value is given by

$$\tan 2\zeta = \frac{-2 s_w s_\epsilon c_\epsilon}{(R^2-1) + s_\epsilon^2(1+s_w^2)} \ . \tag{2.3.1.11}$$

Here we have defined $R \equiv m_X/m_Z$, and we will assume $R > 1$. Note that $\mathbf{M}$ consists of a rotation and a rescaling, otherwise known as a principal axis transformation.

After performing the transformation in Eq. (2.3.1.9), the full Lagrangian becomes

$$\begin{aligned}\mathcal{L} = &|D_\mu \Phi|^2 + |D_\mu S|^2 - U(\Phi, S) - \frac{1}{2} W^-_{\mu\nu} W^{+\,\mu\nu} \\ &- \frac{1}{4} A_{\mu\nu} A^{\mu\nu} - \frac{1}{4} Z_{\mu\nu} Z^{\mu\nu} - \frac{1}{4} X_{\mu\nu} X^{\mu\nu} + \mathcal{L}_{\text{int}}\end{aligned} \tag{2.3.1.12}$$

where we have written each of the field strength tensors in the form $K_{\mu\nu} = \partial_\mu K_\nu - \partial_\nu K_\mu$ for $K = W^-, W^+, A, Z$, and X. The term $\mathcal{L}_{\text{int}}$ corresponds to interactions among the gauge fields, which are at least second order in $W^\pm$. As we discuss below, we can consistently set $W^\pm = 0$ for our dark string analysis and neglect these terms. The scalar field covariant derivatives now become

$$\begin{aligned} D_\mu \Phi &= \begin{pmatrix} D_\mu \Phi^+ - i\frac{g}{\sqrt{2}} W^+_\mu H \\ D_\mu H - i\frac{g}{\sqrt{2}} W^-_\mu \Phi^+ \end{pmatrix} \\ D_\mu S &= \Big(\partial_\mu - i(g^{\text{S}}_{\text{A}} A_\mu + g^{\text{S}}_{\text{Z}} Z_\mu + g^{\text{S}}_{\text{X}} X_\mu)\Big) S \end{aligned} \tag{2.3.1.13}$$

where we have defined

$$\begin{aligned} D_\mu \Phi^+ &\equiv \left(\partial_\mu - i(g^{\Phi^+}_{\text{A}} A_\mu + g^{\Phi^+}_{\text{Z}} Z_\mu + g^{\Phi^+}_{\text{X}} X_\mu)\right) \Phi^+ \\ D_\mu H &\equiv \left(\partial_\mu - i(g^{\text{H}}_{\text{A}} A_\mu + g^{\text{H}}_{\text{Z}} Z_\mu + g^{\text{H}}_{\text{X}} X_\mu)\right) H \end{aligned} \ . \tag{2.3.1.14}$$

The couplings are found to be

$$\begin{array}{lll} g^{\Phi^+}_{\text{A}} = e & g^{\Phi^+}_{\text{Z}} = c_\zeta \frac{e}{2}\left(\frac{1}{t_w} - t_w\right) - s_\zeta \frac{e}{2}\frac{t_\epsilon}{c_w} & g^{\Phi^+}_{\text{X}} = -c_\zeta \frac{e}{2}\frac{t_\epsilon}{c_w} - s_\zeta \frac{e}{2}\left(\frac{1}{t_w} - t_w\right) \\ g^{\text{H}}_{\text{A}} = 0 & g^{\text{H}}_{\text{Z}} = -c_\zeta \frac{e}{2}\frac{1}{s_w c_w} - s_\zeta \frac{e}{2}\frac{t_\epsilon}{c_w} & g^{\text{H}}_{\text{X}} = -c_\zeta \frac{e}{2}\frac{t_\epsilon}{c_w} + s_\zeta \frac{e}{2}\frac{1}{s_w c_w} \\ g^{\text{S}}_{\text{A}} = 0 & g^{\text{S}}_{\text{Z}} = s_\zeta \frac{g_{\text{X}}}{2}\frac{1}{c_\epsilon} & g^{\text{S}}_{\text{X}} = c_\zeta \frac{g_{\text{X}}}{2}\frac{1}{c_\epsilon} \end{array} \tag{2.3.1.15}$$

where $e = g\, s_w = g' c_w = \bar{g} s_w c_w$ is the electromagnetic coupling constant.

Now one can see the consequences of the GKM operator. As reflected in the nonzero couplings $g_{\rm X}^{\Phi^+}$, $g_{\rm X}^{\rm H}$, and $g_{\rm Z}^{\rm S}$, the Higgs acquires an interaction with the mass eigenstate X boson, and similarly the S interacts with the Z boson. However, the vanishing of $g_{\rm A}^{\rm H}$ and $g_{\rm A}^{\rm S}$ implies that the GKM does not induce a coupling between the photon and the electromagnetically neutral scalars; this is a consequence of the residual electromagnetic gauge invariance.

After electroweak symmetry breaking, see Eq. (2.3.1.4), the gauge fields acquire masses

$$\mathcal{L}\big|_{\rm vevs} \ni M_W^2 W_\mu^+ W^{-\,\mu} + \frac{1}{2} M_A^2 (A_\mu)^2 + \frac{1}{2} M_Z^2 (Z_\mu)^2 + \frac{1}{2} M_X^2 (X_\mu)^2 \tag{2.3.1.16}$$

with the spectrum

$$\begin{aligned} M_W^2 &= m_W^2 \\ M_A^2 &= 2(g_{\rm A}^{\rm H})^2 \eta^2 + 2(g_{\rm A}^{\rm S})^2 \sigma^2 = 0 \\ M_Z^2 &= 2(g_{\rm Z}^{\rm H})^2 \eta^2 + 2(g_{\rm Z}^{\rm S})^2 \sigma^2 = m_Z^2 \left(1 + s_w t_\zeta t_\epsilon\right) \\ M_X^2 &= 2(g_{\rm X}^{\rm H})^2 \eta^2 + 2(g_{\rm X}^{\rm S})^2 \sigma^2 = \frac{m_X^2}{c_\epsilon^2 (1 + s_w t_\zeta t_\epsilon)} \end{aligned} \tag{2.3.1.17}$$

Once again, the massless photon is a sign of the residual gauge invariance. As can be seen in Eq. (2.3.1.11), the angles ζ and ϵ always have opposite signs, and therefore one has in general $M_Z < m_Z$ and $M_X > m_X$. The Z and X boson masses are plotted in Fig. 2.1. Over most of the parameter range, these masses are well approximated as $M_Z \approx m_Z$ and $M_X \approx m_X \approx R M_Z$. To provide a reference point, we also show (on the left panel) the relative error bar on the measured Z boson mass, $\delta M_Z / M_Z \simeq 2.3 \times 10^{-5}$ [50], as a dashed line. Roughly speaking, the parameter range above the dashed line is excluded, or conversely, s_ϵ becomes unconstrained in the decoupling limit $R \gg 1$. However, to rigorously ascertain if a model is excluded, all available observables should

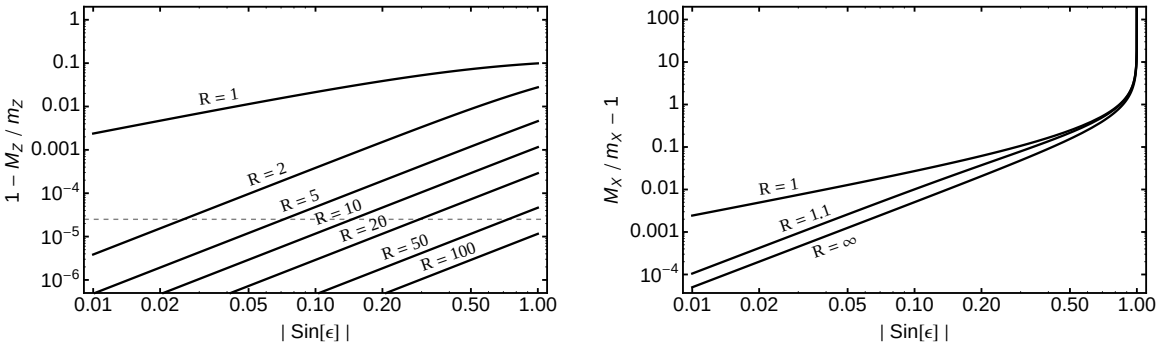

Figure 2.1: The spectrum of gauge bosons, given by Eq. (2.3.1.17), for various values of $\sin\epsilon$ and $R = m_X/m_Z$. We have fixed $g = 0.654$, $g' = 0.359$, and $\eta = 174$ GeV. Roughly speaking, the parameter range above the dashed line is excluded (see text).

be folded in together (see, *e.g.*, [49]). Since it is not the goal of this paper to impose phenomenological constraints, we will reserve that discussion for a future work.

We can now calculate the Euler-Lagrange equations for the diagonalized Lagrangian, Eq. (2.3.1.12). Since we are only interested in string solutions, it is prudent at this point to recognize that because Φ^+ does not acquire a vev, we can consistently set $\Phi^+ = W_\mu^\pm = A_\mu = 0$. That is, these fields are not sourced by the nontrivial profiles of the remaining scalar and gauge fields. Then the remaining field equations become

$$\begin{aligned}
\partial_\nu Z^{\nu\mu} &= g_{\rm Z}^{\rm H} J_H^\mu + g_{\rm Z}^{\rm S} J_S^\mu \\
\partial_\nu X^{\nu\mu} &= g_{\rm X}^{\rm H} J_H^\mu + g_{\rm X}^{\rm S} J_S^\mu \\
D_\mu D^\mu H &= -2\lambda\left(H^*H - \eta^2\right)H - \alpha\left(S^*S - \sigma^2\right)H \\
D_\mu D^\mu S &= -2\kappa\left(S^*S - \sigma^2\right)S - \alpha\left(H^*H - \eta^2\right)S
\end{aligned} \tag{2.3.1.18}$$

where the currents are given by

$$\begin{aligned}
J_H^\mu &\equiv i\big(H(D^\mu H)^* - H^* D^\mu H\big) \\
J_S^\mu &\equiv i\big(S(D^\mu S)^* - S^* D^\mu S\big)
\end{aligned} \quad , \tag{2.3.1.19}$$

and the covariant derivatives are given by Eq. (2.3.1.13). These field equations will be used in Sec. 2.3 to obtain the string equations.

2.3.2 Scalar Sector

After symmetry breaking, both the fields H and S acquire vevs. The three SM would-be Goldstone bosons, Φ^+ and $a_H = \mathrm{Arg}[H]$, and the fourth would-be Goldstone boson, $a_S = \mathrm{Arg}[S]$, are eaten leaving only two massive scalars, $\bar{h} = \sqrt{2}(|H| - \eta)$ and $\bar{s} = \sqrt{2}(|S| - \sigma)$. The Higgs portal operator allows these scalars to mix.

The scalar fields can be parametrized as $H = (\eta + \bar{h}/\sqrt{2}) \exp[ia_H]$ and $S = (\sigma + \bar{s}/\sqrt{2}) \exp[ia_S]$. After defining

$$m_H \equiv \sqrt{4\lambda\eta^2} \qquad \text{and} \qquad m_S \equiv \sqrt{4\kappa\sigma^2} \quad , \tag{2.3.2.1}$$

the scalar potential becomes

$$U \ni \frac{1}{2} \begin{pmatrix} \bar{h} & \bar{s} \end{pmatrix} \begin{pmatrix} m_H^2 & 2\alpha\eta\sigma \\ 2\alpha\eta\sigma & m_S^2 \end{pmatrix} \begin{pmatrix} \bar{h} \\ \bar{s} \end{pmatrix} \tag{2.3.2.2}$$

plus higher order interactions. This mass matrix is diagonalized by

$$\begin{pmatrix} \bar{h} \\ \bar{s} \end{pmatrix} = \begin{pmatrix} \cos\theta & \sin\theta \\ -\sin\theta & \cos\theta \end{pmatrix} \begin{pmatrix} \phi_H \\ \phi_S \end{pmatrix} \tag{2.3.2.3}$$

where the mixing angle, $-\pi/4 < \theta < \pi/4$, is given by

$$\tan 2\theta = \frac{4\alpha\eta\sigma}{m_S^2 - m_H^2} \quad , \tag{2.3.2.4}$$

and the eigenstates ϕ_H and ϕ_S have masses

$$M_H^2 = m_H^2 - \left(m_S^2 - m_H^2\right) \frac{\sin^2\theta}{\cos 2\theta} \tag{2.3.2.5}$$

$$M_S^2 = m_S^2 + \left(m_S^2 - m_H^2\right) \frac{\sin^2\theta}{\cos 2\theta} \quad , \tag{2.3.2.6}$$

respectively. We will assume that $M_S > M_H$ (equivalently, $m_S > m_H$) and that $M_H \approx 125$ GeV is the mass of the Higgs boson measured by the LHC.

The mixing angle can also be written as

$$\tan 2\theta = \frac{\alpha}{\alpha_0} \frac{8 m_H m_S}{m_S^2 - m_H^2} \tag{2.3.2.7}$$

where $\alpha_0 \equiv \sqrt{4\lambda\kappa}$. To ensure that the determinant of the mass matrix in Eq. (2.3.2.2) is positive, we must have $\alpha < \alpha_0$. In the decoupling limit, $m_S \gg m_H$, the mixing angle becomes $|\theta| \approx (|\alpha|/\alpha_0)(4M_H/M_S) \ll 1$, and the eigenvalues become $M_H \approx m_H$ and $M_S \approx m_S$. In this limit, the heavy scalar $\phi_S \approx \bar{s}$ is decoupled from the SM Higgs $\phi_H \approx \bar{h}$. As we reduce the hierarchical ratio, M_S/M_H, the amount of mixing grows larger until it becomes maximal ($\theta = 45°$) and $M_S/M_H = 1$. Observations of the Higgs at the LHC constrain the mixing with a hidden sector scalar to be $\theta \lesssim 40°$ [48]. Since, for the present study, we are not interested in rigorously applying observational constraints, we will simply take $M_H = 125$ GeV and require $M_S > M_H$. The scalar self-couplings are then determined by

$$\begin{aligned} \lambda &= \frac{M_H^2}{4\eta^2} + \frac{M_S^2 - M_H^2}{8\eta^2} \left(1 - \sqrt{1 - \left(\frac{4\alpha\eta\sigma}{M_S^2 - M_H^2} \right)^2} \right) \\ \kappa &= \frac{M_S^2}{4\sigma^2} - \frac{M_S^2 - M_H^2}{8\sigma^2} \left(1 - \sqrt{1 - \left(\frac{4\alpha\eta\sigma}{M_S^2 - M_H^2} \right)^2} \right) \end{aligned} \tag{2.3.2.8}$$

provided that

$$|\alpha| < \alpha_{\max} \equiv \frac{M_S^2 - M_H^2}{4\eta\sigma} \ . \tag{2.3.2.9}$$

Note that Eq. (2.3.2.9) subsumes the previous bound, $\alpha < \alpha_0 = \sqrt{4\lambda\kappa}$, because Eq. (2.3.2.8) gives $\alpha_0 = |\alpha| \sqrt{1 + (M_S M_H / 4\eta\sigma)^2} > |\alpha|$.

In order to discuss the string solutions below, it will be useful here to identify the extrema of the scalar potential Eq. (2.3.1.3). We set $\Phi^+ = 0$ and solve the two equations $\partial U/\partial H = \partial U/\partial S = 0$. There are four solutions with both H and S

nonnegative:

$$\begin{aligned} H=\eta \quad &, \quad S=\sigma \quad \Rightarrow \quad \text{minimum} \\ H=0 \quad &, \quad S=0 \quad \Rightarrow \quad \text{maximum} \\ H=H_0 \quad &, \quad S=0 \quad \Rightarrow \quad \text{saddle point} \\ H=0 \quad &, \quad S=S_0 \quad \Rightarrow \quad \text{saddle point} \end{aligned} \tag{2.3.2.10}$$

where

$$\begin{aligned} H_0 &\equiv \eta\sqrt{1+\tfrac{\alpha\sigma^2}{2\lambda\eta^2}} \\ S_0 &\equiv \sigma\sqrt{1+\tfrac{\alpha\eta^2}{2\kappa\sigma^2}} \end{aligned} \quad . \tag{2.3.2.11}$$

For the case $\alpha < 0$, the saddle point solutions do not exist if $|\alpha| > 2\kappa\sigma^2/\eta^2$.

2.3.3 Dark String Ansatz

Let us now derive the equations for the dark string. We will work in cylindrical coordinates, $\rho = \sqrt{x^2+y^2}$ and $\varphi = \arctan(y/x)$, and we will use the dimensionless radial coordinate $\xi = \rho/\rho_0$ where $\rho_0 = 1/\sigma$. Seeking the straight, static dark string solution, we take the ansatz [4]

$$\begin{aligned} &\Phi^+(x) = 0 \quad , \qquad H(x) = \eta\,\mathrm{h}(\xi)e^{in\varphi} \quad , \qquad Z_\mu(x) = \frac{1}{\rho_0}\frac{\mathrm{z}(\xi)}{\xi}V_\mu(\varphi) \quad , \\ &W^\pm_\mu = A_\mu = 0 \quad , \qquad S(x) = \sigma\,\mathrm{s}(\xi)e^{im\varphi} \quad , \qquad X_\mu(x) = \frac{1}{\rho_0}\frac{\mathrm{x}(\xi)}{\xi}V_\mu(\varphi) \quad , \end{aligned} \tag{2.3.3.1}$$

where $n, m \in \mathbb{Z}$ and $\mathrm{h}, \mathrm{s}, \mathrm{z}, \mathrm{x} \in \mathbb{R}$ and $V_\mu \equiv \rho\partial_\mu\varphi = \big\{0\,,\,-\sin\varphi\,,\,\cos\varphi\,,\,0\big\}$. With this ansatz, the currents in Eq. (2.3.1.19) become

$$J^\mu_H = \frac{2\eta^2}{\rho_0}\frac{\mathrm{h}^2 C_H}{\xi}V^\mu \qquad \text{and} \qquad J^\mu_S = \frac{2\sigma^2}{\rho_0}\frac{\mathrm{s}^2 C_S}{\xi}V^\mu \tag{2.3.3.2}$$

where

$$\begin{aligned} C_H(\xi) &\equiv n - g^{\mathrm{H}}_{\mathrm{Z}}\mathrm{z}(\xi) - g^{\mathrm{H}}_{\mathrm{X}}\mathrm{x}(\xi) \\ C_S(\xi) &\equiv m - g^{\mathrm{S}}_{\mathrm{Z}}\mathrm{z}(\xi) - g^{\mathrm{S}}_{\mathrm{X}}\mathrm{x}(\xi) \end{aligned} \quad . \tag{2.3.3.3}$$

[4] This corresponds to $Z_\mu dx^\mu = \mathrm{z}\,d\varphi$ and $X_\mu dx^\mu = \mathrm{x}\,d\varphi$.

The field equations in Eq. (2.3.1.18) become

$$\left(\frac{\mathrm{z}'}{\xi}\right)' = -2g_{\mathrm{Z}}^{\mathrm{H}}(\rho_0\eta)^2\frac{\mathrm{h}^2 C_H}{\xi} - 2g_{\mathrm{Z}}^{\mathrm{S}}(\rho_0\sigma)^2\frac{\mathrm{s}^2 C_S}{\xi} \tag{2.3.3.4a}$$

$$\left(\frac{\mathrm{x}'}{\xi}\right)' = -2g_{\mathrm{X}}^{\mathrm{H}}(\rho_0\eta)^2\frac{\mathrm{h}^2 C_H}{\xi} - 2g_{\mathrm{X}}^{\mathrm{S}}(\rho_0\sigma)^2\frac{\mathrm{s}^2 C_S}{\xi} \tag{2.3.3.4b}$$

$$(\xi\mathrm{h}')' = C_H^2\frac{\mathrm{h}}{\xi} - 2\lambda(\rho_0\eta)^2\left(1-\mathrm{h}^2\right)\xi\mathrm{h} - \alpha(\rho_0\sigma)^2(1-\mathrm{s}^2)\xi\mathrm{h} \tag{2.3.3.4c}$$

$$(\xi\mathrm{s}')' = C_S^2\frac{\mathrm{s}}{\xi} - 2\kappa(\rho_0\sigma)^2(1-\mathrm{s}^2)\xi\mathrm{s} - \alpha(\rho_0\eta)^2(1-\mathrm{h}^2)\xi\mathrm{s}\ . \tag{2.3.3.4d}$$

Although we take $\rho_0 = 1/\sigma$, we have retained ρ_0 in these expressions so as to avoid confusion as to where the σ enters explicitly as the VEV of S and where it enters as our choice of the radial length scale. If we were to turn off both the GKM and HP operators by taking $\epsilon = \alpha = 0$, then we would regain the string equations for two, uncoupled Nielsen-Olesen strings of winding n and m.

The scalar field boundary conditions can be divided into three cases depending on which of the two winding parameters, n and m, are nonzero. In each case, we must require $\mathrm{h}(\infty) = \mathrm{s}(\infty) = 1$ at spatial infinity and that $H(x)$ and $S(x)$ are regular at the origin. The cases are:

$$\left|\begin{array}{c} \textbf{Case 1}: \\ \\ n \neq 0 \\ m \neq 0 \end{array}\right| \Rightarrow \left|\begin{array}{l} \mathrm{h}(0) = 0 \\ \mathrm{h}(\infty) = 1 \\ \mathrm{s}(0) = 0 \\ \mathrm{s}(\infty) = 1 \end{array}\right| \qquad \left|\begin{array}{c} \textbf{Case 2}: \\ \\ n = 0 \\ m \neq 0 \end{array}\right| \Rightarrow \left|\begin{array}{l} \mathrm{h}'(0) = 0 \\ \mathrm{h}(\infty) = 1 \\ \mathrm{s}(0) = 0 \\ \mathrm{s}(\infty) = 1 \end{array}\right|$$

$$\left|\begin{array}{c} \textbf{Case 3}: \\ \\ n \neq 0 \\ m = 0 \end{array}\right| \Rightarrow \left|\begin{array}{l} \mathrm{h}(0) = 0 \\ \mathrm{h}(\infty) = 1 \\ \mathrm{s}'(0) = 0 \\ \mathrm{s}(\infty) = 1 \end{array}\right| . \tag{2.3.3.5}$$

Case 3 resembles the SM semilocal and electroweak strings [51], which are not topological and therefore not stable. For this reason, we will focus on Cases 1 and 2. In Case 2 we have mixed Neumann and Dirichlet boundary conditions, and we do not expect $\mathrm{h}(0) = 1$ in general. By considering the energetics, it is clear that $\mathrm{h}(0) = 1$ will minimize the gradient contribution to the energy of the string. However, in terms of the potential energy, we expect that the value of the Higgs condensate at the core of the string will relax toward the saddle point at $H = H_0$ and $S = 0$ [see Eq. (2.3.2.10)]. In general we expect

$$\textbf{Case 2}: \quad \begin{cases} h_0 < \mathrm{h}(0) < 1 & \alpha < 0 \\ 1 < \mathrm{h}(0) < h_0 & \alpha > 0 \end{cases} \tag{2.3.3.6}$$

where $h_0 \equiv H_0/\eta = \sqrt{1 + \alpha\sigma^2/(2\lambda\eta^2)}$ and H_0 is given by Eq. (2.3.2.11).

The gauge field boundary conditions are

$$\mathrm{z}(0) = \mathrm{x}(0) = 0 \qquad , \qquad \mathrm{z}(\infty) = \frac{g_{\mathrm{X}}^{\mathrm{S}} n - g_{\mathrm{X}}^{\mathrm{H}} m}{g_{\mathrm{X}}^{\mathrm{S}} g_{\mathrm{Z}}^{\mathrm{H}} - g_{\mathrm{X}}^{\mathrm{H}} g_{\mathrm{Z}}^{\mathrm{S}}} \qquad , \qquad \mathrm{x}(\infty) = \frac{g_{\mathrm{Z}}^{\mathrm{H}} m - g_{\mathrm{Z}}^{\mathrm{S}} n}{g_{\mathrm{X}}^{\mathrm{S}} g_{\mathrm{Z}}^{\mathrm{H}} - g_{\mathrm{X}}^{\mathrm{H}} g_{\mathrm{Z}}^{\mathrm{S}}} \ . \tag{2.3.3.7}$$

These ensure that $Z_\mu(x)$ and $X_\mu(x)$ are regular at the origin and that at spatial infinity

$$C_H(\infty) = C_S(\infty) = 0 \ , \tag{2.3.3.8}$$

and the action is finite. An interesting consequence of the GKM is that both gauge fields have nontrivial profiles if either scalar field has a winding (either n or m is nonzero). This is evident in the limit $s_\epsilon \ll 1$ where

$$\begin{aligned} \mathrm{z}(\infty) &\approx -\frac{\sqrt{2}\eta}{m_Z} n - \frac{\sqrt{2} s_w R^2 \sigma}{m_X (R^2 - 1)} m \, s_\epsilon + O(s_\epsilon^2) \\ \mathrm{x}(\infty) &\approx \frac{\sqrt{2}\sigma}{m_X} m - \frac{\sqrt{2} s_w \eta}{m_Z (R^2 - 1)} n \, s_\epsilon + O(s_\epsilon^2) \ . \end{aligned} \tag{2.3.3.9}$$

For example, taking $n = 0$ and $m = 1$ induces an $O(s_\epsilon)$ expectation value for the Z field.

2.4 Properties of the Dark String

The dark string is the solution of the system of equations given by Eq. (2.3.3.4) along with the boundary conditions in Eqs. (2.3.3.5) and (2.3.3.7). We solve these equations numerically as described in Appendix **??**.

We calculate the dark string solution for various values of the model parameters: (n, m), α, s_ϵ, $g_{\rm X}$, σ, and M_S while fixing $\eta = 174$ GeV, $M_H = 125$ GeV, $g = 0.654$, and $g' = 0.359$ and using Eq. (2.3.2.8) to determine λ and κ. With this choice of parameters, the masses M_Z and M_X are given by Eq. (2.3.1.17). Although these masses depend upon s_ϵ, it is typically the case that $M_Z \approx 91.2$ GeV and $M_X \approx m_X = g_{\rm X}\sigma/\sqrt{2}$. Having obtained the dark string solution, we study its properties and couplings, which are discussed in the remainder of this section.

2.4.1 String Solution

Generally, the strings with higher order windings, (n, m) with $n, m > 1$, are unstable, and they will decay on a microscopic time scale into the lightest strings. The winding m of the singlet scalar S is topological by virtue of the $\mathrm{U}(1)_X$ symmetry, however the winding n of the Higgs field is not topological – just as in the case of the electroweak strings in the SM [51]. This means that any (n, m) string with $n \geq 1$ will fragment and decay into the $(0, 1)$ string, which generally has a lower tension than the $(1, 1)$ string. We will focus on the properties of the $(0, 1)$ string, but we will also compare against the $(1, 1)$ string.

In Figures 2.2, 2.3, and 2.4 we show the profile functions of the $(n, m) = (0, 1)$ and $(1, 1)$ strings for $M_S = M_X = \sigma/\sqrt{2} = 200$ GeV, 1 TeV, and 10 TeV. In the lower

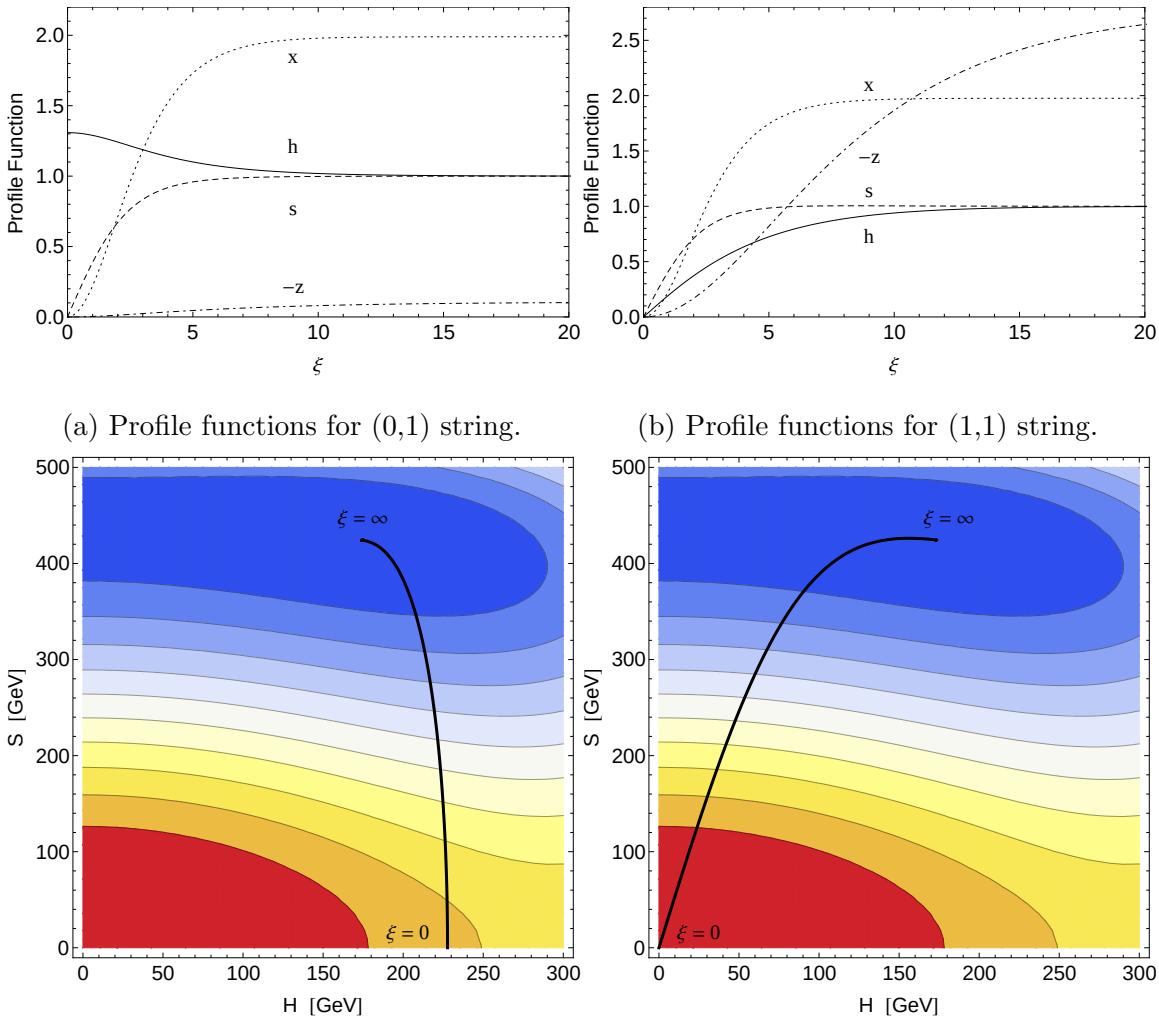

(a) Profile functions for (0,1) string.

(b) Profile functions for (1,1) string.

(c) (0,1) string solution in (H,S) plane.

(d) (1,1) string solution in (H,S) plane.

Figure 2.2: String solutions for $m_X = M_S = \sigma/\sqrt{2} = 200$ GeV, $\alpha = 0.1$, $s_\epsilon = 0.1$, and $g_X = 1$. The bottom panels show the scalar potential, Eq. (2.3.1.3), where the blue (red) contours are lower (higher).

panels, we also show contour plots of the scalar potential, Eq. (2.3.1.3), where we have overlaid the string trajectories $\{H, S\} = \{\eta\, \mathrm{h}(\xi), \sigma\, \mathrm{s}(\xi)\}$. There are a number of qualitative features which can be seen in these figures that we will discuss at length below. First, at the core of the $(0, 1)$ strings the Higgs condensate deviates from its vacuum value. Second, the strings have a tight "core" where the gradients of the S and X^μ fields are large, and this core extends out to $\xi = O(1)$ or equivalently the

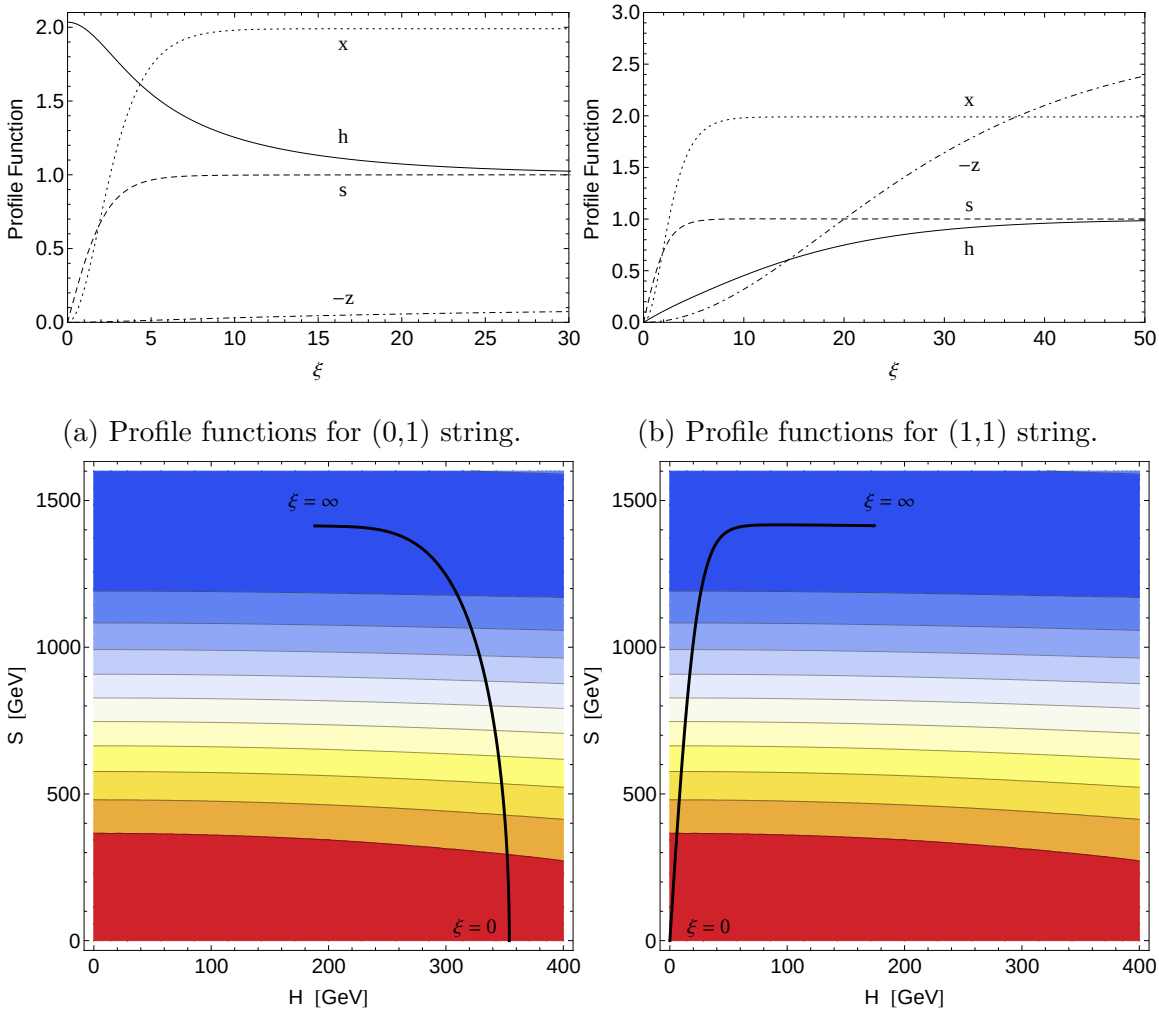

(a) Profile functions for (0,1) string.

(b) Profile functions for (1,1) string.

(c) (0,1) string solution in (H,S) plane.

(d) (1,1) string solution in (H,S) plane.

Figure 2.3: Same as Fig. 2.2 but for $m_X = M_S = \sigma/\sqrt{2} = 1$ TeV.

physical length $\rho = O(1/\sigma)$. The H and Z^μ profiles are much wider than the string core.

For the $(0, 1)$ string, the Higgs field does not wind and satisfies only a Neumann boundary conditions at the origin [see Eq. (2.3.3.5)]. We anticipated in Eq. (2.3.3.6) that the value of the Higgs profile at the core of the $(0, 1)$ string should rise or fall toward $\mathrm{h}(0) = \mathrm{h}_0 = \sqrt{1 + \alpha\sigma^2/2\lambda\eta^2}$ depending on the sign of α. Figures 2.2a, 2.3a, and 2.4a reveal that $\mathrm{h}(0) > 1$, indicating that the Higgs condensate is "attracted"

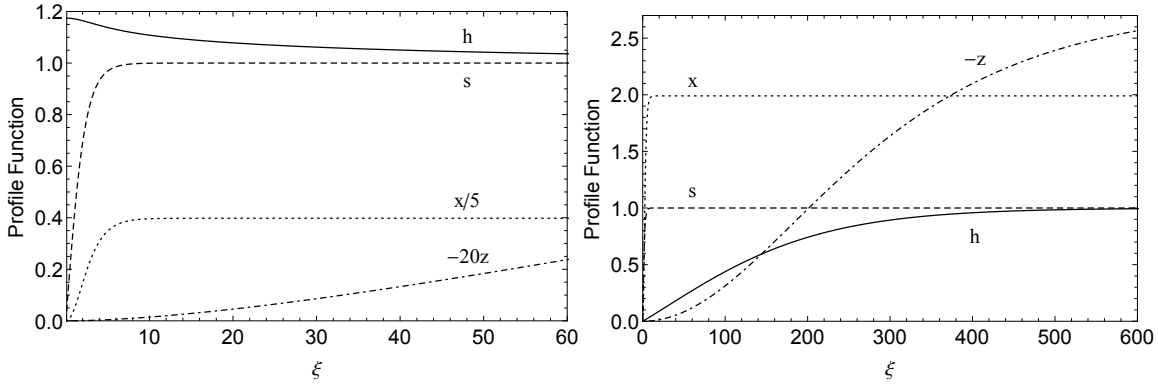

(a) Profile functions for (0,1) string.

(b) Profile functions for (1,1) string.

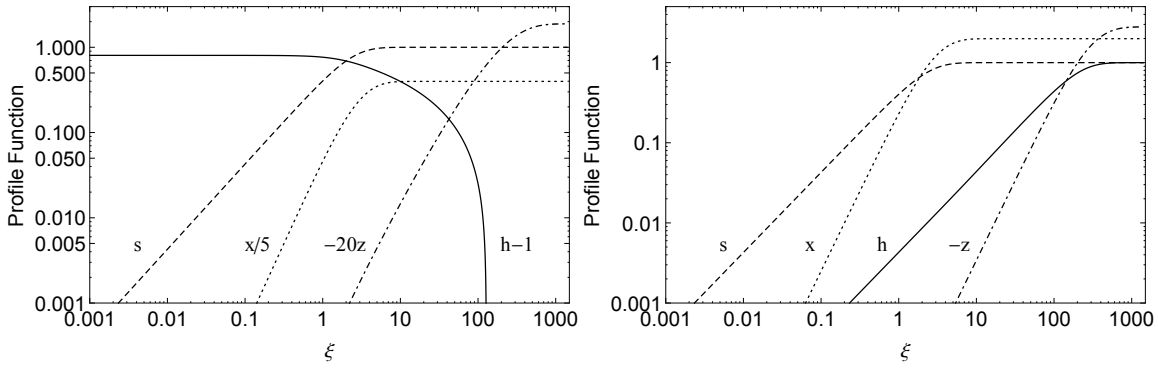

(c) Profile functions for (0,1) string.

(d) Profile functions for (1,1) string.

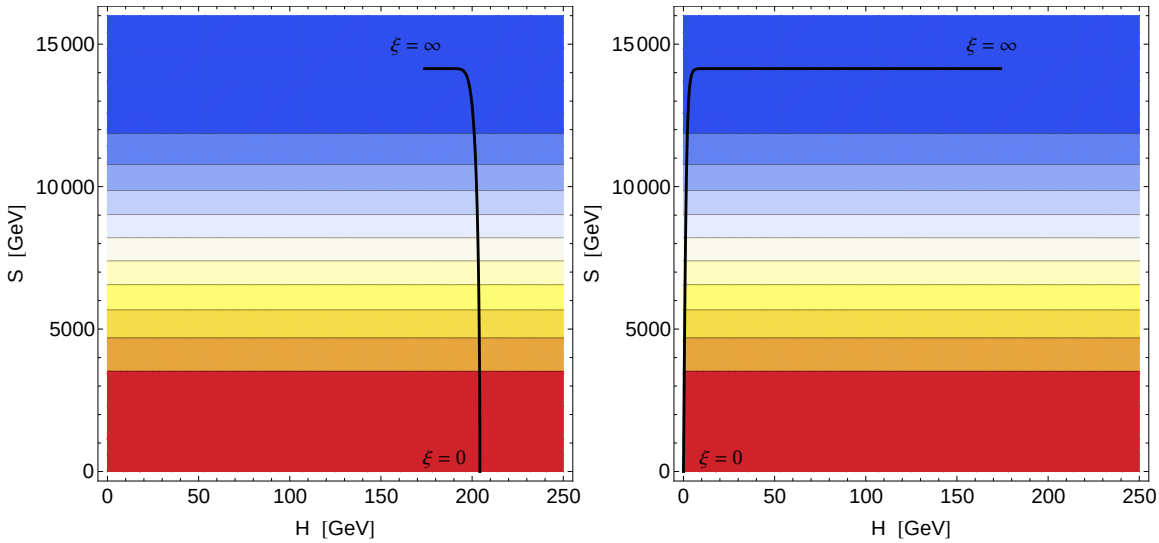

(e) (0,1) string solution in (H,S) plane.

(f) (1,1) string solution in (H,S) plane.

Figure 2.4: Same as Fig. 2.2 but for $m_X = M_S = \sigma/\sqrt{2} = 10$ TeV and $\alpha = 0.01$.

by the string core in the case $\alpha > 0$. Numerically, we find that the magnitude of the deviation is $|\mathrm{h}(0) - 1| \approx O(0.1 - 1)$, depending on the parameter choices. In some cases we find $\mathrm{h}(0) \lesssim \mathrm{h}_0$, which confirms the energetic arguments that led to Eq. (2.3.3.6), whereas in other cases $\mathrm{h}(0) \ll \mathrm{h}_0$ suggesting that the tension is dominated by gradient energy instead of potential energy, and our previous estimate breaks down. We compare $\mathrm{h}(0)$ and h_0 in Fig. 2.5 where we plot both quantities against α (left panel) and σ (right panel). For large values of α, both $\mathrm{h}(0)$ and $\mathrm{h}_0 = \sqrt{1 + \alpha\sigma^2/(2\lambda\eta^2)}$ reach a maximum and turn over. To understand this behavior, recall that λ is allowed to vary with α according to Eq. (2.3.2.8) while M_H and M_S are held fixed, and therefore $\mathrm{h}_0 \sim \sqrt{\alpha/\lambda}$ is not monotonically increasing with α. For negative values of α, Fig. 2.5a reveals that $\mathrm{h}(0)$ asymptotes toward zero whereas h_0 vanishes at $\alpha = -2\lambda\eta^2/\sigma^2$. In this case, the Higgs condensate is "repelled" by the string core. We show the behavior of $\mathrm{h}(0)$ and h_0 in the decoupling limit, $\sigma \gg \eta$, in Fig. 2.5b. In this limit, $\mathrm{h}_0 \sim \sigma/\eta$ grows rapidly, but the value of the condensate at the string core, $\mathrm{h}(0)$, rises much more slowly.

In order to better characterize the string solution, we calculate the "full width at half maximum" of the scalar profile functions. In terms of the dimensionless radial coordinate, these are given by the solutions of $\mathrm{h}(\xi_h/2) = \mathrm{h}(0)/2$ and $\mathrm{s}(\xi_s/2) = \mathrm{s}(0)/2$. Figure 2.6 shows the physical widths

$$\Delta\rho_h = \rho_0\xi_h \qquad \text{and} \qquad \Delta\rho_s = \rho_0\xi_s \tag{2.4.1.1}$$

for the $(0,1)$ and $(1,1)$ strings as a function of σ. In both cases the width of the S condensate falls off like $\Delta\rho_s \simeq 2/M_S = 2\sqrt{2}/\sigma$. The Higgs condensate, on the other hand, has a significantly different behavior in the two cases. For the $(1,1)$ string the width of the Higgs condensate is insensitive to σ and remains approximately equal to $\Delta\rho_h \simeq 2/M_H \approx 16\ \mathrm{TeV}^{-1}$. For the $(0,1)$ string the Higgs condensate is narrower,

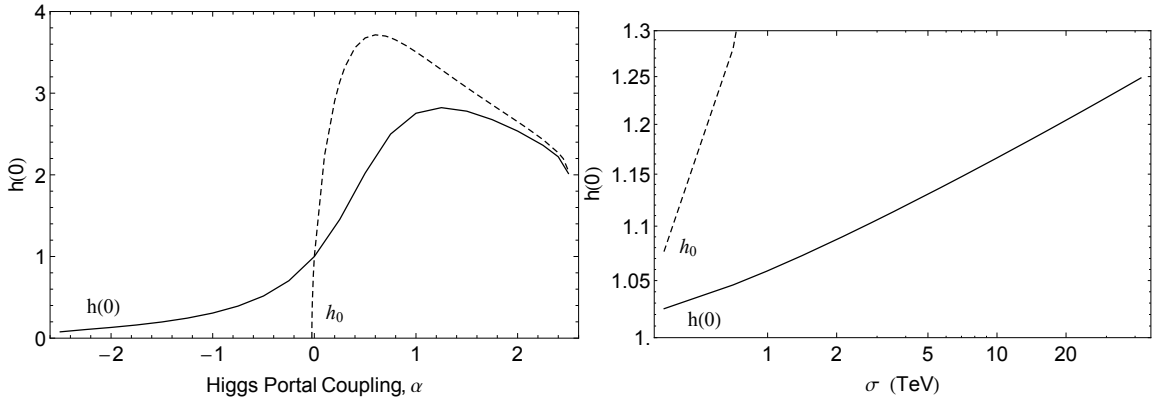

(a) $M_S = 1$ TeV, $M_X = 400$ GeV, $s_\epsilon = 0.1$,(b) $M_X = M_S = \sigma/\sqrt{2}$, $\alpha = 0.01$, $s_\epsilon = 0$, $g_{\rm X} = 1$. $g_{\rm X} = 1$

Figure 2.5: The Higgs profile at the string core, $\mathrm{h}(\xi = 0)$, for the $(0, 1)$ string. For comparison we also show $h_0 = H_0/\eta$ (dashed) where H_0 is given by Eq. (2.3.2.11).

and its width decreases with increasing σ, but not as fast as σ^{-1}.

Let us now take Figures 2.2–2.6 together, and construct a coherent picture of the $(0, 1)$ dark string. The behavior is similar to what is seen in the familiar case of bosonic superconductivity [52]. When $s_\epsilon = \alpha = 0$ the S and X^μ fields form a Nielsen-Olesen string and the Higgs condensate is equal to its vacuum value everywhere. Roughy speaking, the Higgs field is unaware of the presence of the string since there is no coupling between them. For $\alpha > 0$ ($\alpha < 0$) the Higgs condensate is "attracted" ("repelled") by the string and $\mathrm{h}(0) > 1$ ($\mathrm{h}(0) < 1$). In the decoupling limit, $\sigma \sim M_S \gg \eta \sim M_H$, and with $\alpha > 0$, the saddle point moves to $\mathrm{h}_0 \gg 1$, but the tension becomes gradient dominated and $\mathrm{h}(0) \ll \mathrm{h}_0$, contrary to expectations. The S and X profiles fall off on a length scale $2/M_S$, which defines the string core. The Higgs condensate, however, forms a wide halo around the core. For a 10 TeV scale string, the halo is approximately an order of magnitude wider than the core, but it is still

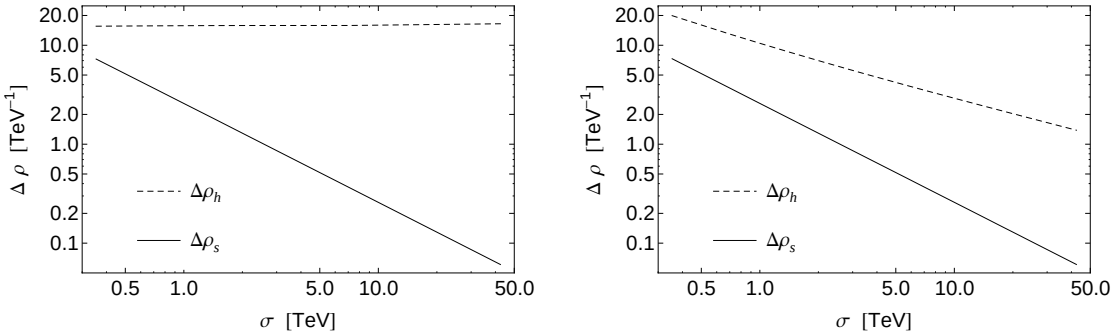

(a) $(n, m) = (1, 1)$ (b) $(n, m) = (0, 1)$

Figure 2.6: The widths of the scalar field condensates (H dashed; S solid) surrounding the dark string. See Eq. (2.4.1.1). The parameters are taken to be $M_X = M_S = \sigma/\sqrt{2}$, $g_{\rm X} = 1$, $\alpha = 0.01$, and $s_\epsilon = 0$. In both cases, $\Delta\rho_s \simeq 2/M_S$, but $\Delta\rho_h \simeq 2/M_H$ for the $(1, 1)$ string, and it decreases gradually for the $(0, 1)$ string.

smaller than $2/M_H$ by another order of magnitude.

2.4.2 Tension

The tension of the dark string is defined by $\mu \equiv \int_0^\infty \rho d\rho \int_0^{2\pi} d\varphi\, T_0^0$ where $T^{\mu\nu}$ is the energy-momentum tensor. Inserting the dark string ansatz, Eq. (2.3.3.1), this becomes [5]

$$\mu = 2\pi\sigma^2 \int_0^\infty \mathcal{E}\, \xi\, d\xi \tag{2.4.2.1}$$

where

$$\mathcal{E} = \mathcal{E}_X + \mathcal{E}_Z + \mathcal{E}_H + \mathcal{E}_S + u \tag{2.4.2.2}$$

is the dimensionless energy density, which consists of contributions from each of the

[5] See Appendix Sec. B

fields:

$$\mathcal{E}_X = \frac{1}{(\sigma\rho_0)^2}\frac{(\mathrm{x}')^2}{2\xi^2} \tag{2.4.2.3a}$$

$$\mathcal{E}_Z = \frac{1}{(\sigma\rho_0)^2}\frac{(\mathrm{z}')^2}{2\xi^2} \tag{2.4.2.3b}$$

$$\mathcal{E}_H = \left(\frac{\eta}{\sigma}\right)^2\left((\mathrm{h}')^2 + \frac{\mathrm{h}^2}{\xi^2}C_H^2\right) \tag{2.4.2.3c}$$

$$\mathcal{E}_S = \left((\mathrm{s}')^2 + \frac{\mathrm{s}^2}{\xi^2}C_S^2\right) \tag{2.4.2.3d}$$

$$u = \lambda(\rho_0\sigma)^2\left(\frac{\eta}{\sigma}\right)^4\left(\mathrm{h}^2-1\right)^2 + \kappa(\rho_0\sigma)^2\left(\mathrm{s}^2-1\right)^2 + \alpha(\rho_0\eta)^2\left(\mathrm{h}^2-1\right)\left(\mathrm{s}^2-1\right)\ . \tag{2.4.2.3e}$$

For the special case $\epsilon = \alpha = 0$ we have $C_H = n - g_{\mathrm{Z}}^{\mathrm{H}}\, z$ and $C_S = m - g_{\mathrm{X}}^{\mathrm{S}}\, x$ [see Eq. (2.3.3.3)]. Thus, as expected, in the absence of interactions between the SM and dark sector the energy reduces to the sum of energies of two separate Nielsen–Olesen strings. In particular, for a $(0,1)$ string with $\epsilon = \alpha = 0$ and $m_S = m_X$, the integral in Eq. (2.4.2.1) numerically evaluates to 1, and we find the tension to be $\mu = 2\pi\sigma^2$. From the individual terms in Eq. (2.4.2.3), we can see that with our choice $\rho_0 = \sigma^{-1}$, some terms are independent of σ and the rest go as $(\eta/\sigma)^2$ or $(\eta/\sigma)^4$. Thus when $\sigma \sim \eta$, the tension will not follow a simple power law, but when $\sigma \gg \eta$, it will increase as σ^2. The terms that scale as inverse powers of σ are more significant for the $(1,1)$ string than for the $(0,1)$ string, so we would expect the $(0,1)$ string tension to essentially scale as σ^2 even for $\sigma \sim \eta$.

Figure 2.7 compares the tension of the $(1,1)$ and $(0,1)$ strings along various slices of parameter space. Each subfigure illustrates that the tension of the $(0,1)$ string is always smaller than the tension of the $(1,1)$ string. The scaling behavior mentioned above is evident in Figures 2.7a and 2.7b. Figure 2.7a shows the tension as a function of the $\mathrm{U}(1)_X$ gauge coupling, g_{X}, and it is seen that the tension scales like $\mu \propto g_{\mathrm{X}}^{-2}$. This scaling is understood by noting that we hold $m_X = g_{\mathrm{X}}\sigma/\sqrt{2}$ fixed and vary

$\sigma \propto g_{\rm X}^{-1}$. Then the figure simply shows that $\mu \propto \sigma^2$. Figure 2.7b shows the tension as a function of the mass of the X gauge boson, and since we are now holding $g_{\rm X}$ fixed and varying $\sigma \propto m_X$, this figure also shows that $\mu \propto \sigma^2$. In both cases, the $(0,1)$ string tension scales as σ^2 for all values of σ, while the $(1,1)$ string tension departs from this behavior at the lower values of σ.

Figures 2.7c and 2.7d show how the tension depends on the GKM parameter s_ϵ. From these it can be seen that the tension decreases monotonically with increasing $|s_\epsilon|$ for the $(0,1)$ string and almost monotonically for the $(1,1)$ string. This behavior can be understood by noting that the gauge kinetic terms of the original Lagrangian, Eq. (2.3.1.1), can be written as

$$\mathcal{L} \ni -\frac{1}{4}\left(\frac{1+s_\epsilon}{2}\right)\left(Y_{\mu\nu}+\hat{X}_{\mu\nu}\right)^2 - \frac{1}{4}\left(\frac{1-s_\epsilon}{2}\right)\left(Y_{\mu\nu}-\hat{X}_{\mu\nu}\right)^2 . \qquad (2.4.2.4)$$

In the limit $s_\epsilon \to \pm 1$ it "costs no energy" to excite the gauge field $Y_\mu \mp \hat{X}_\mu$, and the tension of the string is reduced. Here it is important to note that we hold fixed the parameter $m_X = g_{\rm X}\sigma/\sqrt{2}$, which differs from the mass eigenvalue M_X for nonzero s_ϵ [see Eq. (2.3.1.17)]. In 2.7c, for example, at $s_\epsilon = 0$ we have $M_X = 200$ GeV, while at $|s_\epsilon| = 0.9$ it has increased to $M_X = 450$ GeV.

The dependence of the tension on α is shown in Fig. 2.7e. For the $(1,1)$ string, the tension rises nearly linearly with α, whereas for the $(0,1)$ string the tension is symmetric in α. This parametric behavior is understood by noting that at the core of the $(1,1)$ string the profile functions become $\mathrm{s}(0) = \mathrm{h}(0) = 0$, while at the core of the $(0,1)$ string they become $\mathrm{s}(0) = 0$ and $\mathrm{h}(0) = 1 + O(\alpha)$ [see Eq. (2.3.3.5)]. The tension depends on α primarily through the potential energy density, $u(h,s)$, given by Eq. (2.4.2.3e). The parametric behavior of the tension is estimated by $\mu^{(1,1)} \sim u(0,0) = \lambda\eta^4 + \kappa\sigma^4 + \alpha\eta^2\sigma^2$ for the $(1,1)$ string and by $\mu^{(0,1)} \sim u(1+O(\alpha),0) = \lambda\eta^4 + \kappa\sigma^4 + O(\alpha^2)$ for the $(0,1)$ string. In this way, the dependence on α seen in

Fig. 2.7e is explained.

Finally, let us remark that our string solutions and tension are consistent with the results available in the literature. The authors of Ref. [40] considered a model similar to ours, in which they include a gauge kinetic mixing term but no Higgs portal term. They also take the semilocal limit $s_w = 1$. Our model reduces to theirs upon setting $\alpha = 0$, $s_w = 1$, and $M_H = 125$ GeV. For a particular parameter range given in Figure 3 of Ref. [40], we calculate the string tension and find agreement to better than $O(1\%)$. The author of Ref. [41] considered a model and solutions corresponding to the $(0, 1)$ string in our work with a Higgs portal term but no gauge kinetic mixing term, and also found that the string carries a Higgs condensate.

2.4.3 Coupling of the Higgs to the String

The dark string acts as a source for the scalar fields H and S. This source causes the fields to locally deviate from their vacuum expectation values and to form a long range "cloud" around the string core. As discussed in Sec. 2.3, we can parametrize the fields as $H = (\eta + \bar{h}/\sqrt{2})e^{ia_H}$ and $S = (\sigma + \bar{s}/\sqrt{2})e^{ia_S}$, and the physical scalars, $\bar{h}$ and $\bar{s}$, mix with one another with a mixing angle θ, given by Eq. (2.3.2.4). Only the lighter Higgs-like mass eigenstate, $\phi_H = \cos\theta\,\bar{h} - \sin\theta\,\bar{s}$, can be radiated efficiently from the dark string since the S-like eigenstate, ϕ_S, has a mass comparable to the string tension. We therefore are only interested in the effective coupling of ϕ_H to the dark string.

The field equations for H and S, given previously by Eq. (2.3.1.18), may be written

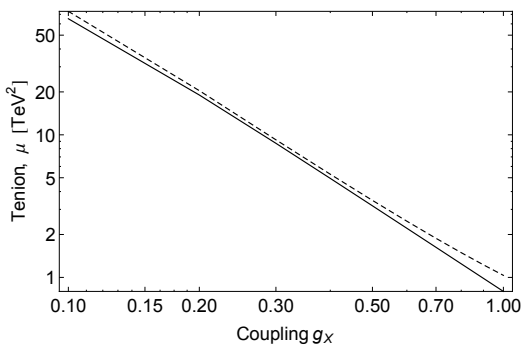

(a) $3m_X = M_S = 600$ GeV, $s_\epsilon = 0.1$, $\alpha = 0.1$.

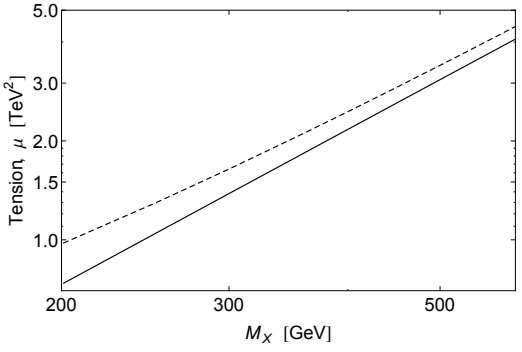

(b) $M_S = 500$ GeV, $s_\epsilon = 0.1$, $\alpha = 0.1$, $g_{\rm X} = 1$.

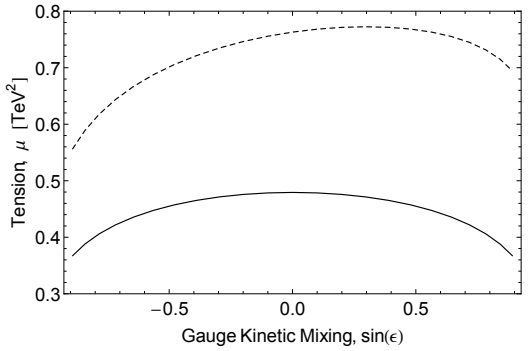

(c) $m_X = M_S = 200$ GeV, $\alpha = 0.1$, $g_{\rm X} = 1$

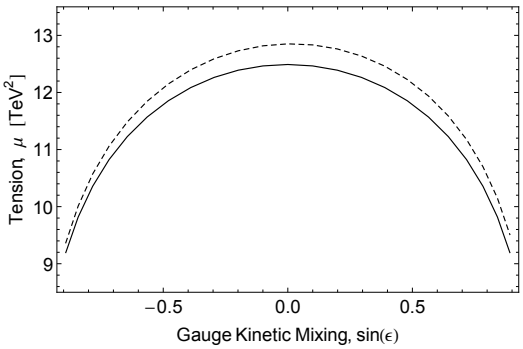

(d) $m_X = M_S = 1$ TeV, $\alpha = 0.1$, $g_{\rm X} = 1$

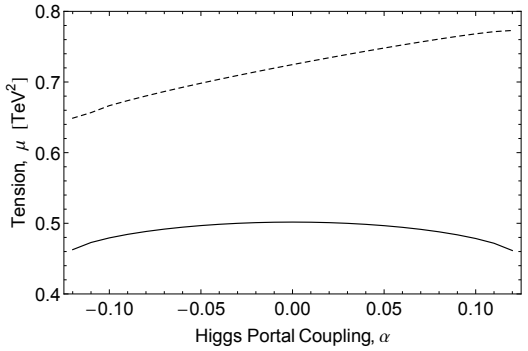

(e) $m_X = M_S = 200$ GeV, $s_\epsilon = 0.1$, $g_{\rm X} = 1$.

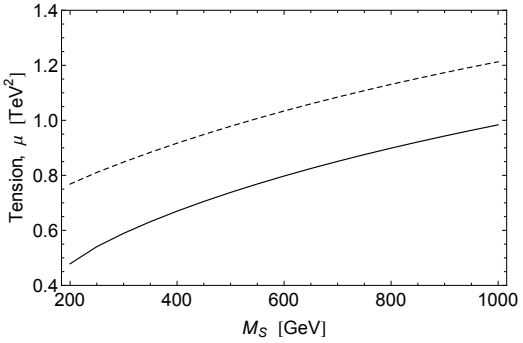

(f) $m_X = 200$ GeV, $s_\epsilon = 0.1$, $\alpha = 0.1$, $g_{\rm X} = 1$.

Figure 2.7: Tension of $(0, 1)$ (solid) and $(1, 1)$ (dashed) strings.

as follows after expanding out the covariant derivatives:

$$\Box H = i\left(g_{\rm Z}^{\rm H}\partial_\mu Z^\mu + g_{\rm X}^{\rm H}\partial_\mu X^\mu\right)H + 2i\left(g_{\rm Z}^{\rm H}Z^\mu + g_{\rm X}^{\rm H}X^\mu\right)\partial_\mu H + \left(g_{\rm Z}^{\rm H}Z^\mu + g_{\rm X}^{\rm H}X^\mu\right)^2 H$$
$$- 2\lambda\left(|H|^2 - \eta^2\right)H - \alpha\left(|S|^2 - \sigma^2\right)H \tag{2.4.3.1}$$
$$\Box S = i\left(g_{\rm Z}^{\rm S}\partial_\mu Z^\mu + g_{\rm X}^{\rm S}\partial_\mu X^\mu\right)S + 2i\left(g_{\rm Z}^{\rm S}Z^\mu + g_{\rm X}^{\rm S}X^\mu\right)\partial_\mu S + \left(g_{\rm Z}^{\rm S}Z^\mu + g_{\rm X}^{\rm S}X^\mu\right)^2 S$$
$$- 2\kappa\left(|S|^2 - \sigma^2\right)S - \alpha\left(|H|^2 - \eta^2\right)S\ . \tag{2.4.3.2}$$

In the vicinity of the dark string, the fields acquire position-dependent expectation values, and the interactions on the right hand side of these equations become source terms. In order to illustrate the nature of this source, we can evaluate the right hand sides of Eqns. (2.4.3.1) and (2.4.3.2), denoted as $\mathcal{S}_H$ and $\mathcal{S}_S$ respectively, in the presence of the string background, given by Eq. (2.3.3.1). Doing so we obtain

$$\mathcal{S}_H = \mathcal{S}_H^{(\rm core)} + \mathcal{S}_H^{(\rm cloud)} \qquad \text{and} \qquad \mathcal{S}_S = \mathcal{S}_S^{(\rm core)} + \mathcal{S}_S^{(\rm cloud)} \tag{2.4.3.3}$$

where

$$\mathcal{S}_H^{(\rm core)} \equiv -\frac{\eta}{\rho_0^2}\frac{\rm h}{\xi^2}\left(g_{\rm Z}^{\rm H}{\rm z}(\infty) + g_{\rm X}^{\rm H}{\rm x}\right)^2 + \alpha\eta\sigma^2\left(1-{\rm s}^2\right){\rm h} + \frac{\eta}{\rho_0^2}\frac{\rm h}{\xi^2}(g_{\rm Z}^{\rm H})^2{\rm z}(\infty)^2(1-{\rm s}^2) \tag{2.4.3.4}$$

$$\mathcal{S}_H^{(\rm cloud)} \equiv -2\lambda\eta^3\left({\rm h}^2-1\right){\rm h} - \frac{\eta}{\rho_0^2}\frac{\rm h}{\xi^2}(g_{\rm Z}^{\rm H})^2\left({\rm z}^2 - {\rm z}(\infty)^2\right) - 2\frac{\eta}{\rho_0^2}\frac{\rm h}{\xi^2}(g_{\rm Z}^{\rm H}g_{\rm X}^{\rm H}){\rm x}\left({\rm z}-{\rm z}(\infty)\right)$$
$$- \frac{\eta}{\rho_0^2}\frac{\rm h}{\xi^2}(g_{\rm Z}^{\rm H})^2{\rm z}(\infty)^2(1-{\rm s}^2) \tag{2.4.3.5}$$

$$\mathcal{S}_S^{(\rm core)} \equiv -\frac{\sigma}{\rho_0^2}\frac{\rm s}{\xi^2}\left(1 - g_{\rm Z}^{\rm S}{\rm z}(\infty) - g_{\rm X}^{\rm S}{\rm x}\right)^2 + 2\kappa\sigma^2\left(1-{\rm s}^2\right){\rm s} \tag{2.4.3.6}$$

$$\mathcal{S}_S^{(\rm cloud)} \equiv -\alpha\sigma\eta^2\left({\rm h}^2-1\right){\rm s} - \frac{\sigma}{\rho_0^2}\frac{\rm s}{\xi^2}\left[(g_{\rm Z}^{\rm S})^2\left({\rm z}+{\rm z}(\infty)\right) - 2g_{\rm Z}^{\rm S}(1-g_{\rm X}^{\rm S}{\rm x})\right]\left({\rm z}-{\rm z}(\infty)\right)\quad , \tag{2.4.3.7}$$

and where ${\rm z}(\infty)$ is given by Eq. (2.3.3.7) with $(n,m)=(0,1)$. We have added and subtracted the term $-\frac{\eta}{\rho_0^2}\frac{\rm h}{\xi^2}(g_{\rm Z}^{\rm H})^2{\rm z}(\infty)^2(1-{\rm s}^2)$ from $\mathcal{S}_H^{(\rm core)}$ and $\mathcal{S}_H^{(\rm cloud)}$ in order to keep these functions finite at the origin. We show these various contributions to the sources

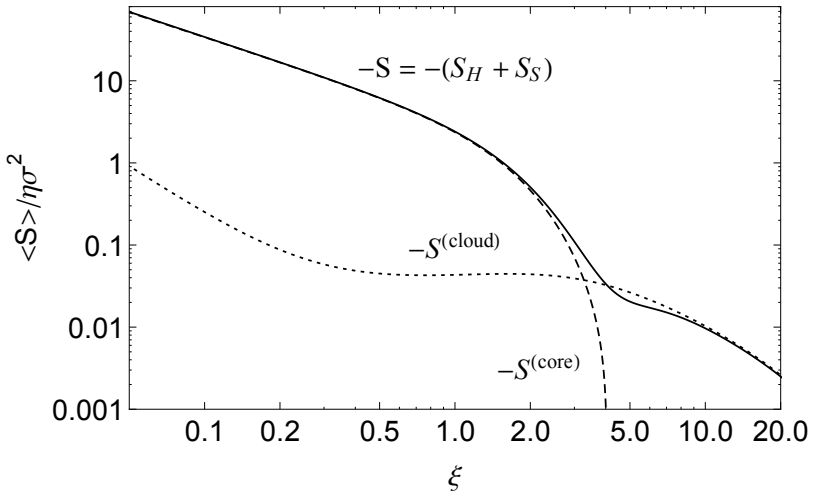

Figure 2.8: Vacuum expectation value of $\mathcal{S}$ as a function of the scaled radial coordinate ξ, where $\mathcal{S}_H$ and $\mathcal{S}_S$ are given by Eq. (2.4.3.3), and we have defined $\mathcal{S}^{(\rm core)} = \mathcal{S}_H^{(\rm core)} + \mathcal{S}_S^{(\rm core)}$ and $\mathcal{S}^{(\rm cloud)} = \mathcal{S}_H^{(\rm cloud)} + \mathcal{S}_S^{(\rm cloud)}$. We have held fixed $M_S = M_X = 1$ TeV, $\alpha = 0.1$, $\epsilon = 0.1$ and $g_{\rm X} = 1$.

in Fig. 2.8. The figure confirms that the sources are characterized by a tight core, which drops off on a scale $\xi \gtrsim$ few corresponding to $\rho \gtrsim \sigma$, surrounded by a wide tail or cloud, which is smaller in magnitude and drops off more slowly. In the decoupling limit, $\sigma \gg \eta$, the cloud can be much wider than the core. This motivates our prescription for calculating the effective couplings, which we employ in this section and the following one. We will consider fluctuations of the light fields ($\phi_H \approx H$ and Z^μ) about their vacuum expectation values in the presence of the background expectation values of the heavy fields ($\phi_S \approx S$ and X^μ), which are determined by the long straight string solution. Then, we can treat the heavy fields which compose the core as providing the source for the light fields which compose the cloud.

To implement the above strategy, we will write

$$S = \left(\sigma\, \mathrm{s}(\xi) - \sin\theta \frac{\phi_H}{\sqrt{2}} + \cos\theta \frac{\phi_S}{\sqrt{2}}\right) e^{i\varphi} \qquad , \qquad X^\mu = \frac{\mathrm{x}(\xi)}{\rho} V^\mu \quad ,$$
$$H = \eta + \cos\theta \frac{\phi_H}{\sqrt{2}} + \sin\theta \frac{\phi_S}{\sqrt{2}} \qquad , \text{ and } \qquad Z^\mu = \frac{\mathrm{z}(\infty)}{\rho} V^\mu \, . \tag{2.4.3.8}$$

By taking the appropriate linear combination of Eqns. (2.4.3.1) and (2.4.3.2), we find the field equation for ϕ_H to be

$$\left(\Box + M_H^2 + \delta M_H^2\right)\phi_H + \delta\mu^2\phi_S = \mathcal{S} + O(\phi_H^2, \phi_H\phi_S) \tag{2.4.3.9}$$

where the mass M_H^2 was given by Eq. (2.3.2.5), the mass shift is defined by

$$\begin{aligned}\delta M_H^2(\xi) \equiv \frac{\cos^2\theta}{\rho_0^2\xi^2}\left(g_{\rm Z}^{\rm H}{\rm z}(\infty) + g_{\rm X}^{\rm H}{\rm x}\right)^2 + \frac{\sin^2\theta}{\rho_0^2\xi^2}\left(1 - g_{\rm Z}^{\rm S}{\rm z}(\infty) - g_{\rm X}^{\rm S}{\rm x}\right)^2 - 2\lambda\eta^2\frac{\sin^2 2\theta}{\cos 2\theta} \\ - 2\kappa\sigma^2\left(1 - 3{\rm s}^2 - 2\sec 2\theta\right)\sin^2\theta - \alpha\sigma\left((1-{\rm s}^2)\sigma\cos\theta + 4\eta\,{\rm s}\,\sin\theta\right)\cos\theta \quad ,\end{aligned} \tag{2.4.3.10}$$

the residual mixing is defined by

$$\begin{aligned}\delta\mu^2(\xi) \equiv \frac{\sin 2\theta}{2\rho_0^2\xi^2}\left[\left(g_{\rm Z}^{\rm H}{\rm z}(\infty) + g_{\rm X}^{\rm H}{\rm x}\right)^2 - \left(1 - g_{\rm Z}^{\rm S}{\rm z}(\infty) - g_{\rm X}^{\rm S}{\rm x}\right)^2\right] \\ + 2\lambda\eta^2\sin 2\theta + \kappa\sigma^2\left(1 - 3{\rm s}^2\right)\sin 2\theta + \frac{\alpha}{2}\sigma\left(4\eta{\rm s}\cos 2\theta - \sigma(1-{\rm s}^2)\sin 2\theta\right) \quad ,\end{aligned} \tag{2.4.3.11}$$

and the source term is defined by

$$\begin{aligned}\mathcal{S}(\xi) \equiv \sqrt{2}\cos\theta\Big[- \frac{\eta}{\rho_0^2}\frac{1}{\xi^2}\left(g_{\rm Z}^{\rm H}{\rm z}(\infty) + g_{\rm X}^{\rm H}{\rm x}\right)^2 + \alpha\eta\sigma^2\left(1-{\rm s}^2\right) + \frac{\eta}{\rho_0^2}\frac{1}{\xi^2}(g_{\rm Z}^{\rm H})^2{\rm z}(\infty)^2(1-s^2)\Big] \\ -\sqrt{2}\sin\theta\Big[\frac{\sigma}{\rho_0^2}{\rm s}'' - \frac{\sigma}{\rho_0^2}\frac{\rm s}{\xi^2}\left(1 - g_{\rm Z}^{\rm S}{\rm z}(\infty) - g_{\rm X}^{\rm S}{\rm x}\right)^2 + 2\kappa\sigma^3\left(1-{\rm s}^2\right){\rm s}\Big] \ .\end{aligned} \tag{2.4.3.12}$$

We have dropped terms in Eq. (2.4.3.9) which are higher order in ϕ_H and ϕ_S, because these represent interactions among the quanta of the scalar fields, and they are not relevant for the particle production calculation. Near the string core, the spectrum is shifted as compared with far from the string. This leads to a residual mixing, $\delta\mu^2(\xi)$, and a position-dependent mass eigenvalue, $M_H^2 + \delta M_H^2(\xi)$. Since these shifts vanish rapidly outside of the string, and we are interested in the dynamics of the long range fields, we can neglect these terms and take $\delta\mu^2 = 0 = \delta M_H^2$.

We would like to reduce the source term, $\mathcal{S}$, down to a single effective coupling parameter $g_{\rm str}^{\rm H}$. This is accomplished by noting that long wavelength modes of the

Higgs field cannot resolve the internal structure of the string, *i.e.*, the core, and for the purposes of studying these modes it is a good approximation to treat the source term as a Dirac delta function:

$$\mathcal{S} \approx g^{\rm H}_{\rm str}\, \eta\sigma^2\, \delta(\sigma x)\delta(\sigma y)\ . \tag{2.4.3.13}$$

The effective, dimensionless coupling constant, $g^{\rm H}_{\rm str} \equiv \eta^{-1}\int dxdy\ \mathcal{S}$, is given by

$$\begin{aligned} g^{\rm H}_{\rm str} &= 2\pi\sqrt{2}\int_0^\infty \xi d\xi \\ &\times \left(-\cos\theta\Big[\frac{1}{\xi^2}\left(g^{\rm H}_{\rm Z}{\rm z}(\infty)+g^{\rm H}_{\rm X}{\rm x}\right)^2 - \alpha(\rho_0\sigma)^2\left(1-{\rm s}^2\right) - \frac{1}{\xi^2}(g^{\rm H}_{\rm Z})^2{\rm z}(\infty)^2(1-{\rm s}^2)\Big]\right. \\ &\left. + \frac{\sigma}{\eta}\sin\theta\Big[-{\rm s}'' + \frac{\rm S}{\xi^2}\big(1-g^{\rm S}_{\rm Z}{\rm z}(\infty)-g^{\rm S}_{\rm X}{\rm x}\big)^2 - 2\kappa(\rho_0\sigma)^2\left(1-{\rm s}^2\right){\rm s}\Big]\right)\ . \end{aligned} \tag{2.4.3.14}$$

This expression simplifies in the decoupling limit where we can write

$${\rm s}(\xi) \approx \begin{cases} \frac{\xi}{\xi_{\rm max}} & \xi \le \xi_{\rm max} \\ 1 & \xi > \xi_{\rm max} \end{cases} \qquad \text{and} \qquad {\rm x}(\xi) \approx \begin{cases} {\rm x}(\infty)\left(\frac{\xi}{\xi_{\rm max}}\right)^2 & \xi \le \xi_{\rm max} \\ {\rm x}(\infty) & \xi > \xi_{\rm max} \end{cases}\ . \tag{2.4.3.15}$$

Using Eq. (2.4.1.1), the parameter $\xi_{\rm max}$ is related to the profile widths as $\xi_{\rm max} \approx (\Delta\rho_s)\sigma$. This can be determined by solving for the full profile functions, but we will take $\xi_{\rm max} = O(1)$ for numerical estimates. Then after expanding in the ratio $(\eta^2/\sigma^2) \ll 1$ we find

$$(g^{\rm H}_{\rm str})^{\rm (dec.)} \simeq \left(\frac{e^2\pi}{\sqrt{2}\,c_w^2 g_{\rm X}^2}\right)s_\epsilon^2 + \frac{\pi}{15\sqrt{2}}\left(\frac{64}{\kappa} - 17\xi^2_{\rm max}\right)\alpha + O\left(\frac{\eta^2}{\sigma^2}\right)\ . \tag{2.4.3.16}$$

Although alternative definitions of the coupling can be proposed, they will differ from our definition in terms that are suppressed by factors of $O(\eta/\sigma)$ and can be ignored in the decoupling limit.

Once the string solution is obtained, it is straightforward to perform the integral in Eq. (2.4.3.14) and evaluate $g^{\rm H}_{\rm str}$. Figures 2.9a and 2.9b show the dependence of $g^{\rm H}_{\rm str}$

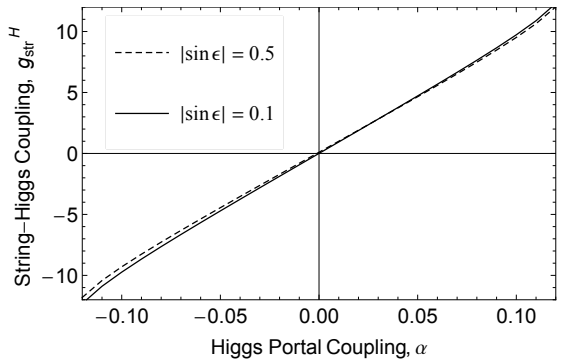

(a) $m_X = M_S = \sigma/\sqrt{2} = 200$ GeV, $g_{\rm X} = 1$

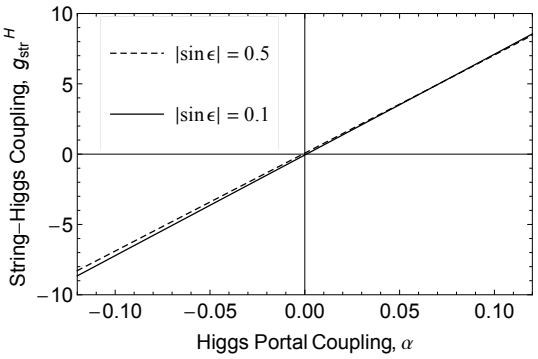

(b) $m_X = M_S = 1$ TeV, $g_{\rm X} = 1$.

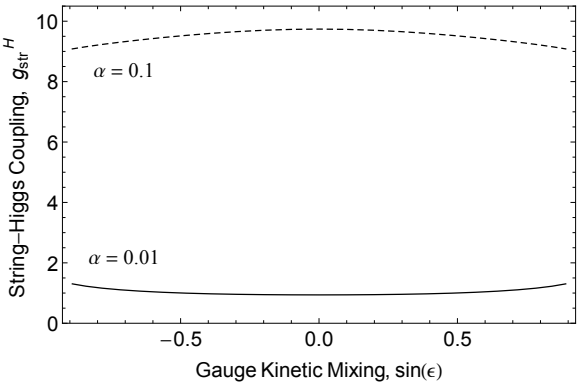

(c) $m_X = M_S = \sigma/\sqrt{2} = 200$ GeV, $g_{\rm X} = 1$

Figure 2.9: Effective coupling of the $(0, 1)$ string with the Higgs field, given by Eq. (2.4.3.14).

on the Higgs portal coupling, and they suggest the approximate relationship $g^{\rm H}_{\rm str} \propto \alpha$. This behavior is understood by noting that $g^{\rm H}_{\rm str}$ depends explicitly on α through one term in Eq. (2.4.3.14) and implicitly through the profile functions. The explicit dependence dominates at small α and gives $g^{\rm H}_{\rm str} \sim \alpha \int \xi d\xi (1 - {\rm s}^2)$, and at larger α the subdominant dependence in s and h emerges. Figure 2.9c shows that $g^{\rm H}_{\rm str}$ has a weak dependence on the gauge kinetic mixing parameter $g^{\rm H}_{\rm str} \sim$ const. $- O(s^2_\epsilon)$. This follows from the relations $g^{\rm H}_{\rm X} \sim g^{\rm S}_{\rm Z} \sim {\rm z}_\infty \sim O(s_\epsilon)$ and $g^{\rm H}_{\rm Z} \sim g^{\rm S}_{\rm X} \sim {\rm x}_\infty \sim O(1)$ and $\sin\theta \sim O(\alpha)$ [see Eq. (2.3.2.4)]. Finally, Fig. 2.10 shows the dependence of $g^{\rm H}_{\rm str}$ on the scale σ. In the decoupling limit, $\sigma \gg \eta$, we see that $g^{\rm H}_{\rm str}$ becomes asymptotically independent of σ, which confirms that dimensionally $\mathcal{S} \sim \eta\sigma^2$, as given by Eq. (2.4.3.13). The

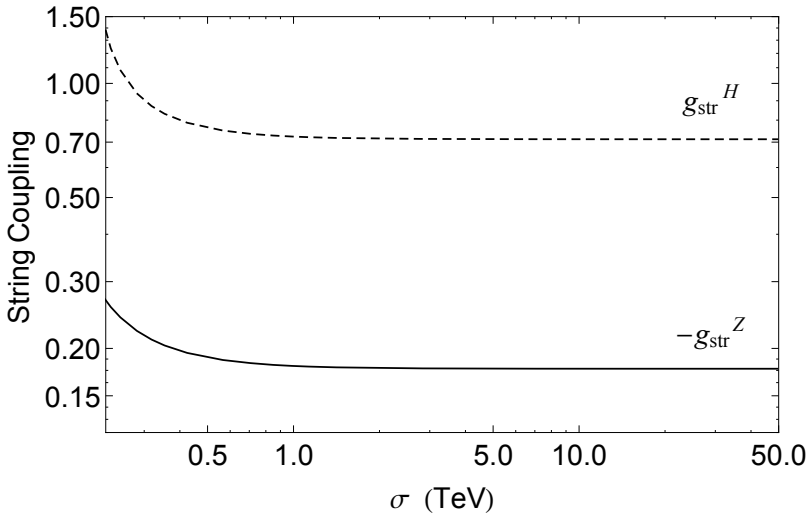

Figure 2.10: Effective couplings of $(0,1)$ string to Z and H fields as the scale σ becomes large. We have held fixed $M_S = M_X = \sigma/\sqrt{2}$, $\alpha = 0.01$, $s_\epsilon = 0.1$, and $g_{\rm X} = 1$. For comparison, the decoupling limit approximations, given by Eqs. (2.4.3.16) and (2.4.4.14), give $(g^{\rm H}_{\rm str})^{\rm (dec.)} \approx 0.70$ and $(g^{\rm Z}_{\rm str})^{\rm (dec.)} \approx -0.17$ for $\xi_{\rm max} = 1.5$ and 2.7, respectively.

appearance of the Higgs VEV, η, is an important result. It reflects the fact that the linear coupling of the Higgs to the string only emerges after electroweak symmetry breaking. Prior to electroweak symmetry breaking, the coupling of the Higgs bosons to the string is higher order in powers of the Higgs field, *i.e.*, the string can only radiate Higgs/anti-Higgs pairs. This result is not totally obvious since it is possible for the string to carry a Higgs condensate, and thereby break the electroweak symmetry locally, even if the Higgs VEV vanishes outside the string, as in the case of bosonic superconductivity [52].

Thus far we have considered the coupling between the Higgs and the straight static string. Now we generalize to the case of an arbitrary Nambu-Goto string with spacetime coordinate $\mathbb{X}^\mu(\tau,\zeta)$ where τ and ζ are the world coordinates. The source term in Eq. (2.4.3.9) derives from the Lagrangian $\mathcal{L} = \phi_H \mathcal{S}$. Upon approximating

the source as a delta function, as in Eq. (2.4.3.13), the action becomes

$$\begin{aligned} S^H_{\rm str} &= \int d^4x\, \phi_H\, \mathcal{S} \\ &= g^{\rm H}_{\rm str}\, \eta \int d^4x\ \phi_H(x) \int d\tau d\zeta \sqrt{-\gamma}\ \delta^{(4)}(x - \mathbb{X}^\mu(\tau,\zeta)) \\ &= g^{\rm H}_{\rm str}\, \eta \int d\tau d\zeta \sqrt{-\gamma}\ \phi_H(\mathbb{X}^\mu) \end{aligned} \tag{2.4.3.17}$$

where the worldsheet metric is defined by $\gamma_{ab} = g_{\mu\nu}\partial_a \mathbb{X}^\mu \partial_b \mathbb{X}^\nu$ $(a, b = 0, 1)$ and $\gamma = \det(\gamma_{ab}) = (1/2)\epsilon^{ac}\epsilon^{bd}\gamma_{ab}\gamma_{cd}$.

2.4.4 Coupling of the Z Boson to the String

As in the case of the Higgs field, the string provides a source for the Z field. Recall that the Z boson field equation, Eq. (2.3.1.18), was given by

$$\begin{aligned} \partial_\nu Z^{\nu\mu} =& g^{\rm H}_{\rm Z} \left[i\left(H\partial^\mu H^* - H^*\partial^\mu H\right) - 2\left(g^{\rm H}_{\rm Z} Z^\mu + g^{\rm H}_{\rm X} X^\mu\right)|H|^2 \right] \\ &+ g^{\rm S}_{\rm Z} \left[i\left(S\partial^\mu S^* - S^*\partial^\mu S\right) - 2\left(g^{\rm S}_{\rm Z} Z^\mu + g^{\rm S}_{\rm X} X^\mu\right)|S|^2 \right] \end{aligned} \tag{2.4.4.1}$$

where we have explicitly written out the currents using Eq. (2.3.1.19). As we discussed in Sec. 2.4, the decoupling approximation, $\sigma \gg \eta$, allows us to replace the heavy fields with the string background and to expand the light fields about their vacuum expectation values:

$$\begin{aligned} & S \to \left(\sigma\, {\rm s}(\xi) + \bar{S}\right) e^{i\varphi} \quad , \quad X^\mu \to \frac{{\rm x}(\xi)}{\rho} V^\mu \quad , \\ & H = \eta + \bar{H} \quad , \text{ and } \quad Z^\mu = \frac{{\rm z}(\infty)}{\rho} V^\mu + \bar{Z}^\mu \quad , \end{aligned} \tag{2.4.4.2}$$

where ${\rm z}(\infty)$ is given by Eq. (2.3.3.7) with $(n, m) = (0, 1)$. Since we are now interested in radiation of the Z field, and we are not concerned with its coupling to the scalar fields, we can take $\bar{S} = \bar{H} = 0$. Inserting Eq. (2.4.4.2) into Eq. (2.4.4.1) yields the field equation for the fluctuation $\bar{Z}^\mu$,

$$\partial_\nu \bar{Z}^{\nu\mu} + M_Z^2 \bar{Z}^\mu + \delta M_Z^2 \bar{Z}^\mu = \mathcal{J}^\mu \quad , \tag{2.4.4.3}$$

where $\bar{Z}^{\mu\nu} \equiv \partial^\mu \bar{Z}^\nu - \partial^\nu \bar{Z}^\mu$, the mass M_Z is given by Eq. (2.3.1.17), the position-dependent mass shift is defined as

$$\delta M_Z^2(\xi) \equiv -2(g_{\rm z}^{\rm S})^2 \sigma^2 \left(1 - {\rm s}^2\right) \quad , \tag{2.4.4.4}$$

and the source current is given by

$$\mathcal{J}^\mu = \frac{\eta^2}{\rho_0}\, j(\xi) V^\mu(\varphi) \tag{2.4.4.5}$$

where

$$j(\xi) \equiv 2 g_{\rm Z}^{\rm H} \frac{1}{\xi}\Big(-g_{\rm Z}^{\rm H}{\rm z}(\infty) - g_{\rm X}^{\rm H}{\rm x}\Big) + 2 g_{\rm Z}^{\rm S} \frac{\sigma^2}{\eta^2}\frac{{\rm s}^2}{\xi}\Big(1 - g_{\rm Z}^{\rm S}{\rm z}(\infty) - g_{\rm X}^{\rm S}{\rm x}\Big) \tag{2.4.4.6}$$

for the $(0,1)$ string. Despite the factor of (σ^2/η^2) in the second term above, both terms in $j(\xi)$ scale like $(\sigma/\eta)^0$ because $g_{\rm z}^{\rm S} \sim \eta^2/\sigma^2$.

Using the complete set of orthonormal basis vectors

$$T_\mu = \partial_\mu t \quad , \quad R_\mu = \partial_\mu \rho \quad , \quad V_\mu = \rho\, \partial_\mu \varphi \quad , \text{ and } \quad L_\mu = \partial_\mu z \tag{2.4.4.7}$$

the current can also be written as

$$\mathcal{J}^\mu = \eta^2\, \epsilon^{\mu\alpha\beta\gamma} \partial_\alpha \Big(k(\xi) T_\beta L_\gamma\Big) \tag{2.4.4.8}$$

where

$$k(\xi) \equiv \int_\infty^\xi d\xi'\, j(\xi') \ . \tag{2.4.4.9}$$

Note that $j(\xi)$ is approximately equal to the right hand side of the string equation, Eq. (2.3.3.4a), and if we were to replace ${\rm h} \to 1$ and ${\rm z} \to {\rm z}(\infty)$, then they would be identical. As such, $k(\xi)$ is approximately given by

$$k(\xi) \approx -\frac{1}{(\rho_0 \eta)^2}\left(\frac{{\rm z}'}{\xi} - \lim_{\xi\to\infty}\frac{{\rm z}'}{\xi}\right) = -\frac{1}{\eta^2} B_Z(\xi) \tag{2.4.4.10}$$

where $B_Z(\xi) \equiv \mathrm{z}'/(\rho_0^2 \xi)$ is the magnitude of the Z-magnetic field,

$$(B_Z)^i = (-1/2)\epsilon^{ijk} Z_{jk} = \epsilon^{ijk} \partial_j A^k. \tag{2.4.4.11}$$

The profile functions s and x both reach their asymptotic values exponentially fast on a scale $\xi = O(1)$ corresponding to $\rho = O(\rho_0 = \sigma^{-1})$. In the decoupling limit, $M_Z \ll \sigma$, long wavelength modes of the Z field cannot resolve the string core, and we can use delta function approximations. The mass shift, given by Eq. (2.4.4.4), becomes negligible outside of the narrow string core. Therefore it is not relevant for the particle radiation calculation, and we will neglect it by taking $\delta M_Z^2 = 0$. The profile function $k(\xi)$ can also be approximated as a delta function

$$k(\xi) \approx g_{\mathrm{str}}^{\mathrm{Z}}\, \sigma^{-2}\, \delta(x)\delta(y) \tag{2.4.4.12}$$

where the effective coupling, $g_{\mathrm{str}}^{\mathrm{Z}} \equiv 2\pi \int_0^\infty \xi d\xi\ k(\xi)$, is given by

$$g_{\mathrm{str}}^{\mathrm{Z}} = 2\pi \int_0^\infty \xi d\xi \int_\infty^\xi d\xi' \left[2 g_{\mathrm{Z}}^{\mathrm{H}} \frac{1}{\xi'} \Big(-g_{\mathrm{Z}}^{\mathrm{H}} \mathrm{z}(\infty) - g_{\mathrm{X}}^{\mathrm{H}} \mathrm{x} \Big) + 2 g_{\mathrm{Z}}^{\mathrm{S}} \frac{\sigma^2}{\eta^2} \frac{\mathrm{s}^2}{\xi'} \Big(1 - g_{\mathrm{Z}}^{\mathrm{S}} \mathrm{z}(\infty) - g_{\mathrm{X}}^{\mathrm{S}} \mathrm{x} \Big) \right] \tag{2.4.4.13}$$

after inserting Eq. (2.4.4.6) into Eq. (2.4.4.9). Note that the approximation given in Eq. (2.4.4.10) would give the effective coupling to be $g_{\mathrm{str}}^{\mathrm{Z}} \approx \Phi_Z/(\rho_0 \eta)^2$ where $\Phi_Z \equiv \int dx dy\, B_Z$ is the Z-magnetic flux. In the decoupling limit [see Eq. (2.4.3.15)] we find

$$(g_{\mathrm{str}}^{\mathrm{Z}})^{(\mathrm{dec.})} \simeq -\left(\frac{11 e^2 \pi}{36 c_w^2 s_w g_{\mathrm{X}}} \xi_{\mathrm{max}}^2 \right) s_\epsilon + O\left(\frac{\eta^2}{\sigma^2} \right) \tag{2.4.4.14}$$

where $\xi_{\mathrm{max}} = O(1)$.

From Fig. 2.10 we see that $g_{\mathrm{str}}^{\mathrm{Z}}$ asymptotes to a constant in the decoupling limit that is given approximately by Eq. (2.4.4.14). Figures 2.11a and 2.11b show that $g_{\mathrm{str}}^{\mathrm{Z}}$ depends weakly on the Higgs portal coupling, with the approximate relationship $g_{\mathrm{str}}^{\mathrm{Z}} \propto -\alpha^2$. Since α does not appear explicitly in Eq. (2.4.4.13), the dependence is

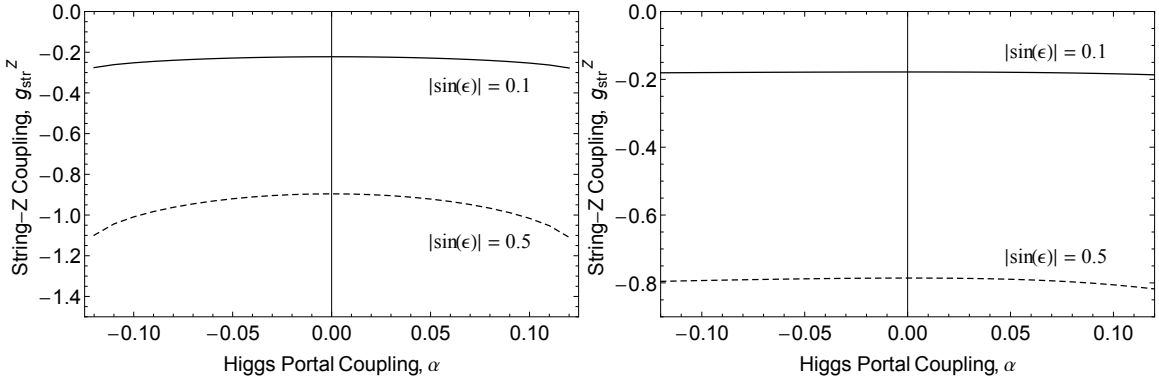

(a) $m_X = M_S = \sigma/\sqrt{2} = 200$ GeV, $g_{\rm X} = 1$

(b) $m_X = M_S = 1$ TeV, $g_{\rm X} = 1$.

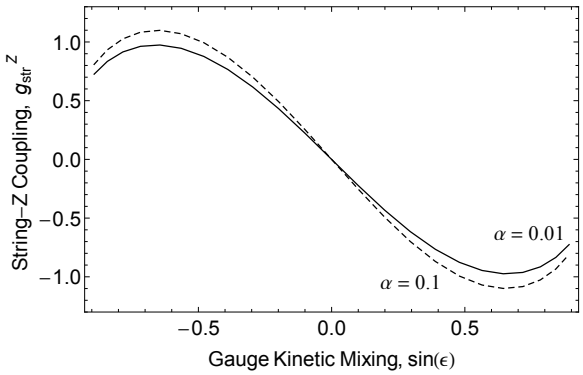

(c) $m_X = M_S = \sigma/\sqrt{2} = 200$ GeV, $g_{\rm X} = 1$

Figure 2.11: Effective coupling of the $(0, 1)$ string with the Z boson, given by Eq. (2.4.4.13).

only through the profile functions. Figure 2.11c shows that $g^{\rm Z}_{\rm str}$ depends linearly on the gauge kinetic mixing parameter $g^{\rm Z}_{\rm str} \sim O(s_\epsilon)$ for small values of s_ϵ, which can be understood from the dependence on $g^{\rm S}_{\rm Z}$ in Eq. (2.4.4.13) and by noting that $g^{\rm S}_{\rm Z}$ is linear in s_ϵ. As $|s_\epsilon|$ increases, the terms that are higher order in s_ϵ begin to have an effect.

Thus far we have been assuming that the string is long and straight. To generalize to an arbitrary Nambu-Goto string, we can write the source term, Eq. (2.4.4.8), as

$$\mathcal{J}^\mu = g^{\rm Z}_{\rm str}(\eta/\sigma)^2 \partial_\nu \int d\sigma^{\mu\nu}\ \delta^{(4)}(x - \mathbb{X}(\tau, \zeta)) \tag{2.4.4.15}$$

where $d\sigma^{\mu\nu} = d\tau d\zeta \epsilon^{\mu\nu\alpha\beta}\epsilon^{ab}\partial_a \mathbb{X}_\alpha \partial_b \mathbb{X}_\beta$ is the areal element of the string worldsheet. A

source of this form was first given in Ref. [53]. This source can be derived from a term in the effective action

$$\begin{aligned} S^{Z}_{\rm str} &= \int d^4x\, Z_\mu \mathcal{J}^\mu \\ &= \frac{g^{\rm Z}_{\rm str}}{2}\left(\frac{\eta}{\sigma}\right)^2 \int d^4x\ Z_{\mu\nu} \int d\sigma^{\mu\nu}\delta^{(4)}(x-\mathbb{X}(\tau,\zeta)) \\ &= \frac{g^{\rm Z}_{\rm str}}{2}\left(\frac{\eta}{\sigma}\right)^2 \int d\sigma^{\mu\nu} Z_{\mu\nu}(\mathbb{X}^\mu) \end{aligned} \tag{2.4.4.16}$$

where total derivative terms have been dropped. We have factored off the $(\eta/\sigma)^2$ scaling such that $g^{\rm Z}_{\rm str}$ is constant in the limit $\eta \ll \sigma$.

2.4.5 Coupling to the Fermions

Finally, let us turn to the coupling between the dark string and the SM fermions. Like the coupling to the bosons, this interaction can give particle radiation from the string [54]. Additionally, as the string passes through the plasma, this interaction induces a drag force that has an important influence on the evolution of the string network as a whole [55].

The interaction that we seek to calculate arises from the kinetic terms for the SM fermions,

$$\mathcal{L} = Q^\dagger i\bar\sigma^\mu D_\mu Q + u_R^\dagger i\sigma^\mu D_\mu u_R + d_R^\dagger i\sigma^\mu D_\mu d_R + L^\dagger i\bar\sigma^\mu D_\mu L + e_R^\dagger i\sigma^\mu D_\mu e_R \tag{2.4.5.1}$$

where we use the two component spinor notation and the doublets are $Q = (u_L\,,\, d_L)$ and $L = (\nu_L\,,\, e_L)$. The covariant derivatives are given by

$$\begin{aligned} D_\mu Q &= \left(\partial_\mu - i\tfrac{g}{2}\sigma^a W^a_\mu - i\tfrac{g'}{2} y_{\rm Q} Y_\mu\right) Q \\ D_\mu u_R &= \left(\partial_\mu - i\tfrac{g'}{2} y_{u_R} Y_\mu\right) u_R \\ D_\mu d_R &= \left(\partial_\mu - i\tfrac{g'}{2} y_{d_R} Y_\mu\right) d_R \\ D_\mu L &= \left(\partial_\mu - i\tfrac{g}{2}\sigma^a W^a_\mu - i\tfrac{g'}{2} y_{\rm L} Y_\mu\right) L \\ D_\mu e_R &= \left(\partial_\mu - i\tfrac{g'}{2} y_{e_R} Y_\mu\right) e_R \end{aligned} \tag{2.4.5.2}$$

where we have turned off the SU(3) gauge coupling, since it does not modify the coupling to the dark string, and the hypercharge assignments are

$$y_{\mathrm{Q}} = \frac{1}{3} \quad , \quad y_{u_R} = \frac{4}{3} \quad , \quad y_{d_R} = -\frac{2}{3} \quad , \quad y_{\mathrm{L}} = -1 \quad , \text{ and } \quad y_{e_R} = -2 \ . \tag{2.4.5.3}$$

After performing the field redefinition given by Eq. (2.3.1.9), the covariant derivatives become

$$D_\mu Q = \begin{pmatrix} D_\mu u_L - i\frac{g}{\sqrt{2}} W_\mu^+ d_L \\ D_\mu d_L - i\frac{g}{\sqrt{2}} W_\mu^- u_L \end{pmatrix} \tag{2.4.5.4}$$

with

$$\begin{aligned} D_\mu u_L &= \big(\partial_\mu - i(g_{\mathrm{A}}^{u_L} A_\mu + g_{\mathrm{Z}}^{u_L} Z_\mu + g_{\mathrm{X}}^{u_L} X_\mu)\big) u_L \\ D_\mu d_L &= \big(\partial_\mu - i(g_{\mathrm{A}}^{d_L} A_\mu + g_{\mathrm{Z}}^{d_L} Z_\mu + g_{\mathrm{X}}^{d_L} X_\mu)\big) d_L \\ D_\mu u_R &= \big(\partial_\mu - i(g_{\mathrm{A}}^{u_R} A_\mu + g_{\mathrm{Z}}^{u_R} Z_\mu + g_{\mathrm{X}}^{u_R} X_\mu)\big) u_L \\ D_\mu d_R &= \big(\partial_\mu - i(g_{\mathrm{A}}^{d_R} A_\mu + g_{\mathrm{Z}}^{d_R} Z_\mu + g_{\mathrm{X}}^{d_R} X_\mu)\big) u_L \end{aligned} \tag{2.4.5.5}$$

and

$$D_\mu L = \begin{pmatrix} D_\mu \nu_L - i\frac{g}{\sqrt{2}} W_\mu^+ e_L \\ D_\mu e_L - i\frac{g}{\sqrt{2}} W_\mu^- \nu_L \end{pmatrix} \tag{2.4.5.6}$$

with

$$\begin{aligned} D_\mu \nu_L &= \big(\partial_\mu - i(g_{\mathrm{A}}^{\nu_L} A_\mu + g_{\mathrm{Z}}^{\nu_L} Z_\mu + g_{\mathrm{X}}^{\nu_L} X_\mu)\big) \nu_L \\ D_\mu e_L &= \big(\partial_\mu - i(g_{\mathrm{A}}^{e_L} A_\mu + g_{\mathrm{Z}}^{e_L} Z_\mu + g_{\mathrm{X}}^{e_L} X_\mu)\big) e_L \\ D_\mu e_R &= \big(\partial_\mu - i(g_{\mathrm{A}}^{e_R} A_\mu + g_{\mathrm{Z}}^{e_R} Z_\mu + g_{\mathrm{X}}^{e_R} X_\mu)\big) e_R \end{aligned} \tag{2.4.5.7}$$

where

$$
\begin{array}{lll}
g_{\rm A}^{u_L} = \frac{2e}{3} & g_{\rm Z}^{u_L} = c_\zeta \frac{e}{6}\left(\frac{3}{t_w} - t_w\right) - s_\zeta \frac{e}{6}\frac{t_\epsilon}{\cos\theta_w} & g_{\rm X}^{u_L} = -c_\zeta \frac{e}{6}\frac{t_\epsilon}{\cos\theta_w} - s_\zeta \frac{e}{6}\left(\frac{3}{t_w} - t_w\right) \\
g_{\rm A}^{u_R} = \frac{2e}{3} & g_{\rm Z}^{u_R} = -c_\zeta \frac{2e}{3} t_w - s_\zeta \frac{2e}{3}\frac{t_\epsilon}{\cos\theta_w} & g_{\rm X}^{u_R} = -c_\zeta \frac{2e}{3}\frac{t_\epsilon}{\cos\theta_w} + s_\zeta \frac{2e}{3} t_w \\
g_{\rm A}^{d_L} = -\frac{e}{3} & g_{\rm Z}^{d_L} = -c_\zeta \frac{e}{6}(\frac{3}{t_w} + t_w) - s_\zeta \frac{e}{6}\frac{t_\epsilon}{\cos\theta_w} & g_{\rm X}^{d_L} = -c_\zeta \frac{e}{6}\frac{t_\epsilon}{\cos\theta_w} + s_\zeta \frac{e}{6}(\frac{3}{t_w} + t_w) \\
g_{\rm A}^{d_R} = -\frac{e}{3} & g_{\rm Z}^{d_R} = c_\zeta \frac{e}{3} t_w + s_\zeta \frac{e}{3}\frac{t_\epsilon}{\cos\theta_w} & g_{\rm X}^{d_R} = c_\zeta \frac{e}{3}\frac{t_\epsilon}{\cos\theta_w} - s_\zeta \frac{e}{3} t_w \\
g_{\rm A}^{e_L} = -e & g_{\rm Z}^{e_L} = -c_\zeta \frac{e}{2}\left(\frac{1}{t_w} - t_w\right) + s_\zeta \frac{e}{2}\frac{t_\epsilon}{\cos\theta_w} & g_{\rm X}^{e_L} = c_\zeta \frac{e}{2}\frac{t_\epsilon}{\cos\theta_w} + s_\zeta \frac{e}{2}\left(\frac{1}{t_w} - t_w\right) \\
g_{\rm A}^{e_R} = -e & g_{\rm Z}^{e_R} = c_\zeta\, e\, t_w + s_\zeta e \frac{t_\epsilon}{\cos\theta_w} & g_{\rm X}^{e_R} = c_\zeta e \frac{t_\epsilon}{\cos\theta_w} - s_\zeta\, e t_w \\
g_{\rm A}^{\nu_L} = 0 & g_{\rm Z}^{\nu_L} = c_\zeta \frac{e}{2}\left(\frac{1}{t_w} + t_w\right) + s_\zeta \frac{e}{2}\frac{t_\epsilon}{\cos\theta_w} & g_{\rm X}^{\nu_L} = c_\zeta \frac{e}{2}\frac{t_\epsilon}{\cos\theta_w} - s_\zeta \frac{e}{2}\left(\frac{1}{t_w} + t_w\right)
\end{array}
\tag{2.4.5.8}
$$

We have included the couplings to the photon field A_μ for completeness, but since the dark string does not contain any electromagnetic flux, these interactions are not relevant for couplings of the string to the SM fermions.

The dominant interaction between fermions and the dark string is the Aharonov-Bohm (AB) interaction [56, 53]. In general when a particle of charge e and momentum $\mathbf{p}$ (in the rest frame of the string) is incident on a string carrying magnetic flux Φ, it will scatter with a differential cross section per unit length $d\sigma/d\theta$. It is useful to define the transport cross section, $\sigma_t \equiv \int_0^{2\pi} d\theta\, (d\sigma/d\theta)(1-\cos\theta)$, which is given by

$$\sigma_t = \frac{2}{|\mathbf{p}|}\sin^2\pi\theta \tag{2.4.5.9}$$

where $\theta \equiv (e/2\pi)\Phi$. In general these need not be electromagnetic charge and flux, and in fact the dark string carries no electromagnetic flux. Instead, the particles scatter off of the Z-flux and X-flux carried by the string.

The fluxes are defined by

$$\Phi_Z \equiv \int \mathbf{B}_Z \cdot d\mathbf{A} \qquad \text{and} \qquad \Phi_X \equiv \int \mathbf{B}_X \cdot d\mathbf{A} \tag{2.4.5.10}$$

where the integral extends over the plane normal to the string and the magnetic fields are given by $\vec{B}_Z = \vec{\nabla} \times \vec{Z}$ where $\vec{Z}_i = Z^i$ and similarly for X_μ. Using Stokes theorem

along with the boundary conditions Eq. (2.3.3.7), the fluxes are easily found to be

$$\Phi_Z = 2\pi \frac{g_{\rm X}^{\rm S} n - g_{\rm X}^{\rm H} m}{g_{\rm X}^{\rm S} g_{\rm Z}^{\rm H} - g_{\rm X}^{\rm H} g_{\rm Z}^{\rm S}} \tag{2.4.5.11}$$

$$\Phi_X = 2\pi \frac{g_{\rm Z}^{\rm H} m - g_{\rm Z}^{\rm S} n}{g_{\rm X}^{\rm S} g_{\rm Z}^{\rm H} - g_{\rm X}^{\rm H} g_{\rm Z}^{\rm S}} \tag{2.4.5.12}$$

Note that Φ_Z is nonzero even for the $(0,1)$ string for which the Higgs field does not wind, but instead $\Phi_Z \propto s_\epsilon$ due to the gauge kinetic mixing.

As a particle moves around the string, its phase changes due to both fluxes. Therefore to calculate the transport cross section for a particle of species i we sum the phases:

$$\sigma_t\Big|_i = \frac{2}{|\mathbf{p}|} \sin^2 \pi\theta_i \tag{2.4.5.13}$$

where

$$\theta_i \equiv \frac{g_{\rm Z}^i \Phi_Z}{2\pi} + \frac{g_{\rm X}^i \Phi_X}{2\pi} \tag{2.4.5.14}$$

and the $g_{\rm Z}^i$ and $g_{\rm X}^i$ are given by Eq. (2.4.5.8). Upon performing the sum in Eq. (2.4.5.14) a remarkable simplification occurs, and we are left with

$$\theta_i = (y_i - 2c_w^2 g_{\rm A}^i) n + \left(-2 \frac{c_w e s_\epsilon}{g_{\rm X}} g_{\rm A}^i \right) m \tag{2.4.5.15}$$

where y_i and $g_{\rm A}^i$ are the hypercharge and electromagnetic charges of species i given by Eqns. (2.4.5.3) and (2.4.5.8). Specifically, for the case $(n,m) = (0,1)$ we find

$$\theta_i = q_i \Theta \qquad \text{with} \qquad \Theta \equiv -2 \frac{c_w s_\epsilon}{g_{\rm X}} \tag{2.4.5.16}$$

and $q_i = e\, g_{\rm A}^i$ is the electromagnetic charge. Note that we have *not expanded* in $s_\epsilon \ll 1$; these expressions are exact. It is remarkable that the phases θ_i are independent of the ratio of mass scales $R = m_X/m_Z$, even though $g_{\rm Z}^i \Phi_Z$ and $g_{\rm X}^i \Phi_X$ separately depend upon R. This has the important and interesting implication that the scattering of particles from the string is unchanged in the decoupling limit $R \gg 1$.

As an example, let us consider the scattering of a few elementary particles from the $(0,1)$ dark string. Upon setting $n=0$ and $m=1$ in Eq. (2.4.5.16) we see that the left- and right-chiral components have identical AB phases, *e.g.*, $\theta_{u_L}=\theta_{u_R}\equiv\theta_u$. We calculate the transport cross section for the electron, proton, neutron, hydrogen atom, and neutrino as

$$\sigma_t\Big|_e = \frac{2}{|\mathbf{p}|}\sin^2\pi\theta_e \approx \frac{1}{|\mathbf{p}|}\frac{8\pi^2 c_w^2 e^2}{g_{\rm X}^2}s_\epsilon^2 + O(s_\epsilon^4) \tag{2.4.5.17}$$

$$\sigma_t\Big|_p = \frac{2}{|\mathbf{p}|}\sin^2\pi(2\theta_u+\theta_d) \approx \frac{1}{|\mathbf{p}|}\frac{8\pi^2 c_w^2 e^2}{g_{\rm X}^2}s_\epsilon^2 + O(s_\epsilon^4) \tag{2.4.5.18}$$

$$\sigma_t\Big|_n = \frac{2}{|\mathbf{p}|}\sin^2\pi(\theta_u+2\theta_d) = 0 \tag{2.4.5.19}$$

$$\sigma_t\Big|_H = \frac{2}{|\mathbf{p}|}\sin^2\pi(2\theta_u+\theta_d+\theta_e) = 0 \tag{2.4.5.20}$$

$$\sigma_t\Big|_\nu = \frac{2}{|\mathbf{p}|}\sin^2\pi\theta_{\nu_L} = 0 \quad , \tag{2.4.5.21}$$

respectively. In the second equalities of Eqns. (2.4.5.17) and (2.4.5.18) we have expanded for $s_\epsilon \ll 1$. In performing this expansion, both terms in Eq. (2.4.5.14) are of the same order because $\Phi_Z \sim g_{\rm X}^{e_L} \sim g_{\rm X}^{e_R} = O(s_\epsilon^1)$ and $\Phi_X \sim g_{\rm Z}^{e_L} \sim g_{\rm Z}^{e_R} = O(s_\epsilon^0)$. After recombination, when the SM particle content of the universe consists mainly of neutral hydrogen and neutrinos, the AB interactions vanish. Then, scattering arises from the typically subdominant hard-core interaction between the fermions and the Higgs and Z boson condensates on the string. If additionally $\alpha \to 0$, then even this interaction vanishes and the string does not feel the SM fermions at all.

If the original model had contained fermion fields charged under the $\mathrm{U}(1)_X$, for example a dark matter candidate, then the interactions of these particles with the string would not vanish even as $s_\epsilon, \alpha \to 0$. For example, let Ψ be a Dirac spinor field with gauge interactions specified by the covariant derivative

$$D_\mu\Psi = \big(\partial_\mu - i g_{\rm X}\frac{q_{\rm X}}{2}\hat{X}_\mu\big)\Psi = \big(\partial_\mu - i(g_{\rm A}^\Psi A_\mu + g_{\rm Z}^\Psi Z_\mu + g_{\rm X}^\Psi X_\mu)\big)\Psi \tag{2.4.5.22}$$

where

$$g_{\rm A}^{\Psi} = 0 \qquad , \qquad g_{\rm Z}^{\Psi} = \frac{g_{\rm X} q_{\rm X}}{2 c_\epsilon} s_\zeta \qquad , \quad \text{and} \qquad g_{\rm X}^{\Psi} = \frac{g_{\rm X} q_{\rm X}}{2 c_\epsilon} c_\zeta \ . \tag{2.4.5.23}$$

Its AB phase is simply $\theta_\Psi = m q_{\rm X}$ and the AB interaction is found to be

$$\sigma_t \Big|_\Psi = \frac{2}{|\mathbf{p}|} \sin^2 \pi q_{\rm X} \ . \tag{2.4.5.24}$$

If $q_{\rm X}$ is an integer, then the transport cross-section vanishes and there is no AB interaction between the dark string and Ψ.

2.5 Conclusion

We have studied the properties and couplings of the dark string including, for the first time, the full electroweak gauge sector, the gauge kinetic mixing, and Higgs portal interaction.

The dark string solution field profiles are discussed in Sec. 2.4. The ansatz of the dark string can include a non-topological winding of the electroweak Higgs, labeled by an integer n, in addition to the topological winding of the new scalar field, S, given by an integer m. We have evaluated $(n, m) = (0, 1), (1, 1)$ classes of solutions. Since the (0,1) string is lighter, and there is no topology protecting the (1,1) solution, we expect that the (1,1) solution will be unstable to decay into the (0,1) solution. Hence, we mainly focus on the (0,1) string which we have also referred to as the "dark string".

In Sec. 2.4 we have evaluated the tension of the dark string and the results can be summarized in the formula

$$\mu \approx 2\pi \frac{\kappa^{1/4}}{g_{\rm X}^{1/2}} \sigma^2 \left[1 + \frac{\eta^2}{\sigma^2} O(\alpha^2, s_\epsilon^2) \right] \tag{2.5.1}$$

where the approximate dependencies are derived from the plots in Fig. 2.7 for small values of the hidden sector scalar self-coupling, κ, the gauge kinetic mixing parameter,

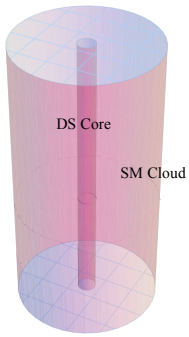

Figure 2.12: Structure of the Dark String.

s_ϵ, the Higgs portal coupling α, and the dark gauge coupling, g_X. In the decoupling limit when the electroweak VEV is much less than the hidden sector VEV, $\eta \ll \sigma$, the expression reduces to that of a Nielsen-Olesen string.

A novel feature of the dark string is that it also carries a condensate of the electroweak Higgs and Z fields. The structure of the string is a core of size $\sim M_X^{-1}$ that contains flux of the dark gauge field X and in which the new scalar S departs from its VEV. This is just as in the case of the Nielsen-Olesen string. Around the Nielsen-Olesen core we also have a "cloud" or "dressing" of Higgs and Z fields that extend out to a radius $\sim M_H^{-1}$ as illustrated in Fig. 2.12.

The presence of the electroweak cloud can be of phenomenological importance because it connects a topological defect in the dark sector to the matter content of the visible sector. In particular, an oscillating loop of dark string may be expected to copiously radiate Higgs bosons [57] and Z gauge bosons (similar to Goldstone boson radiation discussed in [58]). With these effects in mind, we have proposed effective interactions of the dark string with the Higgs excitations, ϕ_H, and Z bosons that take the form

$$S_{\rm int} = g_{\rm str}^{\rm H}\,\eta \int d^2\sigma\sqrt{-\gamma}\;\phi_H(\mathbb{X}^\mu) + \frac{g_{\rm str}^{\rm Z}}{2}\left(\frac{\eta}{\sigma}\right)^2 \int d\sigma^{\mu\nu}\,Z_{\mu\nu}(\mathbb{X}^\mu) \tag{2.5.2}$$

given by Eqs. (2.4.3.17) and (2.4.4.16). The first term carries a factor of η because the

emission of a single Higgs boson can only occur after electroweak symmetry breaking. The factor of $(\eta/\sigma)^2$ in the second term reflects the suppressed interaction of the Z boson with the hidden sector fields in the decoupling limit where the gauge sector mixing is small. The coupling constants in these interactions are shown in Figs. 2.9, 2.10, and 2.11. In the decoupling limit they can be approximated as in Eqs. (2.4.3.16) and (2.4.4.14) by

$$\begin{aligned}(g_{\rm str}^{\rm H})^{\rm (dec.)} &\simeq \left(\frac{e^2\pi}{\sqrt{2}\,c_w^2 g_{\rm X}^2}\right) s_\epsilon^2 + \frac{\pi}{15\sqrt{2}}\left(\frac{64}{\kappa} - 17\xi_{\rm max}^2\right)\alpha \\ (g_{\rm str}^{\rm Z})^{\rm (dec.)} &\simeq -\left(\frac{11e^2\pi}{36c_w^2 s_w g_{\rm X}}\xi_{\rm max}^2\right) s_\epsilon \ . \end{aligned} \tag{2.5.3}$$

up to terms of order η^2/σ^2. The parameter $\xi_{\rm max} = O(1)$ is the rescaled width of the profile functions.

The gauge kinetic mixing term in the model also leads to an Aharonov-Bohm interaction between fermions and the dark string [57]. These interactions are important since, in a cosmological setting, the strings are surrounded by a plasma of fermions that can scatter and affect the evolution of the string network. In addition, the Aharonov-Bohm interaction will allow for dark string loops to radiate standard model fermions [54]. We give the Aharonov-Bohm phases for the fermions in Eq. (2.4.5.16), where we should set $n = 0$ for the (0,1) string. The result is simply that the Aharonov-Bohm phase of a fermion with electric charge q is

$$\theta_q = -\frac{2c_w s_\epsilon}{g_X} q. \tag{2.5.4}$$

Following Ref. [53], we have also calculated the transport cross sections for fermions scattering off dark strings in Sec. 2.4.

Our analysis has not made any assumptions about the nature of the dark matter. Depending on its interaction with the fields that make up the dark string, string loop decays can contribute to the dark matter relic abundance [59, 60].

Having mapped out the properties of the dark string, we plan to explore their cosmological consequences and phenomenological connections in future work. Here we will provide a brief discussion of the nature of that work. The coupling of a dilation (or more general scalar moduli field) to the string takes the same form that we found for the coupling of the Higgs boson to the string, namely Eq. (2.4.3.17). Quanta of this scalar field can be emitted from cusps or kinks on string loops [61, 57]. It has been shown that this radiation leads to astrophysical signals in the form of the diffuse gamma ray flux, cosmic rays, and high energy neutrinos [57, 62]. The non-observation of these signals places constraints on the string model. For the specific case of the dark string discussed here, these constraints may be complimentary to direct laboratory searches for evidence of the hidden sector as discussed in Sec. 2.2.

The coupling of the Z-boson to the string through the interaction in Eq. (2.4.4.16) may allow for a second form of radiation. To our knowledge, the emission of vector bosons has not been studied extensively (see, however, [53]), and this may prove a unique feature of the dark string. The Aharonov-Bohm interaction calculated in Sec. 2.4 will provide a friction force the dark string in the hot, dense conditions of the early universe. This may have a significant impact on the evolution of the network of light strings.

Chapter 3

GRAVITATIONAL WAVES FROM PREHEATING

3.1 Introduction

Inflation leaves the universe cold and nearly empty of particles, so there needs to be a reheating mechanism for energy transfer between inflaton and Standard Model fields in order to create the thermalized particles that existed before Big Bang Nucleosynthesis began. This is typically modeled by a small, direct coupling between inflaton and another field. The first discussions of reheating [63, 64, 65, 66, 67, 68, 69] studied a perturbative calculation of inflaton decay into the coupled field, with energy gradually transferred to matter fields. (Also see the reviews [70, 71].)

However, inflaton decay occurs in the context of large, coherent field oscillations and nonperturbative effects should also be taken into account [72, 68, 69, 73]. Typically, the inflaton ϕ is considered to be coupled to a field χ by an interaction $\frac{1}{2}g^2\phi^2\chi^2$, which is χ's only potential energy term. As the inflaton oscillates about the bottom of its potential after inflation, the phenomenon of parametric resonance leads to some modes of the decay product χ being excited at an exponential rate. This effect, which may occur briefly at the beginning of a longer period of reheating, is called preheating. (Most of the work on this subject has been in the context of direct couplings between inflaton and matter fields; see [74] for a scenario that does not require this.)

Preheating in these models can produce gravitational waves [75, 76, 77, 78, 79, 80], since the exponential amplification of certain modes leads to a large contribution to anisotropic stress, which sources tensor perturbations. Predictions for the resulting spectrum are around $h^2\Omega_{\rm gw} \sim 10^{-10}$ and $f \sim 10^4$ to 10^6 Hz today for massive or $\lambda\phi^4$

inflation or could be as low as 10^2 to 10^3 Hz for hybrid inflation models. Some work [79, 81, 82, 83, 84, 85, 86] has addressed this problem in the context of various models that relate to processes that are more specific. These find a wide range of possibilities. For example, [83] found that decay into fermions after inflation could produce $\Omega_{\rm gw} \sim 10^{-12}$ to 10^{-18}, $f \sim 10^9$ to 10^{10} Hz today, depending on the parameters.

These tend to fall outside the range of current, planned or proposed gravitational wave experiments such as Advanced LIGO and VIRGO, KAGRA, Einstein Telescope, eLISA, DECIGO or BBO (for an exception, see [82]). Roughly speaking, these are most sensitive to frequencies around 10^{-3} to 10^3 Hz and signal strength corresponding to $h^2\Omega_{\rm gw} \sim 10^{-5}$ to possibly 10^{-14}. (See [87, 88] or the review [89]. [1]) LIGO and VIRGO have jointly placed upper bounds on a stochastic gravitational wave background on the order of $\Omega_{\rm gw} \sim 5 \times 10^{-6}$ around 10^2 Hz [90]. Gravitational wave detection at MHz frequencies has also been considered [91, 92, 93]. It has not been a major focus, though, since comparatively reliable astrophysical sources (e.g. neutron star mergers) are not expected in this frequency range.

This motivates the study of how robust are the predictions for the gravitational wave spectrum from preheating. We would expect that a realistic preheating process in the early universe would include couplings of the decay product to other fields, as well as possible self-interactions. It will be useful to know whether these can significantly affect the observability of such a process. [2] Specifically, it would be interesting to answer the question "Given a model of preheating with some self-interaction strength, how does one estimate the overall gravitational wave production?" This is analogous to the discussion in [95], which estimates the maximum energy den-

[1] Note that some results are given in terms of $h^2\Omega_{\rm gw}$, others in terms of $\Omega_{\rm gw}$ and still others in terms of strain h, which is distinct from today's Hubble constant in units of 100 km/s/Mpc that appears in $h^2\Omega_{\rm gw}$. Consistent comparison of experimental sensitivities is discussed in [87].

[2] While this paper was in preparation, another work [94] appeared that addresses some of these questions. We will discuss it in Sec. 3.6.

sity in gravitational waves that could be produced by a cosmological process such as preheating.

Previous work has shown that for self-couplings $\lambda_\chi \sim \mathcal{O}(10^{-2}) \gg g^2$, where g^2 is the coupling between the inflaton and scalar, parametric resonance can be significantly affected [96, 97]. However, there has been little discussion of gravitational wave production in this scenario. [3] Therefore it is difficult to give a thorough answer to the above question based on the existing literature. This also means that it is unclear how general a gravitational wave prediction is when it ignores interactions of the decay products.

In this work, we begin to address this by studying the development and termination of parametric resonance and the production of gravitational waves in the context of $\lambda\phi^4$ chaotic inflation coupled to a self-interacting light scalar field. We verify by lattice simulation that the resonance terminates early for self-coupling $\lambda_\chi \gtrsim g^2$, demonstrating the condition $\rho_\chi^{\rm final} \sim g^2/\lambda_\chi$ mentioned in footnote 19 of [96] (their g is our g^2), and show that this leads to significant suppression of gravitational wave production. The resonance terminates early because the self-interaction term allows more efficient rescattering of particles out of the resonant mode, and this can be characterized by a condition comparing the energy density associated with the self-interaction to the inflaton-scalar interaction energy. The early termination of the resonance means that there is less energy in the light scalar's fluctuations, which directly source gravitational waves. Therefore, gravitational wave production is reduced. For $\lambda_\chi \gtrsim \lambda_\chi^* = g^2$, the energy density goes as $\Omega_{\rm gw}^{(\lambda_\chi)} \sim (g^2/\lambda_\chi)^2\, \Omega_{\rm gw}^{(\lambda_\chi=0)}$.

In Sec. 3.5 we show that this result is robust to changes in initial conditions, and that the same scaling occurs in massive ($m^2\phi^2$) inflation. Although this suggests

[3] A study of gravitational waves in M-flation preheating [98] mentions that a self-interaction can suppress the resonance, but does not quantify this in a way that allows comparison with [96].

generality to inflationary models that are quadratic or quartic about the minimum, we point out that an important goal of future work is to understand the effect of realistic interactions on other models that have predicted gravitational wave spectra.

As an application of this result, one could imagine the universe reheating by a coupling between the Higgs and inflaton, and we argue in Sec. 3.6 that such a scenario would likely produce no observable gravitational radiation. This is due to the size of the Higgs self-coupling, despite its eventual running to zero in the Standard Model. However, we point out that even a resonance too brief to produce observable gravitational waves could be relevant for the issue of vacuum stability. Finally, if the inflaton preheats a scalar field with an extremely small self-coupling, then the gravitational wave spectrum could directly measure this potential.

3.2 Model

Representing the universe by a spatially flat Friedmann-Robertson-Walker metric, we will describe gravitational waves as transverse and traceless perturbations to this metric, specifically as h_{ij} such that

$$ds^2 = a^2(\eta)\left(-d\eta^2 + (\delta_{ij} + h_{ij})dx^i dx^j\right) \tag{3.2.1}$$

with $\partial_i h_{ij} = 0$ and $h_{ii} = 0$. We will take the inflaton to be a real scalar field, $\phi(t, \vec{x})$, and consider it to be coupled to a massless real scalar field $\chi(t, \vec{x})$, with potential given by

$$V = \frac{1}{4}\lambda\phi^4 + \frac{1}{4}\lambda_\chi\chi^4 + \frac{1}{2}g^2\phi^2\chi^2 \tag{3.2.2}$$

Here we have chosen to study $\lambda\phi^4$ chaotic inflation, and this requires some justification since standard slow-roll inflation with this potential is inconsistent with Cosmic Microwave Background (CMB) observations [99]. Much literature on gravitational

waves from preheating takes the potential as $\frac{1}{4}\lambda\phi^4$, in particular the thorough numerical study [78], whose model corresponds to ours with the choice $\lambda_\chi = 0$. We expect the qualitative nature of our results to be relevant to a broad range of inflationary scenarios (this will be discussed further in Sec. 3.6), and it will be useful to refer to specific previous results in order to understand the production of gravitational waves.

We are also studying the behavior of a "light" scalar field, and so we neglect a χ mass term in comparison with the effective χ mass that comes from the interaction term $\frac{1}{2}g^2\phi^2\chi^2$. Comparing these terms using the amplitude of the ϕ oscillations shows that this is roughly equivalent to requiring the χ mass to be $m_\chi \ll \sqrt{g^2/\lambda} \times 10^{12}$ GeV.

Here the inflaton self-coupling is set by the amplitude of the scalar power spectrum of the CMB as $\lambda = 10^{-13}$. The unknown coupling g^2 must be small, but we will also take it to be larger than λ; in terms of the resonance parameter $q \equiv g^2/\lambda$ this means $1 \ll q \ll \lambda^{-1}$; here we will examine the range $10 \lesssim q \lesssim 2000$, which contains most of the region with the largest gravitational wave production [78]. We will see that this peaks around $q \approx 100 - 200$ and falls off slightly as q gets larger or smaller (see Fig. 3.2d), although there are examples with smaller q that do not exactly follow this trend [78]. We consider the light scalar's self-interaction in the range $\lambda < \lambda_\chi < 1$.

We study the dynamics in this model beginning at the end of inflation, $t_0 \equiv 0$, once the comoving horizon $(aH)^{-1}$ begins to expand, with the inflaton as a homogeneous field given everywhere by $\phi_0 = 0.342\, M_{\rm Pl}$. [4] The field χ is a light "spectator" field during inflation, and at the end of inflation each χ mode is in the de Sitter vacuum state. As shown in previous work [100, 101], as the inflaton decays the quantum state quickly approaches a semiclassical regime with large occupation numbers, and the

[4] This particular point along the inflaton's phase space trajectory is identical to that of [78]. This choice is further addressed in Sec. 3.5.

evolution here is equivalent to the classical evolution of an initial classical distribution that gives

$$\langle|\chi_k(0)|^2\rangle = 1/(2\lambda^{3/2}\phi_0^3\omega_k), \qquad \dot{\chi}_k(0) = (i\omega_k + H(0))\,\chi_k(0) \tag{3.2.3}$$

at the beginning of reheating. [5] The dynamics considered here occurs on sub-horizon scales. [6]

Since ϕ is homogeneous, the equations of motion for these fields in a spatially flat Friedmann-Robertson-Walker (FRW) background are

$$\ddot{\phi} + 3H\dot{\phi} + \lambda\phi^3 = 0 \tag{3.2.4}$$

$$\Box\chi + 3H\dot{\chi} + \lambda_\chi\chi^3 + g^2\phi^2\chi = 0 \tag{3.2.5}$$

where $H \equiv \dot{a}/a$ is the Hubble parameter, whose value is related to the total energy density ρ by the Friedmann equation

$$H^2 = \frac{8\pi G}{3}\rho. \tag{3.2.6}$$

In order to study the behavior of ϕ and χ that follows from the above, we will express χ in terms of modes χ_k [7] :

$$\chi(t,\vec{x}) = \frac{1}{(2\pi)^{3/2}}\int d^3k\left(a_k\chi_k(t)e^{-i\vec{k}\cdot\vec{x}} + a_k^\dagger\chi_k^*(t)e^{i\vec{k}\cdot\vec{x}}\right). \tag{3.2.7}$$

The amplitude of ϕ is still very large at the end of inflation, $\lambda_\chi\chi^2 \ll g^2\phi^2$, and Eq. (3.2.5) is approximately linear in χ. We can then use the mode equation

$$\ddot{\chi}_k + 3H\dot{\chi}_k + \left(\frac{k^2}{a^2} + g^2\phi^2\right)\chi_k = 0 \tag{3.2.8}$$

[5] χ_k and ω_k are defined below. The specific implementation for initial field conditions of [100] is as described in the documentation for LATTICEEASY code, available at http://www.felderbooks.com/latticeeasy/.

[6] For the typical example $q = 120$, numerical results show that preheating begins at about $H = 1.1\times10^{-9}\,M_{\rm Pl}$ and $a = 5.5$ (for $a = 1$ at the beginning of the simulation) and the mode $k_* \approx \sqrt{\lambda}\phi_0$ is excited. Then at formation the wavelength of these perturbations is a fraction $R_*/R_{\rm horizon} = (a\,k_*^{-1})H \sim 10^{-2}$ of the horizon size. Since inflation has ended, the comoving horizon $(aH)^{-1}$ is increasing, so aH is decreasing and the modes excited later will be an even smaller fraction of the horizon size.

[7] Here we always use the Fourier Transform convention $f(\vec{x}) = (2\pi)^{-3/2}\int d^3k\, f(\vec{k})\exp(i\vec{k}\cdot\vec{x})$.

to study the beginning of the reheating process. It will be convenient to introduce conformally rescaled fields $\overline{\phi} \equiv a\phi/\phi_0$, $\overline{\chi} \equiv a\chi/\phi_0$, and time $d\eta \equiv dt/a$ and define a dimensionless time parameter and wave number

$$\tau \equiv \sqrt{\lambda}\phi_0\eta, \quad \kappa \equiv k/(\sqrt{\lambda}\phi_0). \tag{3.2.9}$$

Following e.g. [73, 78], we study the field spectrum in terms of a comoving number density for the field χ,

$$n_\kappa = \frac{1}{2}\left(\omega_\kappa|\overline{\chi}_\kappa|^2 + \frac{1}{\omega_\kappa}|\overline{\chi}_\kappa{}'|^2\right), \tag{3.2.10}$$

and comoving energy density $\rho_\kappa = \omega_\kappa n_\kappa$, where

$$\omega_\kappa = \sqrt{\kappa^2 + m_{\rm eff}^2} = \sqrt{\kappa^2 + q\overline{\phi}^{\,2} + 3(\lambda_\chi/\lambda)\overline{\chi}^{\,2}}. \tag{3.2.11}$$

3.3 Preheating in This Model

We begin by briefly outlining some results from previous studies of preheating, beginning with the case $\lambda_\chi = 0$ (see [73] and references therein). We then use these to develop an approximate relation that quantifies the end of preheating and that will be useful in the gravitational wave calculation. After the end of inflation, ϕ oscillates in its potential with period $T \approx 7.416$ (in terms of the dimensionless time parameter τ) [73] while the modes χ_κ can be excited by the phenomenon of parametric resonance. This process is typically described in terms of the resonance parameter $q = g^2/\lambda$. In general, certain modes κ will be excited as $\chi_\kappa \propto \exp(\mu_\kappa\tau)$. The exponential growth factor μ_κ will vary with κ, giving rise to resonance "bands" characterized by some central κ and width $\Delta\kappa$. We will consider the case of "broad resonance" where $q \gg 1$ (as compared with "narrow resonance" when $q < 1$). In this case the spectrum of resonantly excited modes takes the form of a broad peak whose location and width are approximately characterized by

$$\kappa_*,\, \Delta\kappa \;\sim\; q^{1/4}. \tag{3.3.1}$$

For a particular value of q, the maximum growth exponent $\mu_{\max} \equiv \max\{\mu_\kappa\}$ is [73]

$$\mu_{\max} = \frac{1}{\pi} \ln \left(\sqrt{1 + \exp\left[-\pi\kappa^2\sqrt{2/q}\right]} + \exp\left[-\pi\kappa^2/\sqrt{2q}\right] \right) \tag{3.3.2}$$

and the resonance is efficient when $\kappa^2 \leq \sqrt{q/(2\pi^2)}$. Numerically we find that typical resonant momenta are $\kappa_* \sim 1$, so $\mu_{\max} \sim (3/2\pi)\exp\left(-\pi\sqrt{2/q}\right)$ which is $\mathcal{O}(10^{-1})$ for the range of q we consider. Number density $n_\chi \equiv \int d^3\kappa\, n_{\chi\,\kappa}$ increases in steps, twice per ϕ oscillation – every time the inflaton passes through $\phi = 0$ and χ's effective mass-squared $m_\chi^2 = g^2\phi^2$ goes to zero, a burst of χ particles are created.

The exponential amplification of some χ_κ derived from Eq. (3.2.8) is a solution for small χ (approximately zero) and homogeneous ϕ, when the mode equation for χ_κ is linear. As this process evolves, this will become a worse approximation and the problem will become fully nonlinear. Therefore, Eq. (3.2.8) is only useful for understanding the beginning of the reheating process, and in general it is the coupled equations of motion Eq. (3.2.4) and Eq. (3.2.5) that must be solved.

These can be studied by lattice simulation, and we have used the C++ code LATTICEEASY [102] in order to simulate the evolution of these interacting scalar fields in an expanding universe. Fig. 3.1 shows results for $q = 120$. This is a useful example since [78] presents detailed results for preheating and gravitational wave production for $q = 120$ in the absence of a self-coupling. Fig. 3.1a shows the spatially-averaged energy density $\rho_\chi \equiv \langle \frac{1}{2}\dot{\chi}^2 + \frac{1}{2a^2}(\partial_j\chi)^2 + \frac{1}{4}\lambda_\chi\chi^4 \rangle$ as a function of time. Fig. 3.1c shows for $\lambda_\chi = 0$ the sum of the spatially-averaged energy densities $\rho_\phi \equiv \langle \frac{1}{2}\dot{\phi}^2 + \frac{1}{2a^2}(\partial_j\phi)^2 + \frac{1}{4}\lambda\phi^4 \rangle$ and ρ_χ, as well as the energy density only in the interaction term, $\rho_{\rm int} \equiv \langle \frac{1}{2}g^2\phi^2\chi^2 \rangle$. Fig. 3.1e shows the spectrum in χ for the same choice of parameters. The spectrum is shown at several times, and the solid line corresponds to approximately the time when the exponential growth ends.

We can understand how preheating progresses by observing that the transfer of

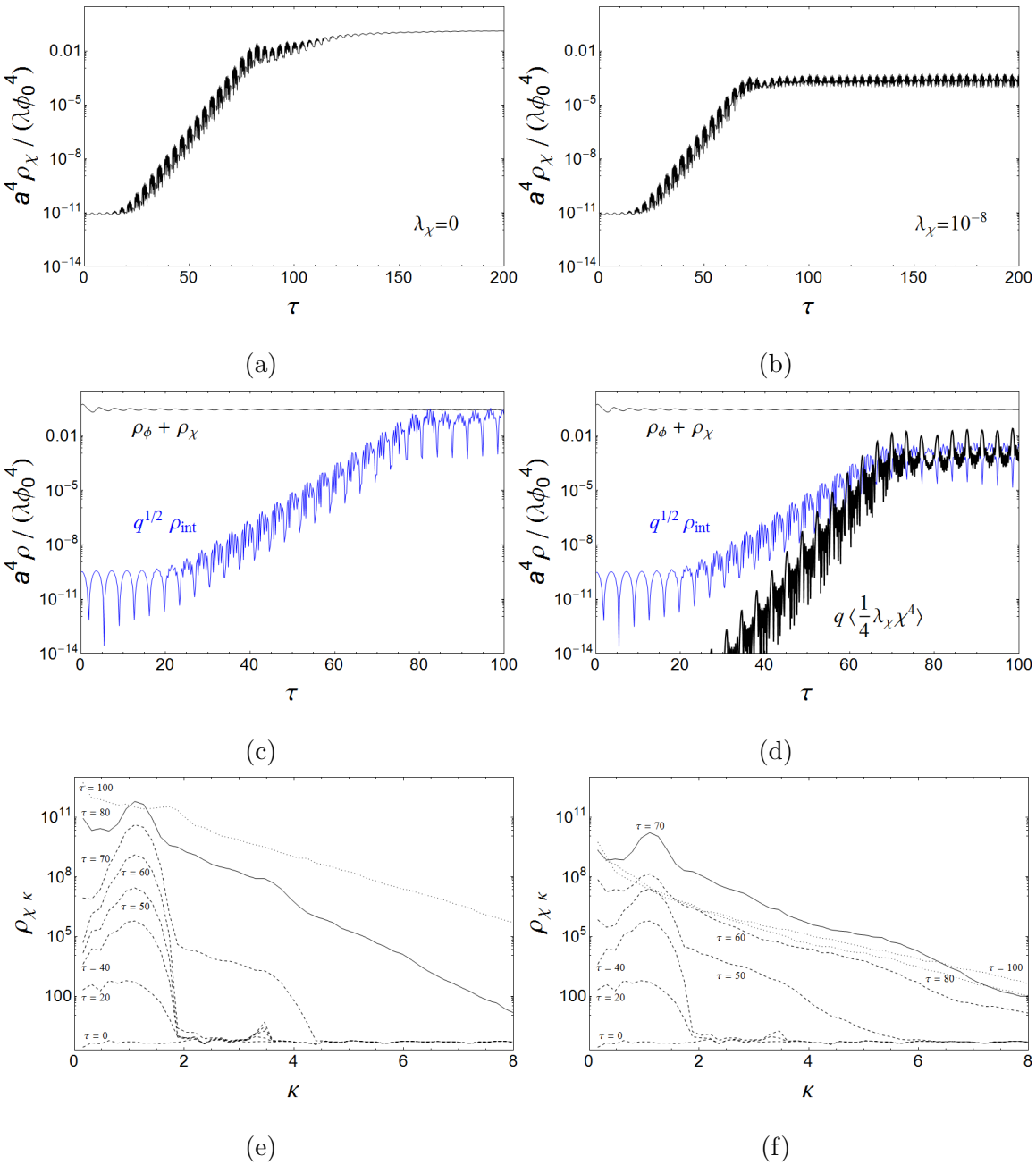

Figure 3.1: Evolution of preheating for $q = 120$. (a) Energy density ρ_χ as a function of time for $\lambda_\chi = 0$. (b) Energy density ρ_χ as a function of time for $\lambda_\chi = 10^{-8}$. (c) Energy density of ϕ and χ, as well as energy density in the interaction term, for $\lambda_\chi = 0$. (d) Same as (c), but for $\lambda_\chi = 10^{-8}$. The spatially averaged quantity $q\langle\frac{1}{4}\lambda_\chi\chi^4\rangle$ is also shown. (e) The spectrum in χ at several times of interest, for $\lambda_\chi = 0$. The solid line corresponds to approximately the time when the exponential growth ends. (f) Same as (e), for $\lambda_\chi = 10^{-8}$.

energy between χ and ϕ, and among different modes χ_κ and ϕ_κ, occurs in the following distinct stages. First, oscillations of the homogeneous ϕ excite modes of χ centered around some $\kappa = \kappa_*$, and the initially small inhomogeneities of χ become large. There is some backreaction onto ϕ, whereby the $\frac{g^2}{2}\phi^2\chi^2$ interaction term broadly excites modes ϕ_κ up through $\approx 2\kappa_*$, and inhomogeneities in ϕ begin to grow.

The second stage occurs once $q^{1/2}\rho_{\rm int} \approx \rho_\phi + \rho_\chi$. This is a useful, approximate numerical result, that is essentially the same as Eq. 6 in [103]. Then χ_{κ_*} efficiently rescatters, i.e. interacts with other modes, and its exponential growth ends. The total energy in χ continues to grow a bit until $\rho_\chi \approx \rho_\phi$. This is evident in Fig. 3.1a. Large field inhomogeneities break up and the spectrum broadens towards larger k. This broad spectrum where energy density becomes approximately evenly distributed among modes is evident in Fig. 3.1e. This figure indicates the spectrum at the time when the exponential growth ends with a solid curve. Spectra before this time are indicated by dashed curves, and spectra after this time are indicated by dotted curves. This stage is discussed and examples of field configurations are shown in [104]. Some work has also examined the final, so-called "turbulent thermalization" stage in detail [105, 106].

We now consider the case of nonzero λ_χ. This has been studied to some extent in [96, 97, 107], and here we find results consistent with theirs. Fig. 3.1b shows ρ_χ as a function of time. The resonance ends earlier in comparison with the $\lambda_\chi = 0$ situation of Fig. 3.1a. Fig. 3.1d shows $\rho_\phi + \rho_\chi$, $\rho_{\rm int}$ and $\langle \frac{1}{4}\lambda_\chi\chi^4 \rangle$ for $\lambda_\chi = 10^{-8}$. Fig. 3.1f shows the spectrum in χ at several times of interest, and the solid line again corresponds to approximately the time when the exponential growth ends. Here the end of this stage still corresponds to a large mixing between modes, but in this case it is the quartic self-interaction that is significant.

In general, we find from numerical simulation that when λ_χ becomes significantly

larger than g^2, the resonance terminates earlier than for the $\lambda_\chi = 0$ case, i.e. for any $\lambda_\chi > \lambda_\chi^* \sim g^2$. In terms of energy transfer, when $q^{1/2}\left\langle \frac{1}{4}\lambda_\chi \chi^4 \right\rangle \approx \rho_{\rm int}$, the resonance ends. This is analogous to the condition we described for $\lambda_\chi = 0$, and will be useful. Depending on the size of λ_χ, this may occur before or after the relation $q^{1/2}\rho_{\rm int} \approx \rho_\phi + \rho_\chi$ becomes true. To summarize, the resonant stage of preheating ends by the following condition:

$$(\rho_\phi + \rho_\chi) \approx q^{1/2}\rho_{\rm int} \qquad \text{for } \lambda_\chi < \lambda_\chi^*, \tag{3.3.3}$$

$$\rho_{\rm int} \approx q^{1/2}\left\langle \frac{1}{4}\lambda_\chi \chi^4 \right\rangle \qquad \text{for } \lambda_\chi > \lambda_\chi^*. \tag{3.3.4}$$

The powers of 1/2 are approximate – when comparing the size of the oscillating energy densities, as in Fig. 3.1c and Fig. 3.1d for example, there is some ambiguity in determining exactly what the value of the energy is when the resonance ends. We can estimate the value λ_χ^* where the condition Eq. (3.3.4) becomes more important than Eq. (3.3.3) in terms of an energy argument. For small enough λ_χ, we will have $\langle \frac{1}{4}\lambda_\chi \chi^4 \rangle \ll \rho_\phi + \rho_\chi$, so the self-interaction will not play a role in ending the resonance. This will no longer be true once

$$q^{1/2}\left\langle \frac{1}{4}\lambda_\chi \chi^4 \right\rangle \sim \rho_\phi + \rho_\chi. \tag{3.3.5}$$

This can be related to the value of χ when the resonance ends by observing that, around this critical value λ_χ^* where behavior transitions from Eq. (3.3.3) to Eq. (3.3.4), we will also have

$$\rho_\phi + \rho_\chi \sim q^{1/2}\left\langle \frac{1}{2} g^2 \phi_{\rm end}^2 \chi_{\rm end}^2 \right\rangle \tag{3.3.6}$$

so that

$$\frac{1}{4}\lambda_\chi \langle \chi_{\rm end}^4 \rangle \sim \frac{1}{2} g^2 \langle \phi_{\rm end}^2 \chi_{\rm end}^2 \rangle \tag{3.3.7}$$

For $(\langle\phi^2\chi^2\rangle/\langle\chi^4\rangle)_{\rm end} \sim \mathcal{O}(1)$ this means that

$$\lambda_\chi^* \sim g^2. \tag{3.3.8}$$

This agrees with numerical results showing that the maximum energy density begins to decrease dramatically with increasing λ_χ around this value. For example, $q = 120$ will give $\lambda_\chi^* \sim 120 \times 10^{-13} \sim 10^{-11}$. We check this by defining for each λ_χ the quantity $\rho_\chi^{\rm max}$ as the time average over several oscillations once ρ_χ has stopped increasing with time. Fig. 3.2b shows that around $\lambda_\chi^* \approx 10^{-11}$, $\rho_\chi^{\rm max}$ begins to decrease as λ_χ^{-1}. We now seek to quantify the effect that this has on gravitational wave production.

3.4 Gravitational Wave Spectrum

The metric perturbation h_{ij} defined in Eq. (3.2.1) can be rescaled as $\overline{h}_{ij} \equiv a h_{ij}$. Neglecting a term that goes as $a''/a \sim (aH)^2$ [78], the equation of motion is

$$\overline{h}_{ij}'' - \nabla^2 \overline{h}_{ij} = 16\pi G a^3 \Pi_{ij}^{\rm TT} \tag{3.4.1}$$

where G is Newton's constant and $\Pi_{ij}^{\rm TT}$ is the transverse traceless projection of the anisotropic stress:

$$\Pi_{ij} = a^{-2} \left(T_{ij} - \langle p \rangle g_{ij} \right), \tag{3.4.2}$$

where p is the pressure. The second term in Eq. (3.4.2) will be neglected since g_{ij} is the sum of a homogeneous, isotropic part whose transverse traceless projection is zero, and a perturbation that is higher order in G. The Fourier Transform of Eq. (3.4.1) is

$$\overline{h}_{ij}''(\vec{k}) + k^2 \overline{h}_{ij}(\vec{k}) = 16\pi G a^3 \Pi_{ij}^{\rm TT}(\vec{k}) \tag{3.4.3}$$

We consider $\Pi_{ij}^{\rm TT}$ to be a source acting continuously during the time interval $\eta_0 < \eta < \eta_f$, solve Eq. (3.4.1) using Green's functions, and use this solution to find

the energy density of the tensor perturbation. As shown in [78], the result of this procedure is

$$\frac{d\rho_{\rm gw}}{d\ln k}(\eta > \eta_f) = \frac{S_k}{a^4(\eta)} \tag{3.4.4}$$

where S_k is defined by

$$S_k = \frac{4\pi G k^3}{V} \int d\Omega \sum_{i,j} \left(\left| \int_{\eta_i}^{\eta_f} d\eta' \cos(k\eta') a(\eta') T_{ij}^{\rm TT}(\eta', \vec{k}) \right|^2 + \left| \int_{\eta_i}^{\eta_f} d\eta' \sin(k\eta') a(\eta') T_{ij}^{\rm TT}(\eta', \vec{k}) \right|^2 \right) \tag{3.4.5}$$

where V is the volume of the box considered and $\int d\Omega$ is an integral over directions in k space. [8] S_k only depends on the dynamics occurring during gravitational wave generation, and the TT part of the energy-momentum tensor is defined in terms of projection operators by

$$T_{ij}^{\rm TT}(\eta, \vec{k}) = \left(P_{il}(\hat{k}) P_{jm}(\hat{k}) - \frac{1}{2} P_{ij}(\hat{k}) P_{lm}(\hat{k}) \right) T_{lm}(\eta, \vec{k}) \tag{3.4.6}$$

$$P_{ij}(\hat{k}) = \delta_{ij} - \hat{k}_i \hat{k}_j \tag{3.4.7}$$

The LATTICEEASY code was modified to in order to compute Eq. (3.4.4) as described above, in order to obtain the spectrum of gravitational waves numerically. We will give results in terms of $\Omega_{\rm gw} = \rho_{\rm gw}/\rho_{\rm total}$, at the "time of production" defined as approximately the time when energy in gravitational waves stops increasing noticeably. This is very well approximated by the value at the end of the simulation at $\tau = 250$, and denote with a subscript "p" quantities evaluated at this time. The relation between the results we give and their present values depends somewhat on the equation of state throughout reheating, but previous works have established that

[8] Our physical results (i.e. energy density) do not scale with box size, as we use a numerical Fourier Transform that takes this into account. This is described in the LATTICEEASY documentation. The number of modes for which results are computed in a given simulation do depend on the box size and number of grid points.

in $\lambda\phi^4$ preheating, the equation of state very rapidly becomes that of radiation, so that the energy density in gravitational waves will be [78]

$$\begin{aligned} h^2\Omega_{\rm gw} &= \left(\frac{S_k}{a^4\rho}\right)_p \left(\frac{g_0}{g_*}\right)^{1/3} h^2\Omega_{\rm rad} \\ &= \left(9.3\times 10^{-6}\right)\left(\Omega_{\rm gw}\right)_p \end{aligned} \tag{3.4.8}$$

where $h^2\Omega_{\rm rad} = 4.3\times 10^{-5}$, $g_*/g_0 \approx 100$. Similarly, frequencies today are related to comoving wave numbers at the time of preheating by

$$f = \left(\frac{k}{a\rho^{1/4}}\right)_p 4\times 10^{10}\,{\rm Hz} \;\sim\; \kappa\times 10^7\,{\rm Hz} \tag{3.4.9}$$

where in the last step we have taken $(a^4\rho)_p \sim \lambda\phi_0^4$ (see e.g. Fig. 3.1a; we begin with $\rho_\chi \approx 0$ and $\rho_\phi \approx 2\times\frac{1}{4}\lambda\phi_0^4$ and throughout the simulation the quantity $a^4(\rho_\phi+\rho_\chi) \approx$ constant).

Fig. 3.2a shows the spectrum obtained in the case $q = 120$, for $\lambda_\chi = 0$ and $\lambda_\chi = 10^{-9}$. The decrease in the energy produced in gravitational waves is evident from this, and Fig. 3.2b shows how this depends on λ_χ, as a fraction of the peak energy density when $\lambda_\chi = 0$. The solid lines in Fig. 3.2c show $\Omega_{\rm gw}$ for the cases $q = 12$ and $q = 1200$. Evidently the effect of λ_χ is to end the resonance early and suppress gravitational wave production. Once preheating ends, the additional contribution of inhomogeneities to the gravitational wave spectrum is negligible [78].

To estimate how this effect depends on the model parameters q and λ_χ, we note that $\Omega_{\rm gw} \sim (T_{ij}^{\rm TT})^2 \sim (\partial_i\chi)^4$. The energy density $\Omega_{\rm gw}$ is dominated by the most recently produced part of the spectrum before the resonance ends (this is particularly clear in Fig. 8 of [78]), so for the purposes of this estimate we will ask how the maximum amplitude of χ depends on q and λ_χ. We have seen that χ grows until the condition Eq. (3.3.4), $\frac{1}{2}q\lambda\langle\phi^2\chi^2\rangle \sim \frac{1}{4}\lambda_\chi\langle\chi^4\rangle$, is satisfied. (Also, comparison of Fig. 3.1a with Fig. 3.1b shows this since $\rho_\chi \sim (\partial_i\chi)^2$.) This suggests a parametric

scaling

$$\chi^2_{\rm end} \propto q\lambda/\lambda_\chi = g^2/\lambda_\chi \tag{3.4.10}$$

Then the expectation that $\Omega_{\rm gw} \sim (\chi^2_{\rm end})^2$ becomes

$$\Omega_{\rm gw} \propto \left(g^2/\lambda_\chi\right)^2 . \tag{3.4.11}$$

Our numerical results confirm this relation as shown in Fig. 3.2b and Fig. 3.2c. For $\lambda_\chi < \lambda^*_\chi$, the peak energy in gravitational waves decreases only very slightly with increasing λ_χ, as the self-interaction term plays a small role in mixing modes and damping inhomogeneities. Once $\lambda_\chi > \lambda^*_\chi$, the energy density in gravitational waves scales in the manner given by Eq. (3.4.11). For $\lambda_\chi \sim 10^{-2}$, we see that ρ_χ and $\Omega_{\rm gw}$ no longer decrease significantly with increasing λ_χ. This is simply because the unstable resonance never begins, and the quartic self-interaction can no longer dramatically decrease $\Omega_{\rm gw}$ by ending the resonance earlier. Fig. 3.2d shows how the value of $\Omega_{\rm gw}$ at the time of production depends on the resonance parameter, q, for both $\lambda_\chi = 0$ and $\lambda_\chi = 10^{-7}$. In the latter case, we also show the prediction of the scaling relation Eq. (3.4.11).

3.5 Generality

So far, we have examined results in the context of $\lambda\phi^4$ chaotic inflation, with the self-coupling λ and the initial condition of the inflaton field identical to a previous work that thoroughly investigated the dynamics of gravitational wave production during preheating [78]. This allows the results of the previous sections to be directly compared with that work. However, observational data indicates that the $\lambda\phi^4$ chaotic potential is not favored [99], so an important question is the generality of the results we have quoted above. In this section we will address this question in two ways,

before pointing out interesting directions for future work. We will consider massive ($m^2\phi^2$) inflation, another standard example in which preheating is studied, and we will also consider a range of initial conditions for ϕ within both the $\lambda\phi^4$ and $m^2\phi^2$ cases.

Specifically, this means that we will begin the numerical situation – corresponding to the end of inflation, with the inflaton's energy about evenly split between kinetic and potential – with the inflaton field at various lower points on its potential than in the original case. Here, we are not primarily concerned with representing a complete model of inflation, but rather are studying how preheating and gravitational wave production proceed within a potential that is quadratic or quartic about the minimum, without regard to the model's behavior at higher (inflationary) field values. In this spirit, we also study the $m^2\phi^2$ case with a few choices of m_ϕ. It is worth pointing out that not all inflationary models end with oscillations of the field responsible for inflation about its zero; see for example the Abelian Higgs and Higgs-dilaton models [82, 108].

For every situation we have tried, the same approximate scaling behavior of reduced gravitational wave production with increased self-interaction λ_χ holds. In particular, we display some typical results in Fig. 3.3 and Fig. 3.4. For the case of $\lambda\phi^4$ inflation, with $q = 120$ and $\phi(0) = \phi_0 \equiv 0.342\, M_{\rm Pl}$, we plot the gravitational wave spectrum in Fig. 3.3 and the scaling behavior with λ_χ in Fig. 3.4a. These results were presented in Sec. 3.4, and they are provided again for direct comparison with alternative scenarios. We label this choice of parameters as $\phi^4 - {\rm I}$. We also show results for $q = 120$ and $\phi(0) = \phi_0/10$, referred to as $\phi^4 - {\rm II}$, as well as $q = 120$ and $\phi(0) = \phi_0/100$, referred to as $\phi^4 - {\rm III}$.

Fig. 3.3 compares the gravitational wave spectra of the $\phi^4-{\rm I}$ and $\phi^4-{\rm II}$ parameter choices, for both $\lambda_\chi = 0$ and $\lambda_\chi = 10^{-9}$. In both cases, evidently, there is a significant

reduction in gravitational wave production that accompanies an increase in λ_χ, despite the difference in overall amplitude of the spectrum. In Fig. 3.4a, we show how this reduction depends on λ_χ for each of the parameter choices $\phi^4 - \mathrm{I}$, $\phi^4 - \mathrm{II}$, $\phi^4 - \mathrm{III}$. We find the same scaling behavior as before: there is a λ_χ^* above which gravitational wave production is suppressed by a factor of $(g^2/\lambda_\chi)^2$.

In the case of massive inflation, we replace Eq. (3.2.2) with the potential

$$V = \frac{1}{2}m_\phi^2\phi^2 + \frac{1}{4}\lambda_\chi\chi^4 + \frac{1}{2}g^2\phi^2\chi^2 \tag{3.5.1}$$

i.e. the light field χ has the same potential and interactions with the inflaton as it did previously, but the inflaton potential is quadratic rather than quartic. In this case we find that, as above, there is some λ_χ^* such that for $\lambda_\chi > \lambda_\chi^*$, gravitational wave production tends to be suppressed by λ_χ^{-2}. We again plot three typical examples. We refer to $q \equiv g^2\phi(0)^2/4m_\phi^2 = 60$, $\phi(0) = 0.1\,M_{\mathrm{Pl}}$, $m_\phi = 10^{-6}M_{\mathrm{Pl}}$ as $\phi^2 - \mathrm{I}$. We refer to $q = 15$, $\phi(0) = 0.01$, $m_\phi = 10^{-9}$ as $\phi^2 - \mathrm{II}$. We refer to $q = 15$, $\phi(0) = 0.001$, $m_\phi = 10^{-9}$ as $\phi^2 - \mathrm{III}$. Fig. 3.4b shows how the gravitational wave spectra in these cases scale with λ_χ. For ease of comparison with the scaling relation λ_χ^{-2} we plot the results as a function of $\lambda_\chi/\lambda_\chi^*$, where $\lambda_\chi^* = 10^{-6}$, 10^{-9}, 10^{-7} for $\phi^2 - \mathrm{I}$, $\phi^2 - \mathrm{II}$, $\phi^2 - \mathrm{III}$ respectively. As before, λ_χ^{-2} fits well (until λ_χ becomes large enough that preheating no longer starts, so that increasing λ_χ won't further decrease the gravitational wave production).

The numerical computations involved make it impractical to check here every imaginable situation of interest to verify this relation. We have shown that gravitational wave production from preheating in potentials with minimum at zero can be extremely sensitive to the value of the light field's self-coupling term, and that result is not exclusive to one particular model or choice of parameters. Therefore, an important goal of future work will be to fully characterize this effect in other realistic

models, and better understand the implications for observability.

3.6 Discussion and Conclusions

In this work we have studied the effect of a nonzero self-interaction on gravitational wave production during preheating of a scalar field. Previous work has considered the dynamics of preheating for a light, self-interacting scalar, as well as gravitational wave production by preheating of a non-self-interacting scalar. This work is an extension of these results, and in particular shows that the spectrum of gravitational waves that survive until today is very sensitive to the light scalar's self-interaction. Our main result within the $\lambda\phi^4$ model is that for self-coupling $\lambda_\chi \gtrsim g^2$, the preheating resonance is terminated early, and the gravitational wave spectrum is significantly reduced:

$$\Omega_{\rm gw} \approx \left(\frac{g^2}{\lambda_\chi}\right)^2 \Omega_{\rm gw}^{(\lambda_\chi=0)} \quad \text{for} \quad \lambda_\chi \gtrsim g^2. \tag{3.6.1}$$

We have also begun to address the question of generality of this result, as discussed in Sec. 3.5. For various choices of the inflaton's initial condition in the $\lambda\phi^4$ model, we have seen that Eq. (3.6.1) holds. Additionally, for an $m^2\phi^2$ inflationary potential, the result that the gravitational waves are suppressed as λ_χ^{-2} is shown, for several parameter choices. While this suggests generality to inflation models with potentials quadratic or quartic about a minimum at zero, an important question for future work is to study the effect of the light field's interactions in other preheating models that have been shown to predict gravitational waves. As our work shows, predictions that neglect such interactions - even if they are extremely small - may not necessarily be accurate.

It is easy to imagine that in a realistic preheating scenario, decay products will have their own self-interactions or further interactions with other fields, that will end the resonance early. Recently, another paper studied the effect of interactions

of χ with further light degrees of freedom, as well as self-interactions in the context of a curvaton decaying to Higgs [94]. Although the model is not identical to ours, it also found that self-interactions can be important in terminating the resonance early. Furthermore, they found that interaction with the additional light scalars, as characterized by the contribution to a thermal term, has the ability to significantly affect the resonance and either end it early or prevent it from occurring at all. They did not consider gravitational wave production, but following the argument given here in Sec. 3.4 it is reasonable to expect that this early termination of the resonance can further reduce any production of gravitational waves. Analyses of other scenarios have shown that preheating can be sensitive to nonlinear interaction terms of decay products [85], or other nonperturbative effects motivated by new physics above the TeV scale [109, 110, 111, 112, 113]. Another interesting goal for future work would be to incorporate the effects of interactions such as those studied in this paper into a more general framework for obtaining order-of-magnitude estimates of gravitational wave production, as in [95]. Although current constraints on MHz gravitational wave backgrounds are not sensitive to these processes [91], this could be very useful in evaluating the potential for observability in future experiments.

One interesting possibility is that reheating occurred through an inflaton-to-Higgs coupling, since the Higgs is a natural candidate to couple to beyond-Standard Model fields [44, 114, 115, 116]. The running of the Higgs self-coupling is sensitive to any new physics that comes in at high energies, but it has not been directly measured and will be difficult to measure at the LHC. One might hope that since $\lambda_{\rm H}$ runs from 0.13 at the weak scale to zero around 10^{10} GeV in the Standard Model [117], the condition $\lambda_{\rm H} \ll 1$ could be satisfied. This would avoid enormous damping of the preheating resonance, and thereby provide a possible cosmological probe of $\lambda_{\rm H}$. The self-coupling remains $\mathcal{O}\left(10^{-1}\right)$ up to $\sim 10^8$ GeV, though, which suggests that there will not be

significant (or any) preheating resonance. However, above this scale the self-coupling decreases and the effective potential reaches a maximum (in the Standard Model – small changes in input parameters or new physics beyond the Standard Model can significantly affect this; see e.g. [118, 119, 120, 121]).

The condition Eq. (3.3.4) suggests that a more relevant condition than the self-coupling may be the magnitude of the Higgs potential. The configuration of χ at the end of inflation (initial configuration for this problem) is certainly sensitive to the potential at large field values, as it corresponds to approximately $\chi_{\rm rms} \sim 10^{12}$ GeV $\sim H_{\rm inf}$. [9] If one takes Eq. (3.3.4) to apply as the condition for whether parametric resonance does or does not occur, then the result could be a resonance pushing Higgs oscillations toward the vacuum instability region. [10] New physics that prevents $\lambda_{\rm H}$ from becoming negative would likely be more than sufficient to prevent a resonance from occuring. These rough estimates also ignore the possibilities of a different running of $\lambda_{\rm H}$ from the new inflaton coupling, as well as thermal effects. We leave the resolution of these questions to future work.

[9] The behavior of the Higgs after inflation, when there is no coupling to the inflaton, is discussed in [122].

[10] There has been much work on the Higgs and vacuum stability, including discussion of the reheat temperature; see e.g. [123, 124, 125] and references therein.

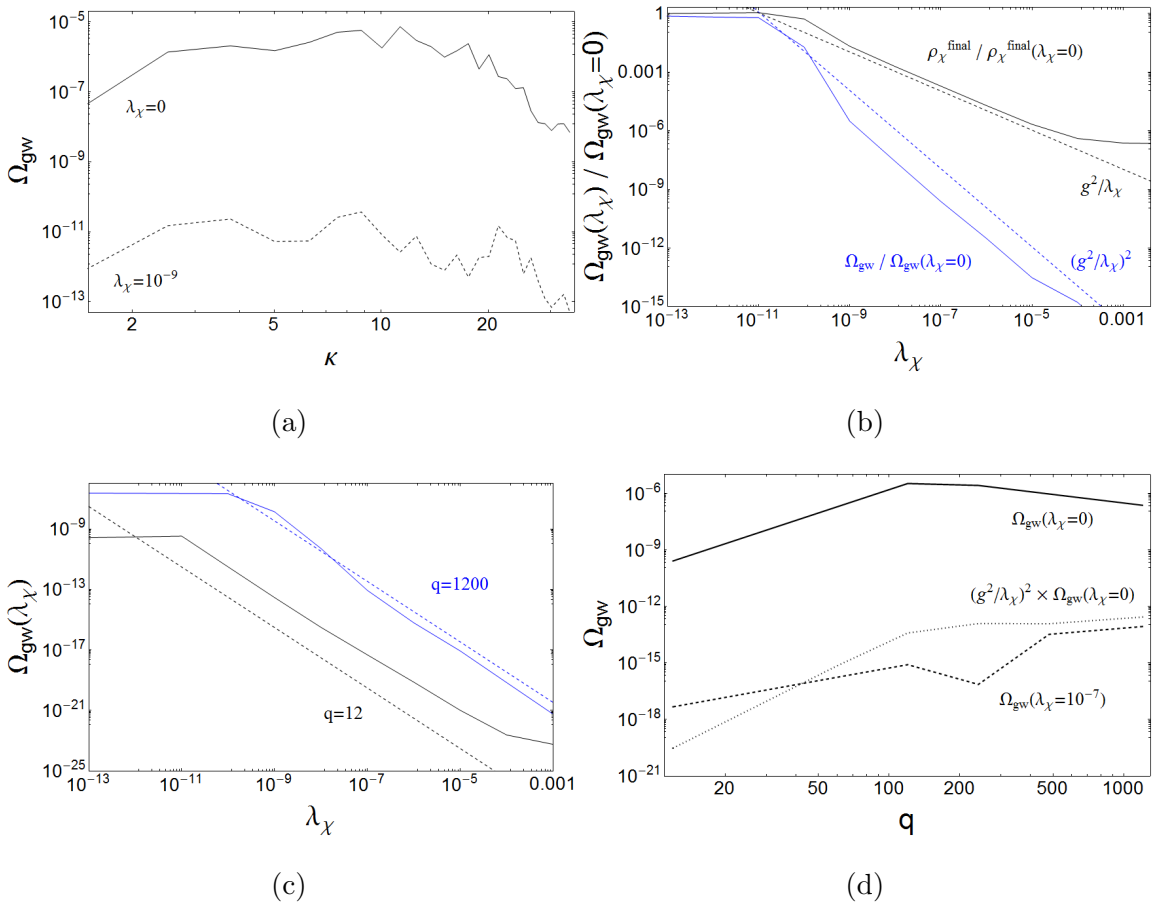

Figure 3.2: Peak of gravitational wave energy density spectrum, defined in Eq. (3.4.4), as a fraction of total energy density at end of preheating stage. (a) Spectrum for $q = 120$ and two choices of self-coupling λ_χ. (b) Amplitude of peak of GW spectrum, and final average value for ρ_χ after preheating ends, for $q = 120$ and as a function of λ_χ. These quantities are presented as fractions of their value in the $\lambda_\chi = 0$ case. For comparison, dashed curves are also shown for the scaling behavior Eq. (3.4.10) and Eq. (3.4.11). (c) Amplitude of peak of GW spectrum, $\Omega^*_{\rm gw}$, as a function of λ_χ for $q = 12$ and $q = 1200$, compared with Eq. (3.4.11). (d) Value of $\Omega_{\rm gw}$ as a function of the resonance parameter, q, for $\lambda_\chi = 0$ and $\lambda_\chi = 10^{-7}$, and the prediction Eq. (3.4.11) applied to the latter case.

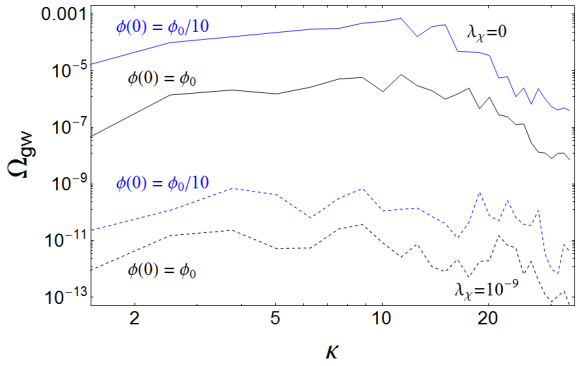

Figure 3.3: Peak of gravitational wave energy density spectrum, defined in Eq. (3.4.4), as a fraction of total energy density at end of preheating stage. Spectrum for $q = 120$ and two choices of self-coupling λ_χ. The curves labeled $\phi(0) = \phi_0$ are identical to those shown in Fig. 3.2a, corresponding to the original initial condition for the inflaton field. The curves labeled $\phi(0) = \phi_0/10$ correspond to starting the inflaton a factor of 10 lower on the potential, as described in the text. The magnitude of the gravitational wave spectrum is changed, but the effect of turning on λ_χ is the same.

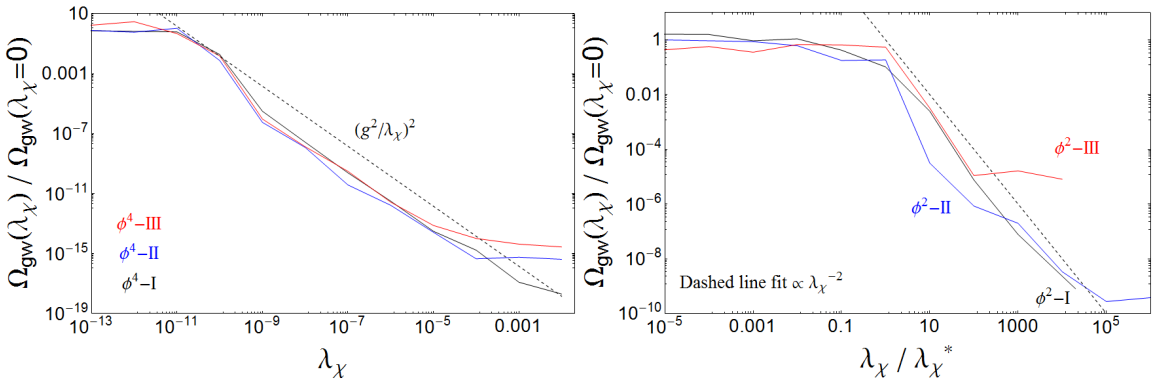

(a) (b)

Figure 3.4: Peak of gravitational wave energy density spectrum, defined in Eq. (3.4.4), as a fraction of total energy density at end of preheating stage and normalized to the value when $\lambda_\chi = 0$. Here we show several typical examples where the initial condition and/or parameters of the model are varied, as described in the text. As in Sec. 3.4, there is some value λ_χ^* above which the peak of the gravitational wave spectrum decreases as λ_χ^{-2}. Once λ_χ is large enough, the preheating resonance never starts and there is no further suppression with increasing λ_χ, an effect also seen in Sec. 3.4. (a) Varying initial conditions for $\lambda\phi^4$ inflaton potential. (b) Varying initial conditions and mass parameter for $m^2\phi^2$ inflaton potential. For ease of comparison, this result is given as a function of λ_χ/λ_*, where $\lambda_*^{\rm I} = 10^{-6}$, $\lambda_*^{\rm II} = 10^{-9}$, $\lambda_*^{\rm III} = 10^{-7}$.

Chapter 4

EFFECT OF STERILE NEUTRINO PARAMETERS ON CP VIOLATION MEASUREMENTS

4.1 Introduction

The phenomenon of neutrino flavor oscillations, first predicted in 1957 [126], is currently well-described by a 3-neutrino mixing matrix. Recent years have seen most parameters of the three-neutrino mixing matrix measured with increasing precision. The remaining questions of the ordering of the mass eigenstates (sign of $m_3^2 - m_1^2$) and the value of the complex phase δ_{13} are targets for on-going and planned experiments. Having measured these parameters, more precise studies of neutrino physics promise to constrain or reveal new physics that deviates from this model.

The on-going experiments directly relevant to the work presented in this chapter include T2K, which has a baseline length of $L = 295$ km and neutrino energy peaked at $E_\nu = 0.6$ GeV, and NOνA, which has a baseline length of $L = 810$ km and neutrino energy peaked at $E_\nu = 2$ GeV. A useful overview of these experiments is provided in [127]. As we will see in Sec. 4.3, these may or may not be able to determine both δ_{13} and the mass ordering, depending on the parameters nature has chosen. However, the planned DUNE experiment, with a baseline length $L = 1300$ km and broad spectrum of neutrino energies $E_\nu \sim 2$ to 3 GeV, will be able to determine both quantities simultaneously.

More specifically, an important goal of these long-baseline neutrino oscillation experiments in the near future will be to measure the presence or absence of CP violation in $\nu_\mu \to \nu_\mathrm{e}$ and $\overline{\nu}_\mu \to \overline{\nu}_\mathrm{e}$ oscillations, and furthermore to determine the

value(s) of the parameter(s) in the underlying theory responsible for it. For mixing among three "active" Dirac neutrinos that are members of weak isospin doublets, CP violation is determined by the value of the single complex phase δ_{13} that appears in the PMNS lepton mixing matrix. If the active neutrinos are Majorana rather than Dirac fermions, there will be two additional phases, but they will not affect the $\nu_\mu \to \nu_\mathrm{e}$ oscillations.

However, if the three active neutrinos mix with one or more sterile neutrinos, the situation will be more complicated. The matrix U relating Dirac mass and weak flavor eigenstates will include more phases (two more beyond δ_{13} for mixing with one additional sterile neutrino), and the expression for $\nu_\mu \to \nu_\mathrm{e}$ oscillation probabilities will include terms that depend on the sum or difference of these phases [128, 129, 130, 131]. In this case, a measurement of $P\left(\nu_\alpha \to \nu_\beta\right) \neq P\left(\overline{\nu}_\alpha \to \overline{\nu}_\beta\right)$ cannot unambiguously be related to one parameter in the underlying model. To what extent can experiments easily break these degeneracies? The goal of this paper is to provide a framework for relating sterile neutrino parameters with observable features.

There is a long history in the literature of considering parameter degeneracies strictly within the 3-neutrino framework. Most notably, the ordering of mass eigenstates (sign of Δm^2_{31}) is degenerate with δ_{13}: flipping the sign of Δm^2_{31} is equivalent to replacing $\delta_{13} \to \pi - \delta_{13}$, up to small corrections that would be difficult to experimentally distinguish [132, 133]. Although the mass ordering - δ_{13} degeneracy for three-neutrino mixing hasn't been experimentally resolved yet, its phenomenology has been well-studied, and provides a useful guide for studying the degeneracy between 3 and 4 neutrino mixing. The effect of a new complex phase was explored in [128] in the context of a general framework for non-standard interactions.

In the following Section, we will review the phenomenology of CP violation in long-baseline oscillation experiments, in particular setting up a consistent notation

that will be useful in the rest of the paper. We will also briefly review some of the considerations that motivate the study of both sterile neutrinos and CP violation, although we will not attempt a thorough review of either topic.

In the remaining Sections of this paper, we will present our results. In particular, we will show the effect that each new parameter has on the CP violation measurement, and discuss the extent to which long-baseline oscillation experiments can distinguish them.

4.2 Formalism

The Standard Model of electroweak interactions includes three active neutrinos that participate in weak interactions as members of weak isospin doublets. Many experiments force us to the conclusion that these three neutrinos have some small mass, and that the mass and flavor eigenstates do not coincide. Strict limits on the invisible decay width of the Z boson restrict the mass of any fourth active neutrino to be greater than half of the Z mass. [1] By contrast, a sterile neutrino is a new state that written in the flavor basis is a singlet of the weak interaction. Just as in the three-neutrino case, though, the change of basis relating flavor and mass eigenstates will induce mixing between the sterile and active neutrinos.

In particular, the fields of definite flavor [2] ν_α (α = e, μ, τ, s) are related to the fields of definite mass ν_i (i = 1, 2, 3, 4) by the mixing matrix U:

$$\nu_\alpha = \sum_{i=1}^{4} U_{\alpha i} \nu_i. \tag{4.2.1}$$

As an approximate relation that turns out to be valid for the long baseline neutrino oscillation experiments considered here [134], one can use Eq. (4.2.1) to represent the

[1] We specifically refer to the fourth mass eigenstate; the new flavor eigenstate would in general be a linear combination of mass eigenstates.

[2] Throughout this paper, we will use Greek indices to refer to flavor basis and Latin indices to refer to mass basis.

flavor eigenstates as linear combinations of mass eigenstates:

$$|\nu_l\rangle = \sum_{i=1}^{3} U_{li}^{*} |\nu_i\rangle \tag{4.2.2}$$

The change of basis between mass and flavor eigenstates leads to neutrino flavor oscillations in the following way. Describing states of definite flavor as linear combinations of mass eigenstates, each of which propagate at a well-defined velocity:

$$|\nu_\alpha(t)\rangle = \sum_{j=1,2,3} U_{\alpha\, j}^{*} \exp(-iE_j t)|\nu_j\rangle \tag{4.2.3}$$

$$= \sum_{\beta=e,\mu,\tau} \sum_{j=1,2,3} U_{\alpha j}^{*} \exp(-iE_j t) U_{\beta j} |\nu_\beta\rangle \tag{4.2.4}$$

Then the $\alpha \to \beta$ flavor transition amplitude is

$$\langle \nu_\beta(t)|\nu_\alpha(0)\rangle = \sum_{j=1,2,3} U_{\alpha j}^{*} U_{\beta j} \exp(-iE_j t) \tag{4.2.5}$$

and the transition probability is

$$P(\alpha \to \beta) = |\langle \nu_\beta(t)|\nu_\alpha(0)\rangle|^2 = \sum_{i=1}^{3}\sum_{j=1}^{3} U_{\beta i} U_{\alpha i}^{*} U_{\beta j}^{*} U_{\alpha j} \exp\left(-i(E_i - E_j)t\right) \tag{4.2.6}$$

We can simplify the energy difference in the exponential by noticing that for relativistic neutrinos ($|\vec{p}|^2 \gg m^2$), it is a very good approximation to take

$$E = \left(p^2 + m^2\right)^{1/2} = p\left(1 + (m^2/p^2)\right)^{1/2} \approx p(1 - \frac{1}{2} m^2/p^2 + \cdots) \approx p - m^2/2p^2 \tag{4.2.7}$$

Then the energy difference that we want is

$$E_k - E_j \approx p - \frac{m_i^2}{2p} - p + \frac{m_j^2}{2p} \approx \frac{m_j^2 - m_i^2}{2p} \equiv \frac{\Delta m_{ji}^2}{2p} \tag{4.2.8}$$

and with $p \approx E$, $t \approx L$ (here $c \equiv 1$, $\hbar \equiv 1$), the transition probability becomes

$$P_{\alpha\to\beta}(E, L) = \sum_{i=1}^{n_\nu}\sum_{j=1}^{n_\nu} U_{\beta i} U_{\alpha i}^{*} U_{\beta j}^{*} U_{\alpha j} \exp\left(i\Delta m_{ij}^2 L/2E\right)$$

$$= \sum_{i=1}^{n_\nu}\sum_{j=1}^{n_\nu} U_{\beta i} U_{\alpha i}^{*} U_{\beta j}^{*} U_{\alpha j} \exp\left(2i\Delta_{ij}\right) \tag{4.2.9}$$

where we have defined $\Delta_{ij} \equiv \Delta m^2_{ij} L/4E$, and allowed for the general case of n_ν neutrino mass eigenstates (correspondingly, n_ν eigenstates of definite flavor). For later use when comparing with experiment, we note that doing the same calculation and keeping all powers of c and $\hbar$, the result is

$$\Delta_{ij} = 1.27 \frac{\left(\Delta m^2_{ij}/(\mathrm{eV}^2/c^4)\right)(L/\mathrm{km})}{(E/\mathrm{GeV})} \tag{4.2.10}$$

Expressing the complex integral in terms of trigonometric functions,

$$\begin{aligned}
P_{\alpha\to\beta}(E,L) = &\sum_{i=1}^{n_\nu}\sum_{j=1}^{n_\nu} U_{\beta i}U^*_{\alpha i}U^*_{\beta j}U_{\alpha j} - 2\sum_{i=1}^{n_\nu}\sum_{j=1}^{n_\nu} U_{\beta i}U^*_{\alpha i}U^*_{\beta j}U_{\alpha j}\sin^2(\Delta_{ij}) \\
&+ i\sum_{i=1}^{n_\nu}\sum_{j=1}^{n_\nu} U_{\beta i}U^*_{\alpha i}U^*_{\beta j}U_{\alpha j}\sin(2\Delta_{ij}) \\
= &\left(\sum_{i=1}^{n_\nu} U_{\beta i}U^*_{\alpha i}\right)\left(\sum_{j=1}^{n_\nu} U^*_{\beta j}U_{\alpha j}\right) \\
&- 2\sum_{j=1}^{n_\nu}\sum_{i<j}\left(U_{\beta i}U^*_{\alpha i}U^*_{\beta j}U_{\alpha j} + (U_{\beta i}U^*_{\alpha i}U^*_{\beta j}U_{\alpha j})^*\right)\sin^2(\Delta_{ij}) \\
&- 2\sum_{i=1}^{n_\nu}\left(U_{\beta i}U^*_{\alpha i}U^*_{\beta i}U_{\alpha i} + (U_{\beta i}U^*_{\alpha i}U^*_{\beta i}U_{\alpha i})^*\right)\sin^2(\Delta_{ii}) \\
&+ i\sum_{j=1}^{n_\nu}\sum_{i<j}\left(U_{\beta i}U^*_{\alpha i}U^*_{\beta j}U_{\alpha j} - (U_{\beta i}U^*_{\alpha i}U^*_{\beta j}U_{\alpha j})^*\right)\sin(2\Delta_{ij}) \\
&+ i\sum_{i=1}^{n_\nu}\left(U_{\beta i}U^*_{\alpha i}U^*_{\beta i}U_{\alpha j} + (U_{\beta i}U^*_{\alpha i}U^*_{\beta i}U_{\alpha i})^*\right)\sin(2\Delta_{ii})
\end{aligned} \tag{4.2.11}$$

The above expression may be further simplified using the unitarity of the mixing matrix $\sum_{i=1}^{3} U_{\beta i}U^*_{\alpha i} = \delta_{\alpha\beta}$, and noticing that $\Delta_{ii} = 0$. Also, for any complex number C, the real and imaginary parts are given by $C + C^* = 2\mathrm{Re}[C]$, $C - C^* = 2i\mathrm{Im}[C]$.

Applying these simplifications to Eq. (4.2.11) gives

$$\begin{aligned} P_{\alpha\to\beta}(E,L) = \delta_{\alpha\beta}\delta_{\alpha\beta} & \\ & - 4\sum_{j=1}^{n_\nu}\sum_{i<j} \mathrm{Re}\left[U_{\beta i}U^*_{\alpha i}U^*_{\beta j}U_{\alpha j}\right]\sin^2\left(\Delta_{ji}\right) \\ & + 2\sum_{j=1}^{n_\nu}\sum_{i<j} \mathrm{Im}\left[U_{\beta i}U^*_{\alpha i}U^*_{\beta j}U_{\alpha j}\right]\sin\left(2\Delta_{ji}\right). \end{aligned} \tag{4.2.12}$$

One transition probability of interest here is the $\nu_\mu \to \nu_\mathrm{e}$ or $\overline{\nu}_\mu \to \overline{\nu}_\mathrm{e}$, since they are relevant to long-baseline oscillation experiments. For four neutrino species, the oscillation probability is

$$\begin{aligned} P(\mu\to \mathrm{e}) = & -4\mathrm{Re}\left[U_{\mu 1}U^*_{\mathrm{e}1}U^*_{\mu 2}U_{\mathrm{e}2}\right]\sin^2\left(\Delta_{21}\right) + 2\mathrm{Im}\left[U_{\mu 1}U^*_{\mathrm{e}1}U^*_{\mu 2}U_{\mathrm{e}2}\right]\sin\left(2\Delta_{21}\right) \\ & - 4\mathrm{Re}\left[U_{\mu 1}U^*_{\mathrm{e}1}U^*_{\mu 3}U_{\mathrm{e}3}\right]\sin^2\left(\Delta_{31}\right) + 2\mathrm{Im}\left[U_{\mu 1}U^*_{\mathrm{e}1}U^*_{\mu 3}U_{\mathrm{e}3}\right]\sin\left(2\Delta_{31}\right) \\ & - 4\mathrm{Re}\left[U_{\mu 2}U^*_{\mathrm{e}2}U^*_{\mu 3}U_{\mathrm{e}3}\right]\sin^2\left(\Delta_{32}\right) + 2\mathrm{Im}\left[U_{\mu 2}U^*_{\mathrm{e}2}U^*_{\mu 3}U_{\mathrm{e}3}\right]\sin\left(2\Delta_{32}\right) \\ & - 4\mathrm{Re}\left[U_{\mu 1}U^*_{\mathrm{e}1}U^*_{\mu 4}U_{\mathrm{e}4}\right]\sin^2\left(\Delta_{41}\right) + 2\mathrm{Im}\left[U_{\mu 1}U^*_{\mathrm{e}1}U^*_{\mu 4}U_{\mathrm{e}4}\right]\sin\left(2\Delta_{41}\right) \\ & - 4\mathrm{Re}\left[U_{\mu 2}U^*_{\mathrm{e}2}U^*_{\mu 4}U_{\mathrm{e}4}\right]\sin^2\left(\Delta_{42}\right) + 2\mathrm{Im}\left[U_{\mu 2}U^*_{\mathrm{e}2}U^*_{\mu 4}U_{\mathrm{e}4}\right]\sin\left(2\Delta_{42}\right) \\ & - 4\mathrm{Re}\left[U_{\mu 3}U^*_{\mathrm{e}3}U^*_{\mu 4}U_{\mathrm{e}4}\right]\sin^2\left(\Delta_{43}\right) + 2\mathrm{Im}\left[U_{\mu 3}U^*_{\mathrm{e}3}U^*_{\mu 4}U_{\mathrm{e}4}\right]\sin\left(2\Delta_{43}\right) \end{aligned} \tag{4.2.13}$$

In the case where all of the mass squared differences $\Delta m^2_{i4} \gg \Delta m^2_{\mathrm{solar}}$, $\Delta m^2_{\mathrm{atmospheric}}$ (for $i = 1, 2, 3$) in any realistic detector these oscillations will be averaged over, making the replacements

$$\sin^2\left(\Delta_{i4}\right) \to \frac{1}{2}, \qquad \sin\left(2\Delta_{i4}\right) \to 0 \tag{4.2.14}$$

valid. Then the above expression becomes

$$\begin{aligned} P(\mu \to \mathrm{e}) = &-4\mathrm{Re}\left[U_{\mu 1}U_{\mathrm{e}1}^{*}U_{\mu 2}^{*}U_{\mathrm{e}2}\right]\sin^2(\Delta_{21}) + 2\mathrm{Im}\left[U_{\mu 1}U_{\mathrm{e}1}^{*}U_{\mu 2}^{*}U_{\mathrm{e}2}\right]\sin(2\Delta_{21}) \\ &- 4\mathrm{Re}\left[U_{\mu 1}U_{\mathrm{e}1}^{*}U_{\mu 3}^{*}U_{\mathrm{e}3}\right]\sin^2(\Delta_{31}) + 2\mathrm{Im}\left[U_{\mu 1}U_{\mathrm{e}1}^{*}U_{\mu 3}^{*}U_{\mathrm{e}3}\right]\sin(2\Delta_{31}) \\ &- 4\mathrm{Re}\left[U_{\mu 2}U_{\mathrm{e}2}^{*}U_{\mu 3}^{*}U_{\mathrm{e}3}\right]\sin^2(\Delta_{32}) + 2\mathrm{Im}\left[U_{\mu 2}U_{\mathrm{e}2}^{*}U_{\mu 3}^{*}U_{\mathrm{e}3}\right]\sin(2\Delta_{32}) \\ &- 2\mathrm{Re}\left(\left(U_{\mu 1}U_{\mathrm{e}1}^{*} + U_{\mu 2}U_{\mathrm{e}2}^{*} + U_{\mu 3}U_{\mathrm{e}3}^{*}\right)U_{\mu 4}^{*}U_{\mathrm{e}4}\right) \end{aligned} \tag{4.2.15}$$

Again using the unitarity condition $\sum_{i=1}^{3} U_{\mathrm{e}i}U_{\mu i}^{*} = \delta_{\mu \mathrm{e}} = 0$, the sum

$$U_{\mu 1}U_{\mathrm{e}1}^{*} + U_{\mu 2}U_{\mathrm{e}2}^{*} + U_{\mu 3}U_{\mathrm{e}3}^{*} = -U_{\mu 4}U_{\mathrm{e}4}^{*}. \tag{4.2.16}$$

So, finally,

$$\begin{aligned} P(\mu \to \mathrm{e}) = &-4\mathrm{Re}\left[U_{\mu 1}U_{\mathrm{e}1}^{*}U_{\mu 2}^{*}U_{\mathrm{e}2}\right]\sin^2(\Delta_{21}) + 2\mathrm{Im}\left[U_{\mu 1}U_{\mathrm{e}1}^{*}U_{\mu 2}^{*}U_{\mathrm{e}2}\right]\sin(2\Delta_{21}) \\ &- 4\mathrm{Re}\left[U_{\mu 1}U_{\mathrm{e}1}^{*}U_{\mu 3}^{*}U_{\mathrm{e}3}\right]\sin^2(\Delta_{31}) + 2\mathrm{Im}\left[U_{\mu 1}U_{\mathrm{e}1}^{*}U_{\mu 3}^{*}U_{\mathrm{e}3}\right]\sin(2\Delta_{31}) \\ &- 4\mathrm{Re}\left[U_{\mu 2}U_{\mathrm{e}2}^{*}U_{\mu 3}^{*}U_{\mathrm{e}3}\right]\sin^2(\Delta_{32}) + 2\mathrm{Im}\left[U_{\mu 2}U_{\mathrm{e}2}^{*}U_{\mu 3}^{*}U_{\mathrm{e}3}\right]\sin(2\Delta_{32}) \\ &+ 2|U_{\mu 4}^{*}U_{\mathrm{e}4}|^2. \end{aligned} \tag{4.2.17}$$

In the literature, there are two popular and nearly identical parametrizations of U:

$$U_{\mathrm{I}}^{4\,\nu} \equiv \tilde{O}(3,4)O(2,4)\tilde{O}(1,4)O(2,3)\tilde{O}(1,3)O(1,2) \tag{4.2.18}$$

$$U_{\mathrm{II}}^{4\,\nu} \equiv \tilde{O}(3,4)\tilde{O}(2,4)O(1,4)O(2,3)\tilde{O}(1,3)O(1,2) \tag{4.2.19}$$

where the matrices $O(i,j)$ ($\tilde{O}(i,j)$) represent real (complex) rotations in the (i,j) plane. We label the plane of rotation within parentheses, so it is part of the name of the entire matrix. Specific elements of a matrix are labeled by subscripts. In general, each $O(i,j)$ will be a 4×4 identity matrix except for "nontrivial elements" responsible for rotations in the (i,j) plane. For a given rotation matrix $O(i,j)$ or $\tilde{O}(i,j)$, the

nontrivial elements of the matrix will be given by

$$\begin{pmatrix} O(i,j)_{ii} & O(i,j)_{ij} \\ O(i,j)_{ji} & O(i,j)_{jj} \end{pmatrix} = \begin{pmatrix} \cos\theta_{ij} & \sin\theta_{ij} \\ -\sin\theta_{ij} & \cos\theta_{ij} \end{pmatrix} \tag{4.2.20}$$

$$\begin{pmatrix} \tilde{O}(i,j)_{ii} & \tilde{O}(i,j)_{ij} \\ \tilde{O}(i,j)_{ji} & \tilde{O}(i,j)_{jj} \end{pmatrix} = \begin{pmatrix} \cos\theta_{ij} & \sin\theta_{ij}\exp(-i\delta_{ij}) \\ -\sin\theta_{ij}\exp(+i\delta_{ij}) & \cos\theta_{ij} \end{pmatrix}. \tag{4.2.21}$$

The parametrizations Eq. (4.2.18) and Eq. (4.2.19) reduce to the usual parametrization of the PMNS three-neutrino mixing matrix when there is no mixing with the fourth state ($\theta_{i4} = 0$ for $i = 1, 2, 3$).

In the vacuum case, it turns out that U_{ei} and $U_{\mu i}$ for $i = 1, 2, 3$ and the term $|U^*_{\mu 4}U_{\mathrm{e}4}|^2$ (see Eq. (4.2.23) below) are identical with the replacement $\delta_{14} \leftrightarrow -\delta_{24}$, so that $P(\delta_{14}) = P(-\delta_{24})$, $\overline{P}(\delta_{14}) = \overline{P}(-\delta_{24})$, and it is easy to convert between the final results. In the matter case, though, there will be additional mixing among terms and this simple replacement won't be true in general. Of course, the physical results are independent of parametrization and the overall range of results for δ_{14} and δ_{24} as each varies from 0 to 2π will be identical. Here we will stick with Parametrization I, with δ_{14}.

The choice of $\tilde{O}(3,4)$ on the far left in Eq. (4.2.18) or Eq. (4.2.19) is convenient for the study of oscillations between electron and muon flavor neutrinos, because these processes end up involving only two independent combinations each of the phases and mixing angles. We will see below that this arrangement of the rotation matrix eliminates θ_{34} and δ_{34} from our probabilities at the outset.

In all of the calculations in this paper, we will take $\Delta m^2_{32} = 2.32 \times 10^{-3}\,\mathrm{eV}^2$, $\Delta m^2_{21} = 7.1 \times 10^{-5}\,\mathrm{eV}^2$, $\theta_{12} = 0.59$, $\theta_{23} = 0.79$, $\theta_{13} = 0.15$. These values are consistent with the Particle Data Group ranges [6] and are identical to those of [135], allowing direct comparison with of our calculations with theirs. We assume a hierarchy between

the fourth mass eigenstate and the usual three: $\Delta m^2_{4i} \gg \Delta m^2_{\rm solar}, \Delta m^2_{\rm atmospheric}$ for $i = 1, 2, 3$. This will correspond to rapid oscillations over a short distance – on the order of meters for $\Delta m^2_{4i} \sim \text{eV}^2$ and $E \sim$ GeV according to Eq. (4.2.10). For the detectors used in long-baseline experiments, these oscillations will be averaged over and the replacements

$$\sin^2(\Delta_{4i}) \to \frac{1}{2}, \qquad \sin(2\Delta_{4i}) \to 0 \tag{4.2.22}$$

will be valid. Then the oscillation probability is

$$\begin{aligned} P(\nu_\mu \to \nu_{\rm e}) = &-4\text{Re}\left[U_{\mu 1}U^*_{\rm e1}U^*_{\mu 2}U_{\rm e2}\right]\sin^2(\Delta_{21}) + 2\text{Im}\left[U_{\mu 1}U^*_{\rm e1}U^*_{\mu 2}U_{\rm e2}\right]\sin(2\Delta_{21}) \\ &- 4\text{Re}\left[U_{\mu 1}U^*_{\rm e1}U^*_{\mu 3}U_{\rm e3}\right]\sin^2(\Delta_{31}) + 2\text{Im}\left[U_{\mu 1}U^*_{\rm e1}U^*_{\mu 3}U_{\rm e3}\right]\sin(2\Delta_{31}) \\ &- 4\text{Re}\left[U_{\mu 2}U^*_{\rm e2}U^*_{\mu 3}U_{\rm e3}\right]\sin^2(\Delta_{32}) + 2\text{Im}\left[U_{\mu 2}U^*_{\rm e2}U^*_{\mu 3}U_{\rm e3}\right]\sin(2\Delta_{32}) \\ &+ 2|U^*_{\mu 4}U_{\rm e4}|^2 \end{aligned} \tag{4.2.23}$$

where the last line has been simplified by using the unitarity of U. [3] The antineutrino oscillation probability $P(\overline{\nu}_\mu \to \overline{\nu}_{\rm e})$ is found in the same way as above; the mixing of the CP-conjugate antineutrino fields is described by

$$\overline{\nu}_\alpha = \sum_{i=1}^{4} U^*_{\alpha\, i}\overline{\nu}_i \tag{4.2.24}$$

where $\alpha = {\rm e}, \mu, \tau, {\rm s}$ and $i = 1, 2, 3, 4$. The oscillation probability between the muon and electron flavors can then be put into a similar form, differing only in the coeffi-

[3] Here the convenience of placing $\tilde{O}(3,4)$ to the far left in the parametrization is apparent. The probability only involves elements $U_{\mu i}$, U_{ei} (i.e. "top two rows" of U), while $\tilde{O}(3,4)$ only has nontrivial elements in the bottom two rows. Multiplying on the far left ensures that the top two rows of U include no factors of θ_{34} or δ_{34}.

cients of $\sin(2\Delta_{ij})$:

$$\begin{aligned} P\left(\overline{\nu}_\mu \to \overline{\nu}_\mathrm{e}\right) = &-4\mathrm{Re}\left[U_{\mu 1}U_{\mathrm{e}1}^* U_{\mu 2}^* U_{\mathrm{e}2}\right]\sin^2\left(\Delta_{21}\right) - 2\mathrm{Im}\left[U_{\mu 1}U_{\mathrm{e}1}^* U_{\mu 2}^* U_{\mathrm{e}2}\right]\sin\left(2\Delta_{21}\right) \\ &- 4\mathrm{Re}\left[U_{\mu 1}U_{\mathrm{e}1}^* U_{\mu 3}^* U_{\mathrm{e}3}\right]\sin^2\left(\Delta_{31}\right) - 2\mathrm{Im}\left[U_{\mu 1}U_{\mathrm{e}1}^* U_{\mu 3}^* U_{\mathrm{e}3}\right]\sin\left(2\Delta_{31}\right) \\ &- 4\mathrm{Re}\left[U_{\mu 2}U_{\mathrm{e}2}^* U_{\mu 3}^* U_{\mathrm{e}3}\right]\sin^2\left(\Delta_{32}\right) - 2\mathrm{Im}\left[U_{\mu 2}U_{\mathrm{e}2}^* U_{\mu 3}^* U_{\mathrm{e}3}\right]\sin\left(2\Delta_{32}\right) \\ &+ 2|U_{\mu 4}^* U_{\mathrm{e}4}|^2 \end{aligned} \tag{4.2.25}$$

Since we will have much to say about the relative size of each probability, we define the simplified notation $P \equiv P(\nu_\mu \to \nu_\mathrm{e})$ and $\overline{P} \equiv P(\overline{\nu}_\mu \to \overline{\nu}_\mathrm{e})$ for these specific processes. Violation of CP symmetry will be observed if the asymmetry

$$A_{\mu\mathrm{e}} \equiv P - \overline{P} \tag{4.2.26}$$

is nonzero. Use of the expressions Eq. (4.2.23) and Eq. (4.2.25) provides a representation of this asymmetry in terms of the elements of the mixing matrix:

$$\begin{aligned} A_{\mu\mathrm{e}} = &\ 4\mathrm{Im}\left[U_{\mu 1}U_{\mathrm{e}1}^* U_{\mu 2}^* U_{\mathrm{e}2}\right]\sin\left(2\Delta_{12}\right) + 4\mathrm{Im}\left[U_{\mu 1}U_{\mathrm{e}1}^* U_{\mu 3}^* U_{\mathrm{e}3}\right]\sin\left(2\Delta_{13}\right) \\ &+ 4\mathrm{Im}\left[U_{\mu 2}U_{\mathrm{e}2}^* U_{\mu 3}^* U_{\mathrm{e}3}\right]\sin\left(2\Delta_{23}\right) \end{aligned} \tag{4.2.27}$$

It is interesting that, even though the term $2|U_{\mu 4}^* U_{\mathrm{e}4}|^2$ cancels, there can still be significant effects of δ_{14}. While the measurement of $A_{\mu\mathrm{e}} \neq 0$ indicates CP violation, it only represents the value along one "direction" in the space of possible $(P, \overline{P})$ values. In Sec. 4.3, we will show a convenient way to represent the full $(P, \overline{P})$ information and its role in possibly breaking some degeneracy between parameters. The expressions for the P and $\overline{P}$ in terms of the specific parametrization of U are lengthy and not central to the story we are telling, but for reference and to point out some features, we present them in Appendix C.1.

Now we consider matter effects. Coherent forward scattering of active neutrinos off of electrons and nuclei in matter provides an interaction Hamiltonian that modifies the

above oscillation probabilities. Electron neutrinos will see weak charged-current (CC) scattering from electrons in atoms as well as weak neutral-current (NC) scattering from neutrons (as the contributions from protons and electrons come in with opposite sign, and cancel in an electrically neutral medium). Therefore they experience an interaction potential $V_{\rm e} = V_{\rm NC} + V_{\rm CC} = \sqrt{2} G_{\rm F} \left(N_{\rm e} - N_{\rm n}/2 \right)$, where $N_{\rm e}$ is the number density of electrons and $N_{\rm n}$ is the number density of neutrons. Muon and tau flavor neutrinos will only interact via NC scattering, so their interaction potentials will be $V_\mu = V_\tau = -G_{\rm F} N_{\rm n}/\sqrt{2}$. Antineutrinos of flavor α will have an interaction potential $V_{\overline{\alpha}} = -V_\alpha$. The sterile neutrino will, by definition, not interact with matter via the weak interaction. In terms of the average matter density,

$$V_{\rm CC} = 7.63 \times \left(\frac{\rho}{\rm g/cm^3} \right) \times 10^{-5} \, {\rm eV}^2. \tag{4.2.28}$$

For all of the calculations in this paper, we will take $\rho = 3 \, {\rm g/cm^3}$. The precise values for oscillation probabilities depend on ρ, of course, but the qualitative features of this paper's results do not.

In the flavor basis, the interaction Hamiltonian is then $H_{\rm int} = {\rm diag} \left(V_{\rm e}, \, V_\mu, \, V_\tau, \, 0 \right)$ for neutrinos and $H_{\overline{\rm int}} = -H_{\rm int}$ for antineutrinos; the full Hamiltonian will be

$$H_{\rm flavor} = U^\dagger H_{\rm mass} U + H_{\rm int}. \tag{4.2.29}$$

where $H_{\rm mass} \equiv {\rm diag} \left(0, \, \Delta m^2_{21}, \, \Delta m^2_{31} \, \Delta m^2_{41} \right)$. In order to study neutrino oscillations, it is again useful to transform to a basis where the Hamiltonian is diagonal. We will define here a mixing matrix U' which diagonalizes $H_{\rm flavor}$:

$$\begin{aligned} H_{\rm matter} \equiv U' H_{\rm flavor} U'^\dagger &\equiv \frac{1}{2E} {\rm diag} \left(m'^2_1, \, m'^2_2, \, m'^2_3, \, m'^2_4 \right) \\ &= \frac{1}{2E} {\rm diag} \left(0, \, \Delta m'^2_{21}, \, \Delta m'^2_{31}, \, \Delta m'^2_{41} \right) \\ &\quad + \frac{1}{2E} {\rm diag} \left(m'^2_1, \, m'^2_1, \, m'^2_1, \, m'^2_1 \right). \end{aligned} \tag{4.2.30}$$

We have factored out the constant matrix proportional to the identity since it doesn't affect relative phases, and therefore has no effect on oscillation probabilities. Using Eq. (4.2.30), the description of neutrino oscillations in matter is formally identical to the starting point for the vacuum case, which led to Eq. (4.2.12). Therefore Eq. (4.2.12) may still be used, with the replacements $U \to U'$ and $m_i \to m'_i$: finding U' gives the required elements U'_{e1}, $U'_{\mu 1}$, U'_{e2}, $U'_{\mu 2}$, U'_{e3}, $U'_{\mu 3}$, U'_{e4}, $U'_{\mu 4}$, and finding H_{matter} gives the quantities Δ'_{21}, Δ'_{32}, Δ'_{31} to substitute into Eq. (4.2.23).

4.3 Quantifying the Effect of New Parameters

As mentioned in Sec. 4.1, there is a long history in the literature of considering parameter degeneracies strictly within the 3-neutrino framework. Most notably, the ordering of mass eigenstates (sign of Δm^2_{31}) is degenerate with δ_{13}: flipping the sign of Δm^2_{31} is equivalent to replacing $\delta_{13} \to \pi - \delta_{13}$, up to small corrections [132, 133]. This degeneracy is illustrated here in Fig. 4.1, showing curves relevant for the T2K experiment.

This approximate degeneracy is important because the separation between these curves is much finer than experiments are capable of measuring. In fact, up until now, experiments have not been able to determine the mass ordering or rule out any values of δ_{13}. At long enough baseline, the curves for the inverted and normal hierarchies separate enough so that there is no overlap. One of the main goals of the upcoming Deep Underground Neutrino Experiment (DUNE) is to take advangate of a long baseline measurement optimized to determine the mass ordering and the value of δ_{13}, using a high-intensity beam of muon neutrinos. [4]

In the original work of Minakata and Nunokawa [133] that introduced biprobability curves as a useful tool, they showed that in vacuum oscillations, the biprobability

[4] For an overview of DUNE's science goals and experimental setup, see [136, 137].

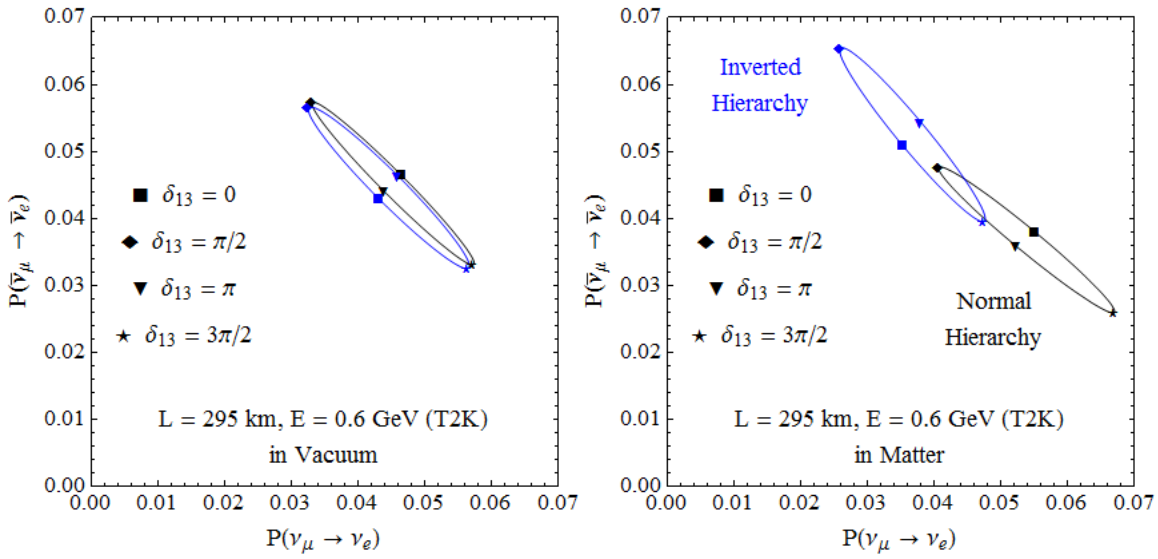

(a) (b)

Figure 4.1: Muon neutrino to electron neutrino flavor oscillation probabilities in $(P, \overline{P})$ plane with each curve representing δ_{13} varying from 0 to 2π. This shows the existence of a near degeneracy between the mass ordering (or "mass hierarchy") and the complex phase δ_{13} in vacuum, and the role of the matter effect to partially remove it. This also illustrates the useful role of biprobability curves in understanding parameter degeneracies.

curves are always elliptical; for neutrino oscillations in matter, they remain very nearly elliptical. Much subsequent work has made use of this idea; see e.g. [138]. Some recent discussions of sterile-active neutrino mixing has made use of biprobability plots and the range covered by this expanded parameter space, but have not explicitly shown the relation between the new parameters and the resulting curves [135].

Here, we quantify the effect of each new parameter (θ_{14}, θ_{24}, θ_{34}, δ_{14}, δ_{34}) on the biprobability ellipses, as a first step towards understanding exactly how neutrino oscillation experiments can unravel the possible effects of these new parameters. First, we will study oscillations in vacuum. The insight gained from this simplification will then be useful for the experimentally-relevant case of neutrino oscillations in matter.

It turns out that in the more general case here, it will still be true that varying δ_{13} while keeping all other parameters fixed traces out an ellipse in the $(P, \overline{P})$ plane.

However, the size, location and (to a lesser extent) orientation of this ellipse depend on the hidden sector parameters θ_{14}, θ_{24}, and δ_{14}. For some values of the hidden sector parameters, the $(P, \overline{P})$ prediction will lie outside the realm of possibility for the 3-neutrino scenario. In that case, the effect of the sterile sector parameters on the biprobability plots provides a framework for interpreting the results phenomenologically.

Since the proof of ellipticity and derivation of the parametric dependence is a technical detour, we will present the details in Appendix C.2 and simply quote the results here. A principal axis transformation allows us to put the probabilities P and $\overline{P}$ into the form of an expression for an ellipse. Such a transformation can be represented as a rotation along with a rescaling, and the rotation angle and rescaling can be expressed in terms of the parameters L, E as well as the mixing angles and phases. In general these are not very simple, but after choosing values for L and E a dual series expansion in the small parameters θ_{i4} is possible. To lowest order in the parameters θ_{14} and θ_{24}, the biprobability ellipses are rotated by an angle α and have lengths $L_{\pm}$ of major / minor axes changed relative to the usual case by an angle

$$\Delta\alpha \propto \theta_{14}\theta_{24}, \quad \Delta L \propto \theta_{14}\theta_{24}, \tag{4.3.1}$$

with a more complex dependence on δ_{14}. The proportionality depends on the choice of neutrino energy E and baseline length L appropriate to a particular experiment, but this provides a good approximation to the behavior in vacuum. As mentioned in Sec. 4.2, θ_{34} and δ_{34} are irrelevant for neutrino oscillations in vacuum, so they have no effect here.

Does the result described in Eq. (4.3.1) and the surrounding discussion extend to the case of neutrino oscillations in matter? As discussed following Eq. (4.2.30), P and $\overline{P}$ will have the same form as in the vacuum case, so it is no surprise that even

with the new parameters, the resulting curves are elliptical. Doing a series expansion in θ_{14} and θ_{24} to find a rotation angle and rescaling, analogous to the vacuum case, is prohibitively complex. However, the important features of the biprobability ellipses for neutrino oscillations in matter are easily seen by plotting the results.

Fig. 4.3 and Fig. 4.4 show how the biprobability ellipses change as δ_{14} varies between 0 and π with fixed θ_{14} and θ_{24}, for parameter choices of experimental interest. Fig. 4.2 shows how the biprobability ellipses change as the product $\theta_{14}\theta_{24}$ varies with fixed δ_{14}. It provides examples of the more general case that the product $\theta_{14}\theta_{24}$, rather than the individual mixing angles, controls the variation in the biprobability curves. In other words, this result from the study of vacuum oscillations remains true in the presence of matter effects.

Fig. 4.5 and Fig. 4.6 show more clearly the regions in which δ_{13} and δ_{14} are or are not degenerate. For several experimental setups, the biprobability curve for $\theta_{14} = \theta_{24} = 0.1$, $\delta_{14} = 0$ is plotted, along with several points corresponding to the choices $\delta_{13} = 0, \pi/2, \pi, 3\pi/2$ and $\delta_{14} = n\pi/4$ with $n = 0, \ldots, 7$. As detailed within the figure, these points are color coded by δ_{14}, while the shape of the plot marker is determined by the value of δ_{13}.The measurement of a point in some regions of biprobability space corresponds to unique values of both phases, while in others there is still ambiguity. This is apparent when comparing Fig. 4.5 and Fig. 4.6.

4.4 Summary and Conclusions

In this paper, we have shown how biprobability curves, a convenient tool for understanding neutrino and antineutrino oscillation probabilities, are affected by the new parameters present when the active neutrinos mix with a sterile neutrino. The mixing angles θ_{14} and θ_{24} affect the angle and size of the ellipses in a manner proportional to $\theta_{14}\theta_{24}$. The most important result concerns degeneracies between δ_{13} and δ_{14}. For

a given experimental setup, there will be regions where a measurement would have difficulty distinguishing between the predictions of different values for these complex phases, while other regions would allow them to be easily distinguished. This makes it sound like the possibility of experimentally determining δ_{14} and δ_{24} separately depends only on the parameters nature has chosen. However, as seen by comparing Fig. 4.5 and Fig. 4.6, different experimental setups may have different values of these parameters that are degenerate. Since DUNE is expected to be able to determine whether the mass ordering follows the normal hierarchy or inverted hierarchy, experiments with shorter baselines will no longer have to worry about the sign(Δ_{31}) ambiguity, and could be more useful in breaking a $\delta_{13} - \delta_{14}$ degeneracy.

In order to fully explore the ability of combinations of experiments to fully determine both δ_{13} and a possible δ_{14}, we would need to take into account each detector's characteristics, i.e. the "resolution" on the biprobability plot which can be distinguished. This is beyond the scope of this work. Another useful goal for future work is to further develop the analytical understanding that relates each new mixing parameter with features of the biprobability plots.

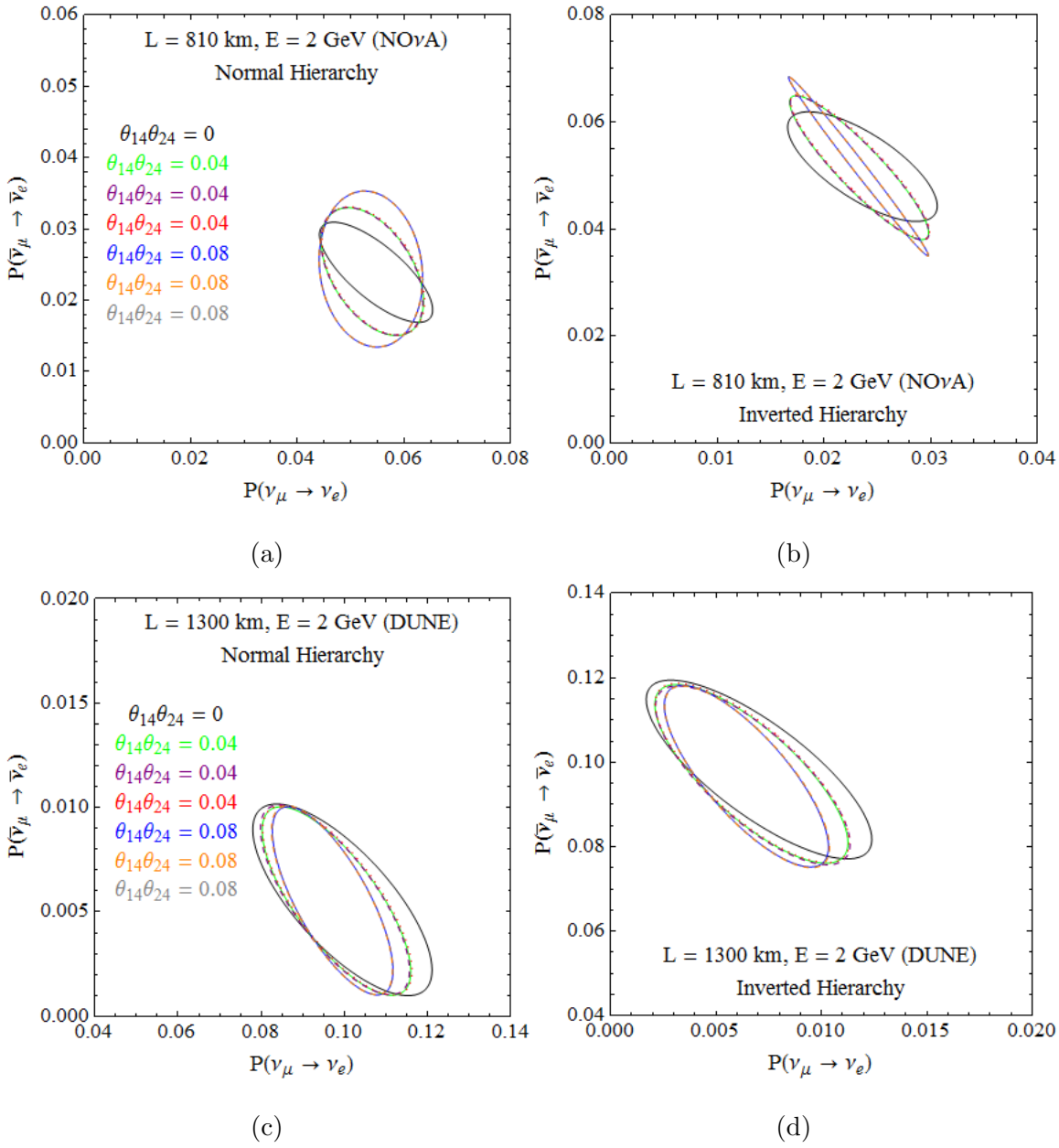

Figure 4.2: Ellipses in $(P, \overline{P})$ plane with each curve representing δ_{13} varying from 0 to 2π, for various choices of the product $\theta_{14}\theta_{24}$ with fixed $\delta_{14} = \pi/4$. Results for nonzero θ_{i4} are plotted for the following combinations ($\theta_{14} = 0.1$, $\theta_{24} = 0.04$); ($\theta_{14} = 0.04$, $\theta_{24} = 0.1$); ($\theta_{14} = 0.06325$, $\theta_{24} = 0.06325$); ($\theta_{14} = 0.1$, $\theta_{24} = 0.08$); ($\theta_{14} = 0.08$, $\theta_{24} = 0.1$); ($\theta_{14} = 0.08944$, $\theta_{24} = 0.08944$). The curves corresponding to the same values of $\theta_{14}\theta_{24}$ almost exactly coincide.

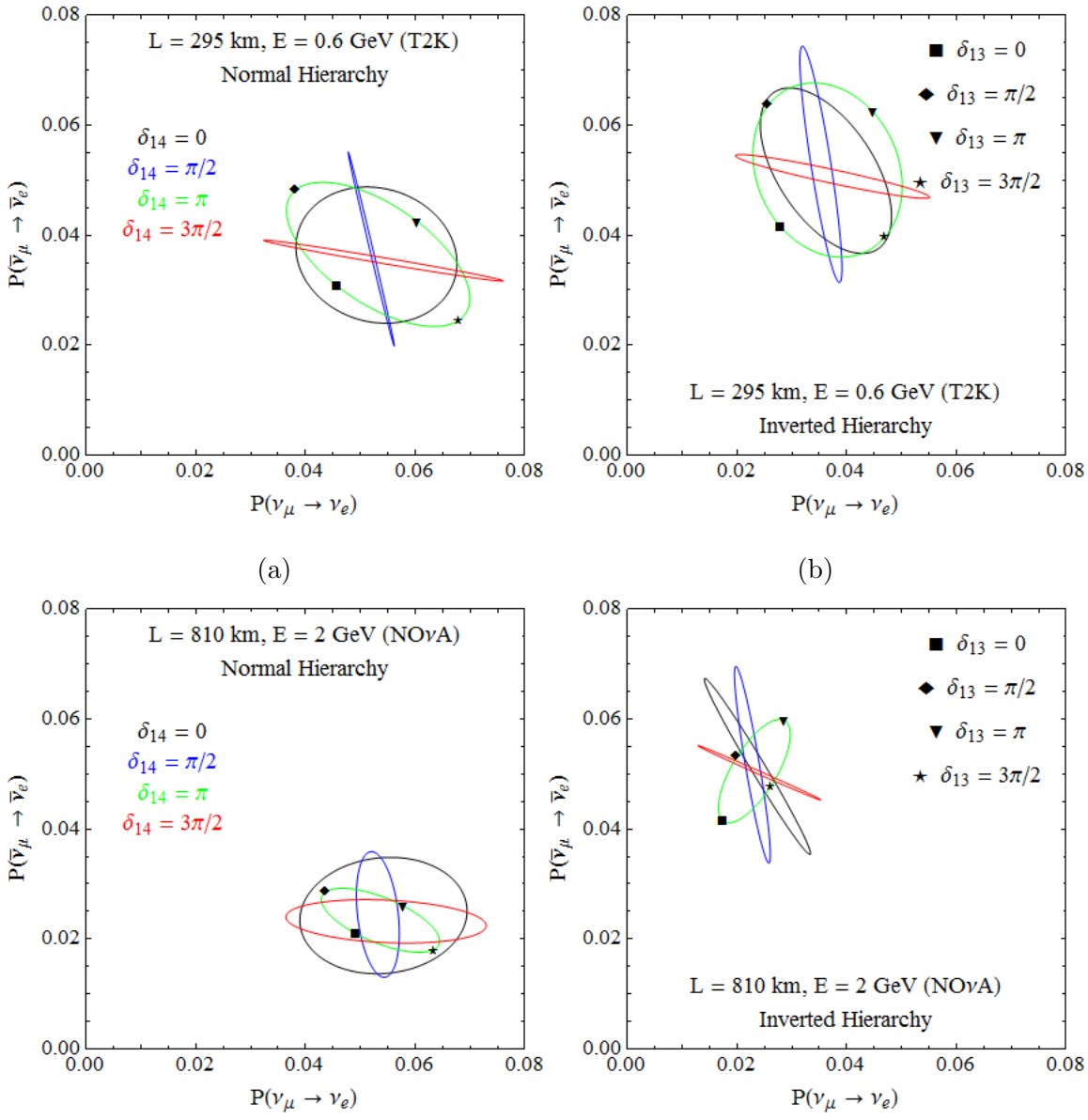

Figure 4.3: Ellipses in $(P, \overline{P})$ plane with each curve representing δ_{13} varying from 0 to 2π, for one specific choice of δ_{14} and for fixed $\theta_{14} = \theta_{24} = 0.1$ and θ_{34}, $\delta_{34} = 0$. The dependence of the θ_{13} points on a varying δ_{14} will be show in Fig. 4.5 and Fig. 4.6.

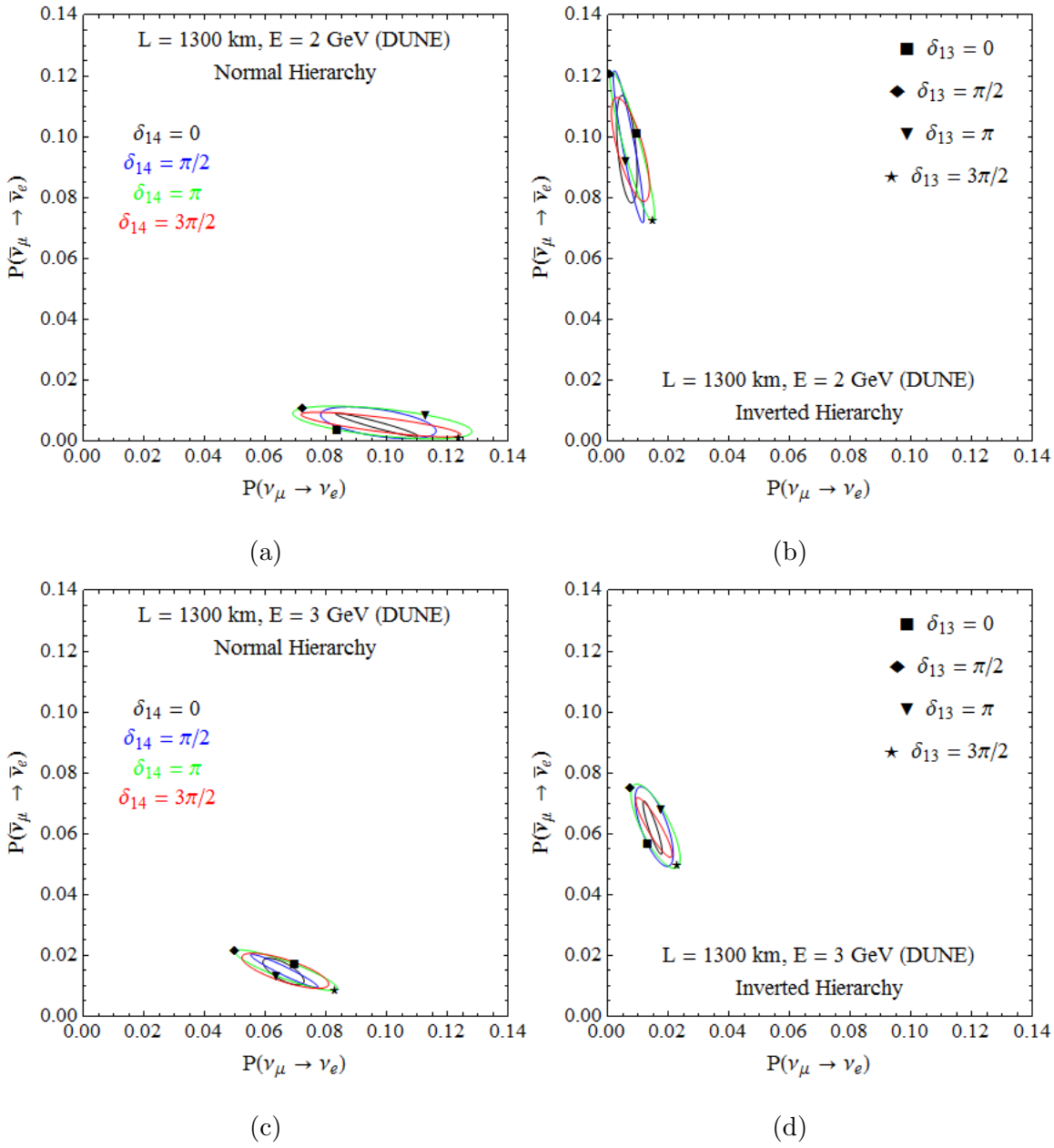

Figure 4.4: Ellipses in $(P, \overline{P})$ plane with each curve representing δ_{13} varying from 0 to 2π, for one specific choice of δ_{14} and for fixed $\theta_{14} = \theta_{24} = 0.1$ and θ_{34}, $\delta_{34} = 0$. The dependence of the θ_{13} points on a varying δ_{14} will be show in Fig. 4.5 and Fig. 4.6.

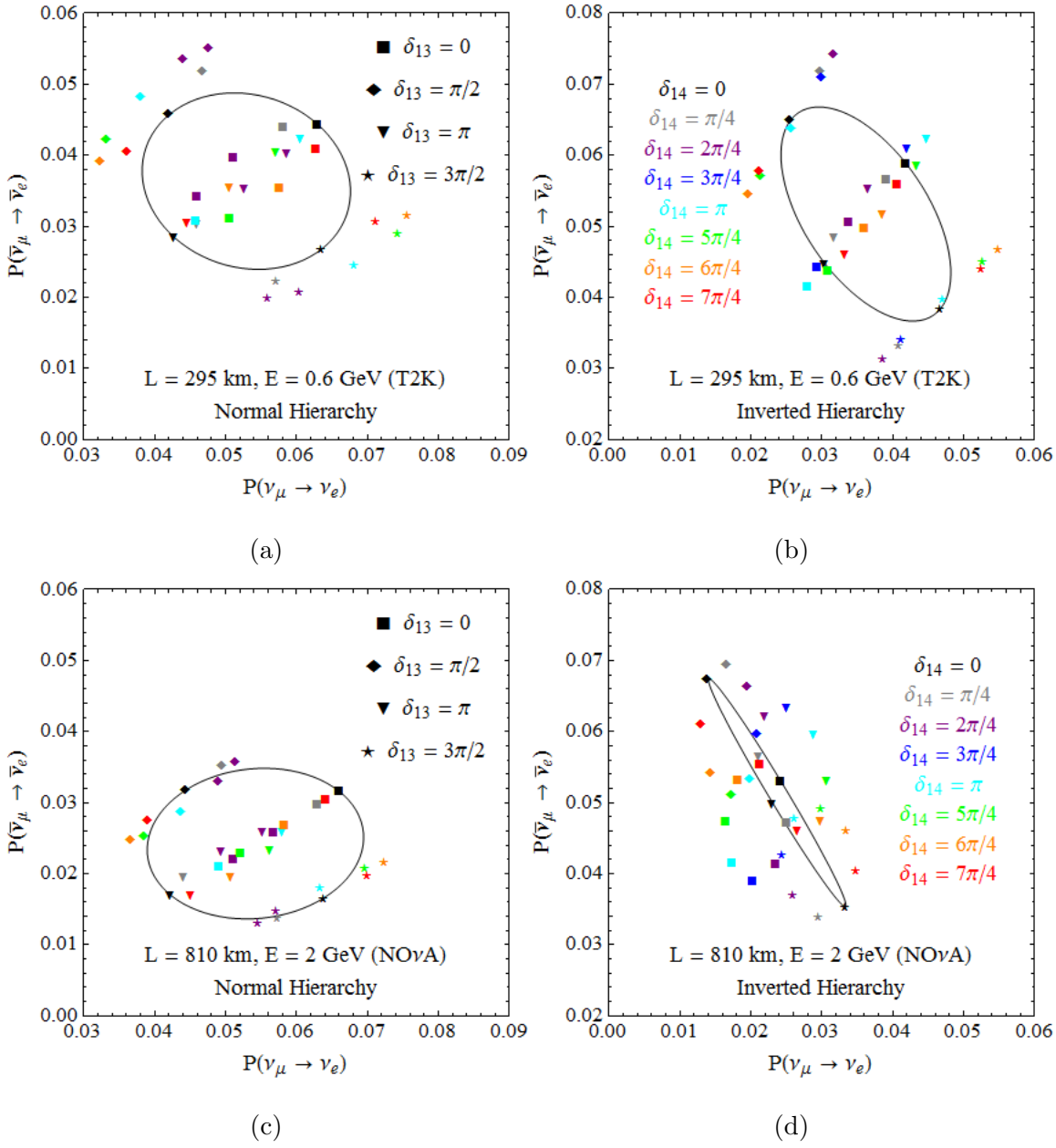

Figure 4.5: Points in $(P, \overline{P})$ plane corresponding to various choices of δ_{13} and δ_{14}, for fixed $\theta_{14} = \theta_{24} = 0.1$ and θ_{34}, $\delta_{34} = 0$. Evidently some regions of parameter space are more amenable than others to simultaneous determination of δ_{13} and δ_{14}. The black curve corresponds to the biprobability ellipse when $\delta_{14} = 0$.

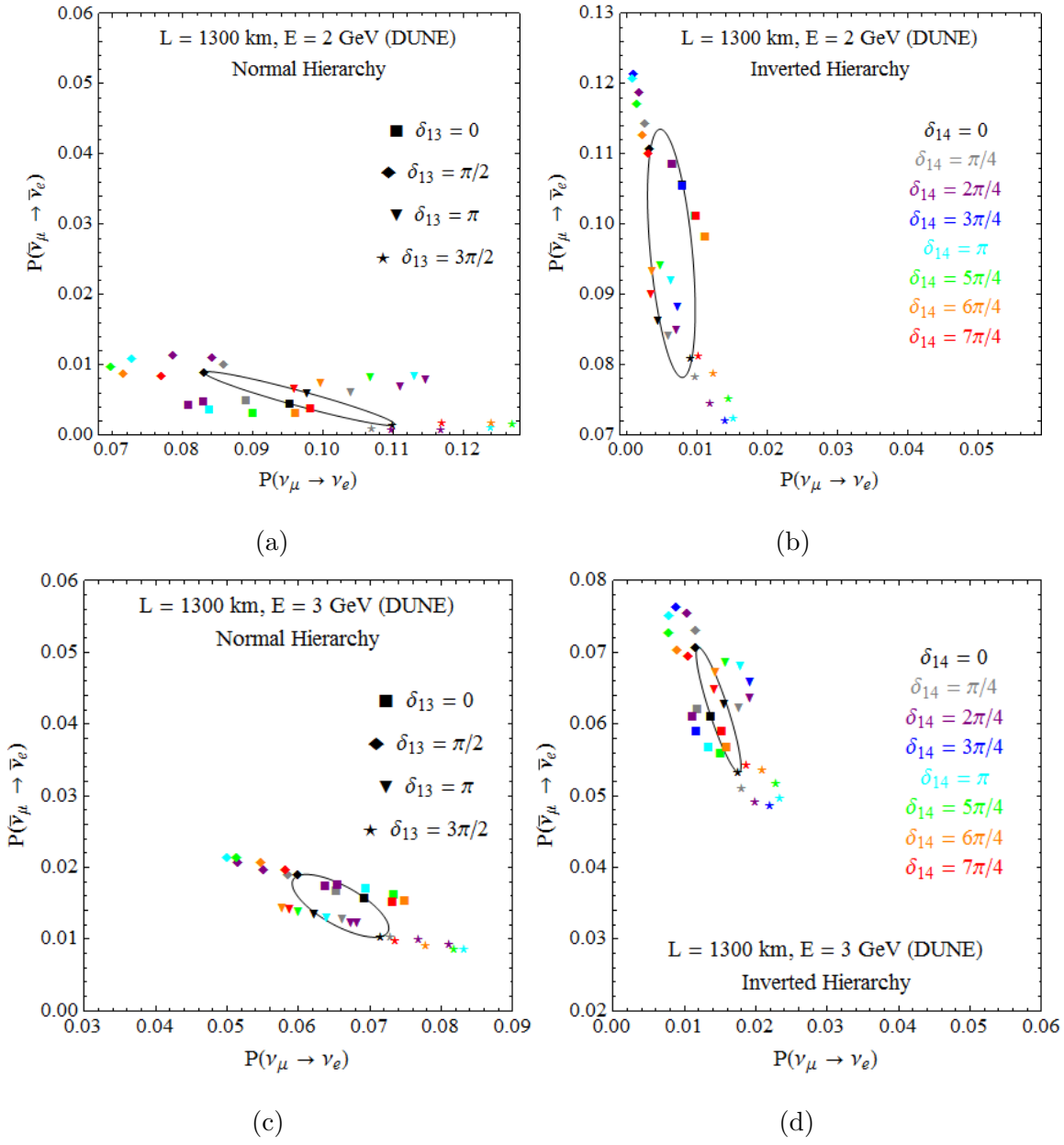

Figure 4.6: Points in $(P, \overline{P})$ plane corresponding to various choices of δ_{13} and δ_{14}, for fixed $\theta_{14} = \theta_{24} = 0.1$ and θ_{34}, $\delta_{34} = 0$. Evidently some regions of parameter space are more amenable than others to simultaneous determination of δ_{13} and δ_{14}. The black curve corresponds to the biprobability ellipse when $\delta_{14} = 0$.

Chapter 5

CONCLUSION

> "Yes, but here I come to a stop! Gentlemen, you must excuse me for being over-philosophical; it's the result of forty years underground!"
>
> –Fyodor Dostoevsky, *Notes From Underground*

This dissertation has examined several aspects of high energy physics relevant to violent processes in the early universe. Early universe processes such as phase transitions and out-of-equilibrium particle production can provide a unique connection between observation and physics far above the TeV scale.

The work presented in Chapter 2 describes a possible way to constrain new models of particle physics which contain a scalar field that gets a vacuum expectation value as a "dark sector" $U(1)$ is spontaneously broken. The scalar S and the gauge boson X_μ of the $U(1)$ can couple to the Standard Model by Higgs Portal and Kinetic Mixing operators. Many experiments constrain the strengths α, ϵ of these operators when the dark symmetry breaking scale σ or dark photon mass m_X is below $\mathcal{O}\,(\text{TeV})$ but there is little constraint at higher energies. When the $U(1)_X$ is spontaneously broken in the early universe, though, a network of cosmic string topological defects would have been formed and would still exist today.

Previous works had noted that these dark strings can radiate particles (e.g. [36]), and that one can consider an "effective coupling" whereby the string acts as a delta-function source of standard model fields, with coupling constants $g^{\text{H}}_{\text{str}}$ and $g^{\text{Z}}_{\text{str}}$ for the Higgs and Z boson, respectively. The decay of these particles would contribute to the diffuse gamma ray flux as measured, for example, by Fermi-LAT. However, it was

not clear from previous works (i) how to calculate the effective coupling of the string action to Higgs or Z fields directly from strength of HP and KM terms in $\mathcal{L}$, (ii) how the coupling scales with the relevant parameters – previous works assumed that the coupling was proportional to the hidden sector symmetry breaking scale σ. It was therefore unclear how to provide a quantitative constraint on these models.

The work described in Chapter 2 found the "string solution" - the field profiles with nonzero hidden-sector winding number that are solutions of the equations of motion for the model. This is a boundary-value problem that is difficult to solve because the Higgs Portal and Kinetic Mixing introduce significant nonlinearities that couple the solutions. It is especially problematic when there is a large hierarchy between the electroweak and hidden sector symmetry breaking scales. The solution to this included development of a numerical method that is able to handle the problem's nonlinearities by "bootstrapping" prior solutions in a way that takes advantage of simpler, limiting cases. As a result, and contrary to assumptions made in some previous works, it was found that the effective coupling depends on the electroweak scale η, rather than the hidden sector scale σ, with big implications for the observability of dark strings.

Integrating these solutions produced the relevant coupling constants $g_{\mathrm{H}}^{\mathrm{str}}$ and $g_{\mathrm{Z}}^{\mathrm{str}}$. With these effective couplings in hand, in order to evaluate phenomenological constraints it is necessary to know the power spectrum emitted by features known as cusps and kinks that occur as the string network evolves, the subject of the follow-up paper [139]. Finally, [140] went on to show that for the range of parameters considered in the papers [141, 139], there won't be an observable contribution to gamma ray flux. On the other hand, a different group has argued [142] that for large Higgs Portal coupling *and* large separation of scales, there will be an observable effect. This region is very difficult to solve numerically, so at the moment it is still not clear whether

there is any constraint – it is an important question to address in future work.

The inflationary scenario requires a reheating mechanism by which the inflaton field's energy density is converted into a thermal spectrum of particles, the subject of Chapter 3. Its nature is not known but much work has gone into the study of simplified models; for example, an inflaton ϕ oscillates about its minimum and excites a light field χ, whose only interaction is a coupling $\Delta\mathcal{L} = -\frac{1}{2}g^2\phi^2\chi^2$ (where g^2 is a coupling constant). In this context, there can be an unstable resonance as some field modes are excited at an exponential rate, for a brief "preheating" phase. Previous work has shown that this produces anisotropic stress that sources gravitational waves. Today this spectrum would be outside the sensitivity of existing or proposed experiments, but in principle detectable.

The result described above leads to the question of how robust are the predictions. Successful reheating into (ultimately) Standard Model particles requires more than the simple field modeled by χ, but previous work had not shown explicitly the effect of introducing new interactions. If we ask generically what interactions a light field such as χ may have, either as fundamental terms or from integrating out a heavy field, a well-motivated addition is a quartic self-interaction with self-coupling λ_χ. (An example could be a small, effective coupling of Higgs to inflaton.) Then the potential is

$$V = V_{\text{inflaton}}(\phi) + \frac{1}{2}g^2\phi^2\chi^2 + \frac{1}{4}\lambda_\chi\chi^4. \tag{5.0.1}$$

This work [143] showed how the spectrum of gravitational waves depends directly on the light field's quartic self-coupling, λ_χ, for a range of parameters and two often-studied inflaton potentials.

A full understanding of reheating in this scenario requires both analytic and numerical methods. At first, the mode equations for the small-amplitude χ field decouple

and become independent harmonic oscillators with time-dependent frequencies (due to the background inflaton oscillations). Parametric resonance leads to exponential amplification of some modes, leading to an anisotropic stress in the fields' energy momentum tensor, which sources gravitational wave production. The source term for gravitational waves grows exponentially.

The size of the gravitational wave spectrum is therefore directly tied to how long the resonance lasts, so any effect that tends to terminate the resonance early will result in a reduced spectrum of gravitational waves. Early termination of the resonance is exactly the effect of $\lambda_\chi \neq 0$. Heuristically, once χ becomes large the self-interaction term will become more efficient in coupling different modes, so that energy is taken from the resonant mode, ending its exponential growth. A full lattice simulation of the field dynamics is necessary in order to understand when the nonlinear effects become important. I found numerically that whether (and when) the quartic term significantly affects the results depends on the variances of ϕ and χ as well as the coupling constants g^2 and λ_χ.

The above result was used to understand that the gravitational wave spectrum scales with λ_χ as

$$\Omega_{\rm gw}^{(\lambda_\chi)}/\Omega_{\rm gw}^{(\lambda_\chi=0)} \sim (g^2/\lambda_\chi)^2 \tag{5.0.2}$$

for λ_χ greater than some small critical value, a typical example being $\lambda_\chi^* \sim 10^{-10}$. I also verified Eq. (5.0.2) numerically, by computing the anisotropic stress in the energy-momentum tensor, and using it as a source for the wave equation for transverse-traceless tensor perturbations (gravitational waves), solved by using Green's functions. I found Eq. (5.0.2) to be true whether $V_{\rm inflaton}(\phi)$ takes a quartic or quadratic form, and holds for several choices of initial condition for ϕ at the end of inflation. (Even without $V \sim \phi^2$ or ϕ^4 at inflationary field values, oscillations about the bottom

of the potential may have this form.)

There are important questions remaining for future work. In particular, numerical simulations show a relationship between the variances of ϕ and χ that determined whether the $\lambda_\chi \chi^4$ term plays a significant role, and a calculation using nonequilibrium field theory would be very useful in understanding the generality of this result. Also, a recent paper estimates the *maximum* gravitational wave production from early universe processes [95]. It would be interesting to see how the result of Chapter 3 could be incorporated into that picture, to estimate how specific interactions in a model relate to features of the observable gravitational wave spectrum.

Chapter 4 showed how biprobability curves, a convenient tool for understanding neutrino and antineutrino oscillation probabilities, are affected by the new parameters present when the active neutrinos mix with a sterile neutrino. The mixing angles θ_{14} and θ_{24} affect the angle and size of the ellipses in a manner proportional to $\theta_{14}\theta_{24}$. The most important result concerns degeneracies between δ_{13} and δ_{14}. For a given experimental setup, there will be regions where a measurement would have difficulty distinguishing between the predictions of different values for these complex phases, while other regions would allow them to be easily distinguished. This experimental ambiguity makes it sound like the possibility of experimentally determining δ_{13} and δ_{14} separately depends only on the parameters nature has chosen. However, different experimental setups may have different values of these parameters that are degenerate. Since the DUNE experiment is expected to be able to determine whether the mass ordering follows the normal hierarchy or inverted hierarchy, experiments with shorter baselines will no longer have to worry about the sign(Δ_{31}) ambiguity, and could be more useful in breaking a $\delta_{13} - \delta_{14}$ degeneracy.

In order to fully explore the ability of combinations of experiments to fully determine both δ_{13} and a possible δ_{14}, it would need to take into account each detector's

characteristics, i.e. the "resolution" on the biprobability plot which can be distinguished. Incorporating these experimental details is beyond the scope of this work. Another useful goal for future work is to further develop the analytical understanding that relates each new mixing parameter with features of the biprobability plots.

REFERENCES

[1] Chris Quigg. *Gauge Theories of the Strong, Weak, and Electromagnetic Interactions*. Princeton University Press, USA, 2013.

[2] J. F. Donoghue, E. Golowich, and Barry R. Holstein. Dynamics of the standard model. *Camb. Monogr. Part. Phys. Nucl. Phys. Cosmol.*, 2:1–540, 1992.

[3] Frank Wilczek. "prizes have been given and won't be given back". From this author's personal observation of his lecture on axions given at ASU on January 12, 2016.

[4] Y. Fukuda et al. Evidence for oscillation of atmospheric neutrinos. *Phys. Rev. Lett.*, 81:1562–1567, 1998.

[5] Q. R. Ahmad et al. Direct evidence for neutrino flavor transformation from neutral current interactions in the Sudbury Neutrino Observatory. *Phys. Rev. Lett.*, 89:011301, 2002.

[6] K. A. Olive et al. Review of Particle Physics. *Chin. Phys.*, C38:090001, 2014.

[7] Adam G. Riess et al. Observational evidence from supernovae for an accelerating universe and a cosmological constant. *Astron. J.*, 116:1009–1038, 1998.

[8] S. Perlmutter et al. Measurements of Omega and Lambda from 42 high redshift supernovae. *Astrophys. J.*, 517:565–586, 1999.

[9] P. A. R. Ade et al. Planck 2015 results. XIII. Cosmological parameters. 2015.

[10] Steven Weinberg. *Cosmology*. 2008.

[11] Daniel Baumann. Inflation. In *Physics of the large and the small, TASI 09, proceedings of the Theoretical Advanced Study Institute in Elementary Particle Physics, Boulder, Colorado, USA, 1-26 June 2009*, pages 523–686, 2011.

[12] Jerome Martin, Christophe Ringeval, and Vincent Vennin. Encyclopaedia Inflationaris. *Phys. Dark Univ.*, 5-6:75–235, 2014.

[13] P. A. R. Ade et al. Planck 2015 results. XX. Constraints on inflation. 2015.

[14] Edmund Bertschinger. Cosmological perturbation theory and structure formation. In *Cosmology 2000*, pages 1–25, 2001.

[15] A. D. Sakharov. Violation of CP Invariance, c Asymmetry, and Baryon Asymmetry of the Universe. *Pisma Zh. Eksp. Teor. Fiz.*, 5:32–35, 1967. [Usp. Fiz. Nauk161,61(1991)].

[16] A. E. Nelson, D. B. Kaplan, and Andrew G. Cohen. Why there is something rather than nothing: Matter from weak interactions. *Nucl. Phys.*, B373:453–478, 1992.

[17] A. Leike. The Phenomenology of extra neutral gauge bosons. *Phys.Rept.*, 317:143–250, 1999.

[18] Gordan Krnjaic. Probing Light Thermal Dark-Matter With a Higgs Portal Mediator. 2015.

[19] Ogan Özsoy, Gizem Sengor, Kuver Sinha, and Scott Watson. A Model Independent Approach to (p)Reheating. 2015.

[20] Mustafa A. Amin and Daniel Baumann. From Wires to Cosmology. *JCAP*, 1602(02):045, 2016.

[21] A. Vilenkin and E. P. S. Shellard. *Cosmic Strings and Other Topological Defects*. Cambridge University Press, 2000.

[22] Tanmay Vachaspati, Levon Pogosian, and Daniele Steer. Cosmic Strings. *Scholarpedia*, 10(2):31682, 2015.

[23] Tanmay Vachaspati and Alexander Vilenkin. Gravitational Radiation from Cosmic Strings. *Phys. Rev.*, D31:3052, 1985.

[24] Paul Langacker. The Physics of Heavy Z' Gauge Bosons. *Rev.Mod.Phys.*, 81:1199–1228, 2009.

[25] Shinya Kanemura, Shigeki Matsumoto, Takehiro Nabeshima, and Nobuchika Okada. Can WIMP Dark Matter overcome the Nightmare Scenario? *Phys.Rev.*, D82:055026, 2010.

[26] Oleg Lebedev, Hyun Min Lee, and Yann Mambrini. Vector Higgs-portal dark matter and the invisible Higgs. *Phys.Lett.*, B707:570–576, 2012.

[27] Yasaman Farzan and Amin Rezaei Akbarieh. VDM: A model for Vector Dark Matter. *JCAP*, 1210:026, 2012.

[28] Seungwon Baek, P. Ko, Wan-Il Park, and Eibun Senaha. Higgs Portal Vector Dark Matter : Revisited. 2012.

[29] Thomas Hambye. Hidden vector dark matter. *JHEP*, 0901:028, 2009.

[30] Nima Arkani-Hamed and Neal Weiner. LHC Signals for a SuperUnified Theory of Dark Matter. *JHEP*, 0812:104, 2008.

[31] S. Cassel, D.M. Ghilencea, and G.G. Ross. Electroweak and Dark Matter Constraints on a Z-prime in Models with a Hidden Valley. *Nucl.Phys.*, B827:256–280, 2010.

[32] Eung Jin Chun, Jong-Chul Park, and Stefano Scopel. Dark matter and a new gauge boson through kinetic mixing. *JHEP*, 1102:100, 2011.

[33] Xiaoyong Chu, Thomas Hambye, and Michel H.G. Tytgat. The Four Basic Ways of Creating Dark Matter Through a Portal. *JCAP*, 1205:034, 2012.

[34] Bogdan A. Dobrescu. Massless gauge bosons other than the photon. *Phys.Rev.Lett.*, 94:151802, 2005.

[35] Lotty Ackerman, Matthew R. Buckley, Sean M. Carroll, and Marc Kamionkowski. Dark Matter and Dark Radiation. *Phys.Rev.*, D79:023519, 2009.

[36] Tanmay Vachaspati. Dark Strings. *Phys. Rev.*, D80:063502, 2009.

[37] P.A.R. Ade et al. Planck 2013 results. XXV. Searches for cosmic strings and other topological defects. 2013.

[38] Jose J. Blanco-Pillado, Ken D. Olum, and Benjamin Shlaer. The number of cosmic string loops. 2013.

[39] Richard Battye and Adam Moss. Updated constraints on the cosmic string tension. *Phys.Rev.*, D82:023521, 2010.

[40] Yves Brihaye and Betti Hartmann. The Effect of dark strings on semilocal strings. *Phys.Rev.*, D80:123502, 2009.

[41] Patrick Peter. Low mass current carrying cosmic strings. *Phys.Rev.*, D46:3322–3334, 1992.

[42] Georges Aad et al. Observation of a new particle in the search for the Standard Model Higgs boson with the ATLAS detector at the LHC. *Phys.Lett.B*, 2012.

[43] Serguei Chatrchyan et al. Observation of a new boson at a mass of 125 GeV with the CMS experiment at the LHC. *Phys.Lett.B*, 2012.

[44] Brian Patt and Frank Wilczek. Higgs-field portal into hidden sectors. 2006.

[45] Bob Holdom. Two U(1)'s and Epsilon Charge Shifts. *Phys.Lett.*, B166:196, 1986.

[46] Robert Foot and Xiao-Gang He. Comment on Z Z-prime mixing in extended gauge theories. *Phys.Lett.*, B267:509–512, 1991.

[47] K.S. Babu, Christopher F. Kolda, and John March-Russell. Implications of generalized Z - Z-prime mixing. *Phys.Rev.*, D57:6788–6792, 1998.

[48] Dean Carmi, Adam Falkowski, Eric Kuflik, and Tomer Volansky. Interpreting LHC Higgs Results from Natural New Physics Perspective. *JHEP*, 1207:136, 2012.

[49] Anson Hook, Eder Izaguirre, and Jay G. Wacker. Model Independent Bounds on Kinetic Mixing. *Adv.High Energy Phys.*, 2011:859762, 2011.

[50] J. Beringer et al. Review of Particle Physics (RPP). *Phys.Rev.*, D86:010001, 2012.

[51] Ana Achucarro and Tanmay Vachaspati. Semilocal and electroweak strings. *Phys.Rept.*, 327:347–426, 2000.

[52] Edward Witten. Superconducting Strings. *Nucl.Phys.*, B249:557–592, 1985.

[53] Mark G. Alford and Frank Wilczek. Aharonov-Bohm Interaction of Cosmic Strings with Matter. *Phys.Rev.Lett.*, 62:1071, 1989.

[54] Yi-Zen Chu, Harsh Mathur, and Tanmay Vachaspati. Aharonov-Bohm Radiation of Fermions. *Phys.Rev.*, D82:063515, 2010.

[55] C.J.A.P. Martins and E.P.S. Shellard. String evolution with friction. *Phys.Rev.*, D53:575–579, 1996.

[56] Y. Aharonov and D. Bohm. Significance of electromagnetic potentials in the quantum theory. *Phys.Rev.*, 115:485–491, 1959.

[57] Tanmay Vachaspati. Cosmic Rays from Cosmic Strings with Condensates. *Phys.Rev.*, D81:043531, 2010.

[58] Alexander Vilenkin and Tanmay Vachaspati. RADIATION OF GOLDSTONE BOSONS FROM COSMIC STRINGS. *Phys.Rev.*, D35:1138, 1987.

[59] R. Jeannerot, X. Zhang, and Robert H. Brandenberger. Non-thermal production of neutralino cold dark matter from cosmic string decays. *JHEP*, 9912:003, 1999.

[60] Mark Hindmarsh, Russell Kirk, and Stephen M. West. Dark Matter from Decaying Topological Defects. 2013.

[61] Eray Sabancilar. Cosmological Constraints on Strongly Coupled Moduli from Cosmic Strings. *Phys.Rev.*, D81:123502, 2010.

[62] Cecilia Lunardini and Eray Sabancilar. Cosmic Strings as Emitters of Extremely High Energy Neutrinos. *Phys.Rev.*, D86:085008, 2012.

[63] Andrei D. Linde. A New Inflationary Universe Scenario: A Possible Solution of the Horizon, Flatness, Homogeneity, Isotropy and Primordial Monopole Problems. *Phys.Lett.*, B108:389–393, 1982.

[64] Andreas Albrecht, Paul J. Steinhardt, Michael S. Turner, and Frank Wilczek. Reheating an Inflationary Universe. *Phys.Rev.Lett.*, 48:1437, 1982.

[65] A.D. Dolgov and Andrei D. Linde. Baryon Asymmetry in Inflationary Universe. *Phys.Lett.*, B116:329, 1982.

[66] L.F. Abbott, Edward Farhi, and Mark B. Wise. Particle Production in the New Inflationary Cosmology. *Phys.Lett.*, B117:29, 1982.

[67] Jennie H. Traschen and Robert H. Brandenberger. Particle Production During Out-of-equilibrium Phase Transitions. *Phys.Rev.*, D42:2491–2504, 1990.

[68] Lev Kofman, Andrei D. Linde, and Alexei A. Starobinsky. Reheating after inflation. *Phys.Rev.Lett.*, 73:3195–3198, 1994.

[69] Lev Kofman, Andrei D. Linde, and Alexei A. Starobinsky. Towards the theory of reheating after inflation. *Phys.Rev.*, D56:3258–3295, 1997.

[70] Rouzbeh Allahverdi, Robert Brandenberger, Francis-Yan Cyr-Racine, and Anupam Mazumdar. Reheating in Inflationary Cosmology: Theory and Applications. *Ann.Rev.Nucl.Part.Sci.*, 60:27–51, 2010.

[71] Mustafa A. Amin, Mark P. Hertzberg, David I. Kaiser, and Johanna Karouby. Nonperturbative Dynamics Of Reheating After Inflation: A Review. *Int.J.Mod.Phys.*, D24:1530003, 2015.

[72] Y. Shtanov, Jennie H. Traschen, and Robert H. Brandenberger. Universe reheating after inflation. *Phys.Rev.*, D51:5438–5455, 1995.

[73] Patrick B. Greene, Lev Kofman, Andrei D. Linde, and Alexei A. Starobinsky. Structure of resonance in preheating after inflation. *Phys.Rev.*, D56:6175–6192, 1997.

[74] Stephon Alexander, Sam Cormack, Antonino Marcianò, and Nicolás Yunes. Gravitational-Wave Mediated Preheating. 2014.

[75] S.Y. Khlebnikov and I.I. Tkachev. Relic gravitational waves produced after preheating. *Phys.Rev.*, D56:653–660, 1997.

[76] Richard Easther and Eugene A. Lim. Stochastic gravitational wave production after inflation. *JCAP*, 0604:010, 2006.

[77] Richard Easther, Jr. Giblin, John T., and Eugene A. Lim. Gravitational Wave Production At The End Of Inflation. *Phys.Rev.Lett.*, 99:221301, 2007.

[78] Jean Francois Dufaux, Amanda Bergman, Gary N. Felder, Lev Kofman, and Jean-Philippe Uzan. Theory and Numerics of Gravitational Waves from Preheating after Inflation. *Phys.Rev.*, D76:123517, 2007.

[79] Juan Garcia-Bellido, Daniel G. Figueroa, and Alfonso Sastre. A Gravitational Wave Background from Reheating after Hybrid Inflation. *Phys.Rev.*, D77:043517, 2008.

[80] Jean-Francois Dufaux, Gary Felder, Lev Kofman, and Olga Navros. Gravity Waves from Tachyonic Preheating after Hybrid Inflation. *JCAP*, 0903:001, 2009.

[81] Juan Garcia-Bellido, Daniel G. Figueroa, and Javier Rubio. Preheating in the Standard Model with the Higgs-Inflaton coupled to gravity. *Phys.Rev.*, D79:063531, 2009.

[82] Jean-Francois Dufaux, Daniel G. Figueroa, and Juan Garcia-Bellido. Gravitational Waves from Abelian Gauge Fields and Cosmic Strings at Preheating. *Phys.Rev.*, D82:083518, 2010.

[83] Kari Enqvist, Daniel G. Figueroa, and Tuukka Meriniemi. Stochastic Background of Gravitational Waves from Fermions. *Phys.Rev.*, D86:061301, 2012.

[84] Kari Enqvist, Daniel G. Figueroa, and Rose N. Lerner. Curvaton Decay by Resonant Production of the Standard Model Higgs. *JCAP*, 1301:040, 2013.

[85] Kari Enqvist, Sami Nurmi, and Stanislav Rusak. Non-Abelian dynamics in the resonant decay of the Higgs after inflation. *JCAP*, 1410(10):064, 2014.

[86] Daniel G. Figueroa. A gravitational wave background from the decay of the standard model Higgs after inflation. *JHEP*, 1411:145, 2014.

[87] C.J. Moore, R.H. Cole, and C.P.L. Berry. Gravitational-wave sensitivity curves. *Class.Quant.Grav.*, 32(1):015014, 2015.

[88] Eric Thrane and Joseph D. Romano. Sensitivity curves for searches for gravitational-wave backgrounds. *Phys.Rev.*, D88(12):124032, 2013.

[89] K. Riles. Gravitational Waves: Sources, Detectors and Searches. *Prog.Part.Nucl.Phys.*, 68:1–54, 2013.

[90] J. Aasi et al. Improved Upper Limits on the Stochastic Gravitational-Wave Background from 2009–2010 LIGO and Virgo Data. *Phys.Rev.Lett.*, 113(23):231101, 2014.

[91] Tomotada Akutsu et al. Search for a stochastic background of 100-MHz gravitational waves with laser interferometers. *Phys. Rev. Lett.*, 101:101101, 2008.

[92] Atsushi Nishizawa, Seiji Kawamura, Tomotada Akutsu, Koji Arai, Kazuhiro Yamamoto, Daisuke Tatsumi, Erina Nishida, Masa-aki Sakagami, Takeshi Chiba, Ryuichi Takahashi, and Naoshi Sugiyama. Laser-interferometric detectors for gravitational wave backgrounds at 100 mhz: Detector design and sensitivity. *Phys. Rev. D*, 77:022002, Jan 2008.

[93] Maxim Goryachev and Michael E. Tobar. Gravitational Wave Detection with High Frequency Phonon Trapping Acoustic Cavities. *Phys.Rev.*, D90(10):102005, 2014.

[94] Rose Lerner and Anders Tranberg. Thermal blocking of preheating. 2015.

[95] John T. Giblin and Eric Thrane. Estimates of maximum energy density of cosmological gravitational-wave backgrounds. *Phys.Rev.*, D90(10):107502, 2014.

[96] Tomislav Prokopec and Thomas G. Roos. Lattice study of classical inflaton decay. *Phys.Rev.*, D55:3768–3775, 1997.

[97] Rouzbeh Allahverdi and Bruce A. Campbell. Cosmological reheating and self-interacting final state bosons. *Phys.Lett.*, B395:169–177, 1997.

[98] Amjad Ashoorioon, Brandon Fung, Robert B. Mann, Marius Oltean, and M.M. Sheikh-Jabbari. Gravitational Waves from Preheating in M-flation. *JCAP*, 1403:020, 2014.

[99] P.A.R. Ade et al. Planck 2015. XX. Constraints on inflation. 2015.

[100] S. Yu. Khlebnikov and I.I. Tkachev. Classical decay of inflaton. *Phys.Rev.Lett.*, 77:219–222, 1996.

[101] David Polarski and Alexei A. Starobinsky. Semiclassicality and decoherence of cosmological perturbations. *Class.Quant.Grav.*, 13:377–392, 1996.

[102] Gary N. Felder and Igor Tkachev. LATTICEEASY: A Program for lattice simulations of scalar fields in an expanding universe. *Comput.Phys.Commun.*, 178:929–932, 2008.

[103] S. Yu. Khlebnikov and I.I. Tkachev. Resonant decay of Bose condensates. *Phys.Rev.Lett.*, 79:1607–1610, 1997.

[104] Gary N. Felder and Lev Kofman. Nonlinear inflaton fragmentation after preheating. *Phys.Rev.*, D75:043518, 2007.

[105] Raphael Micha and Igor I. Tkachev. Relativistic turbulence: A Long way from preheating to equilibrium. *Phys.Rev.Lett.*, 90:121301, 2003.

[106] Raphael Micha and Igor I. Tkachev. Turbulent thermalization. *Phys.Rev.*, D70:043538, 2004.

[107] Andrei V. Frolov. DEFROST: A New Code for Simulating Preheating after Inflation. *JCAP*, 0811:009, 2008.

[108] Juan Garcia-Bellido, Javier Rubio, Mikhail Shaposhnikov, and Daniel Zenhausern. Higgs-Dilaton Cosmology: From the Early to the Late Universe. *Phys. Rev.*, D84:123504, 2011.

[109] Alexander Kusenko and Anupam Mazumdar. Gravitational waves from fragmentation of a primordial scalar condensate into Q-balls. *Phys.Rev.Lett.*, 101:211301, 2008.

[110] Alexander Kusenko, Anupam Mazumdar, and Tuomas Multamaki. Gravitational waves from the fragmentation of a supersymmetric condensate. *Phys.Rev.*, D79:124034, 2009.

[111] Takeshi Chiba, Kohei Kamada, and Masahide Yamaguchi. Gravitational Waves from Q-ball Formation. *Phys. Rev.*, D81:083503, 2010.

[112] Shuang-Yong Zhou, Edmund J. Copeland, Richard Easther, Hal Finkel, Zong-Gang Mou, et al. Gravitational Waves from Oscillon Preheating. *JHEP*, 1310:026, 2013.

[113] Shuang-Yong Zhou. Gravitational waves from Affleck-Dine condensate fragmentation. 2015.

[114] Kaushik Bhattacharya, Joydeep Chakrabortty, Suratna Das, and Tanmoy Mondal. Higgs vacuum stability and inflationary dynamics after BICEP2 and PLANCK dust polarisation data. *JCAP*, 1412(12):001, 2014.

[115] Kohei Kamada. Inflationary cosmology and the standard model Higgs with a small Hubble induced mass. *Phys. Lett.*, B742:126–135, 2015.

[116] Christian Gross, Oleg Lebedev, and Marco Zatta. Higgs-inflaton coupling from reheating and the metastable Universe. 2015.

[117] K.G. Chetyrkin and M.F. Zoller. Three-loop β-functions for top-Yukawa and the Higgs self-interaction in the Standard Model. *JHEP*, 1206:033, 2012.

[118] Oleg Lebedev. On Stability of the Electroweak Vacuum and the Higgs Portal. *Eur.Phys.J.*, C72:2058, 2012.

[119] Vincenzo Branchina and Emanuele Messina. Stability, Higgs Boson Mass and New Physics. *Phys.Rev.Lett.*, 111:241801, 2013.

[120] Vincenzo Branchina, Emanuele Messina, and Alessia Platania. Top mass determination, Higgs inflation, and vacuum stability. *JHEP*, 1409:182, 2014.

[121] Vincenzo Branchina, Emanuele Messina, and Marc Sher. Lifetime of the electroweak vacuum and sensitivity to Planck scale physics. *Phys.Rev.*, D91:013003, 2015.

[122] Kari Enqvist, Tuukka Meriniemi, and Sami Nurmi. Generation of the Higgs Condensate and Its Decay after Inflation. *JCAP*, 1310:057, 2013.

[123] J.R. Espinosa, G.F. Giudice, and A. Riotto. Cosmological implications of the Higgs mass measurement. *JCAP*, 0805:002, 2008.

[124] Archil Kobakhidze and Alexander Spencer-Smith. Electroweak Vacuum (In)Stability in an Inflationary Universe. *Phys.Lett.*, B722:130–134, 2013.

[125] Giuseppe Degrassi, Stefano Di Vita, Joan Elias-Miro, Jose R. Espinosa, Gian F. Giudice, et al. Higgs mass and vacuum stability in the Standard Model at NNLO. *JHEP*, 1208:098, 2012.

[126] B. Pontecorvo. Inverse beta processes and nonconservation of lepton charge. *Sov. Phys. JETP*, 7:172–173, 1958. [Zh. Eksp. Teor. Fiz.34,247(1957)].

[127] Andreas Hoecker. Moriond Electroweak and Unified Theories 2016 - Experimental Summary. In *51st Rencontres de Moriond on EW Interactions and Unified Theories La Thuile, Italy, March 12-19, 2016*, 2016.

[128] A. M. Gago, H. Minakata, H. Nunokawa, S. Uchinami, and R. Zukanovich Funchal. Resolving CP Violation by Standard and Nonstandard Interactions and Parameter Degeneracy in Neutrino Oscillations. *JHEP*, 01:049, 2010.

[129] N. Klop and A. Palazzo. Imprints of CP violation induced by sterile neutrinos in T2K data. *Phys. Rev.*, D91(7):073017, 2015.

[130] Raj Gandhi, Boris Kayser, Mehedi Masud, and Suprabh Prakash. The impact of sterile neutrinos on CP measurements at long baselines. *JHEP*, 11:039, 2015.

[131] David V. Forero and Patrick Huber. Hints for leptonic CP violation or New Physics? 2016.

[132] G. C. Branco, R. Gonzalez Felipe, and F. R. Joaquim. Leptonic CP Violation. *Rev. Mod. Phys.*, 84:515–565, 2012.

[133] Hisakazu Minakata and Hiroshi Nunokawa. Exploring neutrino mixing with low-energy superbeams. *JHEP*, 10:001, 2001.

[134] Andrew G. Cohen, Sheldon L. Glashow, and Zoltan Ligeti. Disentangling Neutrino Oscillations. *Phys. Lett.*, B678:191–196, 2009.

[135] Sanjib Kumar Agarwalla, Sabya Sachi Chatterjee, and Antonio Palazzo. Physics Reach of DUNE with a Light Sterile Neutrino. 2016.

[136] C. Adams et al. The Long-Baseline Neutrino Experiment: Exploring Fundamental Symmetries of the Universe. 2013.

[137] R. Acciarri et al. Long-Baseline Neutrino Facility (LBNF) and Deep Underground Neutrino Experiment (DUNE). 2016.

[138] V. Barger, D. Marfatia, and K. Whisnant. Breaking eight fold degeneracies in neutrino CP violation, mixing, and mass hierarchy. *Phys. Rev.*, D65:073023, 2002.

[139] Andrew J. Long, Jeffrey M. Hyde, and Tanmay Vachaspati. Cosmic Strings in Hidden Sectors: 1. Radiation of Standard Model Particles. *JCAP*, 1409(09):030, 2014.

[140] Andrew J. Long and Tanmay Vachaspati. Cosmic Strings in Hidden Sectors: 2. Cosmological and Astrophysical Signatures. *JCAP*, 1412(12):040, 2014.

[141] Jeffrey M. Hyde, Andrew J. Long, and Tanmay Vachaspati. Dark Strings and their Couplings to the Standard Model. *Phys. Rev.*, D89:065031, 2014.

[142] H. F. Santana Mota and Mark Hindmarsh. Big-Bang Nucleosynthesis and Gamma-Ray Constraints on Cosmic Strings with a large Higgs condensate. *Phys. Rev.*, D91(4):043001, 2015.

[143] Jeffrey M. Hyde. Sensitivity of gravitational waves from preheating to a scalar field's interactions. *Phys. Rev.*, D92(4):044026, 2015.

[144] G Bader and U. Ascher. A New Basis Implementation for a Mixed Order Boundary Value ODE Solver. *SIAM J. Sci. Stat. Comput.*, 8:483, 1987.

[145] Uri Ascher, Robert Mattheij, and Robert Russell. *Numerical Solution of Boundary Value Problems for Ordinary Differential Equations*. Society for Industrial and Applied Mathematics, Philadelphia, PA, 1987.

APPENDIX A

NUMERICAL SOLUTION OF DARK STRING FIELD EQUATIONS

The dark string is the solution of the system of equations given by 2.3.3.4 along with the boundary conditions in Eqs. (2.3.3.5) and (2.3.3.7). We solve these equations numerically using the Fortran solver *Colnew*, which implements collocation to solve boundary value problems (BVPs) involving systems of ordinary differential equations (ODEs) [144]. In order to obtain convergence, nonlinear BVPs frequently require a very good initial guess as input to an iterative method of solution, and this is the case with our problem.

We obtain this using the method of continuation [145]. In the absence of the HP and GKM operators, the dark and standard model sectors decouple. In the $(1,1)$ case this reduces to two independent Nielsen–Olesen strings, and in the $(0,1)$ case this reduces to a Nielsen–Olesen string along with a vacuum solution. In either case, their solution is straightforward. We then use continuation, which relies on the following observation: given two sets of model parameters whose values are very close, we expect the corresponding solutions of Eq. (2.3.3.4) to be nearly identical. Thus, we begin with the solution to the decoupled problem and then solve the system of equations with the HP or GKM small but nonzero. This is the beginning of a series of problems, each using the previous solution as *Colnew's* initial guess and returning a solution for incrementally larger HP and GKM. The final step in this procedure solves Eq. (2.3.3.4) for the desired choice of parameters.

We impose the $\xi = \infty$ boundary conditions at some ξ_∞ and solve numerically on $[0, \xi_\infty]$. When σ and η are comparable, ξ_∞ of 200 to 400 is typically sufficient to ensure that the profiles and relevant integrals (tension and couplings) are insensitive to the value of ξ_∞. In the $(1,1)$ case and for $\sigma \gg \eta$ we begin with two Nielsen–Olesen strings varying on significantly different scales (as in Fig. 2.4, for example), and we use ξ_∞ of order 1000.

APPENDIX B

CALCULATION OF DARK STRING TENSION

This appendix presents the calculation behind Eq. (2.4.2.1). For a system of several fields ϕ_i described by action $S = \int d^4x\ \mathcal{L}(\phi_i, \partial_\alpha \phi_i)$, the energy–momentum tensor is

$$T_\mu{}^\nu = \sum_i \partial_\mu \phi_i \frac{\partial \mathcal{L}}{\partial(\partial_\nu \phi_i)} - \delta_\mu^\nu \mathcal{L} \tag{B.0.1}$$

For a static solution, time derivatives of all field components vanish, so the energy density (energy per unit volume) is

$$\begin{aligned} \mathcal{E} &= T_0{}^0 \\ &= \sum_i \partial_0 \phi_i \frac{\partial \mathcal{L}}{\partial(\partial_0 \phi_i)} - \mathcal{L} \\ &= -\mathcal{L} \end{aligned} \tag{B.0.2}$$

The string tension is energy per unit length, so it is the above quantity integrated over directions transverse to the string axis:

$$\mu = \int dA_\perp\ \mathcal{E} \tag{B.0.3}$$

This is done on the assumption that the string's radius of curvature is much larger than its width, so that it can be reliably described as axially symmetric.

Since our ansatz is given in cylindrical polar coordinates, it will be easiest to use this choice for the entire calculation. We will use the notation $f' \equiv \frac{df}{d\xi}$. The line element is

$$\begin{aligned} ds^2 = g_{\mu\nu} dx^\mu dx^\nu &= dr^2 + r^2 d\phi^2 + dz^2 \\ &= \frac{1}{\eta^2}(dx^\xi)^2 + \frac{\xi^2}{\eta^2}(dx^\phi)^2 + \frac{1}{\eta^2}(dx^z)^2 \end{aligned} \tag{B.0.4}$$

where $dx^\xi = d\xi = \eta dr$, $dx^\phi = d\phi$, $dx^z = \eta dz$. This gives the components of the metric

$$g_{\xi\xi} = \frac{1}{\eta^2},\ g_{\phi\phi} = \frac{\xi^2}{\eta^2},\ g_{zz} = \frac{1}{\eta^2},\ g_{ij} = 0 \text{ for } i \neq j \tag{B.0.5}$$

and the inverse metric

$$g^{\xi\xi} = \eta^2,\ g^{\phi\phi} = \frac{\eta^2}{\xi^2},\ g^{zz} = \eta^2,\ g^{ij} = 0 \text{ for } i \neq j \tag{B.0.6}$$

Since we have defined

$$Z_\mu dx^\mu = g_{\mu\nu} Z^\nu dx^\mu = z(\xi) dx^\phi \tag{B.0.7}$$

we get

$$g_{\phi\phi} Z^\phi dx^\phi = \frac{\xi^2}{\eta^2} Z^\phi dx^\phi = z(\xi) dx^\phi \tag{B.0.8}$$

or the nonzero component of the gauge field Z is

$$Z^\phi = \frac{\eta^2 z(\xi)}{\xi^2} \tag{B.0.9}$$

Similarly,

$$X^\phi = \frac{\eta^2 x(\xi)}{\xi^2} \tag{B.0.10}$$

In order to compute the string tension, we will need the following quantities:

$$X_\mu X^\mu = g_{\mu\nu} X^\mu X^\nu = g_{\phi\phi} X^\phi X^\phi = \frac{\xi^2}{\eta^2}\frac{\eta^2 x(\xi)}{\xi^2}\frac{\eta^2 x(\xi)}{\xi^2} = \frac{\eta^2 x(\xi)^2}{\xi^2} \tag{B.0.11}$$

$$\partial_\mu S^* \partial^\mu S = g^{\mu\nu}\partial_\mu S^* \partial_\nu S = g^{\xi\xi}\partial_\xi S^* \partial_\xi S + g^{\phi\phi}\partial_\phi S^* \partial_\phi S = \eta^2 \partial_\xi S^* \partial_\xi S + \frac{\eta^2}{\xi^2}\partial_\phi S^* \partial_\phi S \tag{B.0.12}$$

$$(\partial_\mu S^*) Z^\mu = (\partial_\phi S^*) Z^\phi = (\partial_\phi S^*)\frac{\eta^2 z(\xi)}{\xi^2} \tag{B.0.13}$$

$$Z_\mu (\partial^\mu S) = g_{\phi\phi} g^{\phi\phi} Z^\phi (\partial_\phi S) = \frac{\eta^2 z(\xi)}{\xi^2}(\partial_\phi S) \tag{B.0.14}$$

Now,

$$\begin{aligned}
|D_\mu S|^2 &= D_\mu S^* D^\mu S \\
&= \left(\partial_\mu S^* + i g_z^S Z_\mu S^* + i g_X^S X_\mu S^*\right)\left(\partial^\mu S - i g_z^S Z^\mu S - i g_X^S X^\mu S\right) \\
&= \eta^2 \partial_\xi S^* \partial_\xi S + \frac{\eta^2}{\xi^2}\partial_\phi S^* \partial_\phi S - i g_z^S \partial_\phi S^* \frac{\eta^2 z(\xi)}{\xi^2} S - i g_X^S \partial_\phi S^* \frac{\eta^2 x(\xi)}{\xi^2} S \\
&\quad + i g_z^S S^* \frac{\eta^2 z(\xi)}{\xi^2}\partial_\phi S + (g_z^S)^2 \frac{\eta^2 z(\xi)^2}{\xi^2} + g_z^S g_X^S \frac{\eta^2 z(\xi) x(\xi)}{\xi^2}|S|^2 \\
&\quad + i g_X^S S^* \frac{\eta^2 x(\xi)}{\xi^2}\partial_\phi S + g_X^S g_z^S \frac{\eta^2 x(\xi) z(\xi)}{\xi^2}|S|^2 + (g_X^S)^2 \frac{\eta^2 x(\xi)^2}{\xi^2}|S|^2 \\
&= \eta^2 \sigma^2 (s(\xi)')^2 \\
&\quad + \frac{\eta^2 \sigma^2 s(\xi)^2}{\xi^2}\left(m^2 - 2[g_z^S z(\xi) + g_X^S x(\xi)] + [g_z^S z(\xi) + g_X^S x(\xi)]^2\right) \\
&= \eta^2 \sigma^2 (s(\xi)')^2 + \frac{\eta^2 \sigma^2 s(\xi)^2}{\xi^2}\left([g_z^S z(\xi) + g_X^S x(\xi)] - m\right)^2
\end{aligned} \tag{B.0.15}$$

To find $|D_\mu \Phi|^2$ we do the same calculation with $m \to n$, $\sigma \to \eta$, $s, s' \to h, h'$, $g_z^S \to g_z^H$, $g_X^S \to g_X^H$ which gives

$$|D_\mu \Phi|^2 = \eta^4 (h(\xi)')^2 + \frac{\eta^4 h(\xi)^2}{\xi^2}\left([g_z^H z(\xi) + g_X^H x(\xi)] - n\right)^2 \tag{B.0.16}$$

The potential is

$$\begin{aligned} U &= \lambda\left(\Phi^\dagger\Phi-\eta^2\right)^2+\kappa\left(S^*S-\sigma^2\right)^2+\alpha\left(\Phi^\dagger\Phi-\eta\right)\left(S^*S-\sigma\right) \\ &= \lambda\eta^4\left(h(\xi)^2-1\right)^2+\kappa\sigma^4\left(s(\xi)^2-1\right)^2+\alpha\eta^2\sigma^2\left(h(\xi)^2-1\right)\left(s(\xi)^2-1\right) \\ &= \eta^4\left[\lambda\left(h(\xi)^2-1\right)^2+\kappa\left(\frac{\sigma}{\eta}\right)^4\left(s(\xi)^2-1\right)^2+\alpha\left(\frac{\sigma}{\eta}\right)^2\left(h(\xi)^2-1\right)\left(s(\xi)^2-1\right)\right] \end{aligned} \tag{B.0.17}$$

Finally, the kinetic terms for the gauge fields are

$$\begin{aligned} -\frac{1}{4}X_{\mu\nu}X^{\mu\nu} &= -\frac{1}{2}\left(\partial_\mu X_\nu\partial^\mu X^\nu-\partial_\mu X_\nu\partial^\nu X^\mu\right) \\ &= -\frac{1}{2}\left(\partial_\mu g_{\phi\phi}X^\phi g^{\beta\mu}\partial_\beta X^\phi-\partial_\mu g_{\phi\phi}X^\phi g^{\phi\phi}\partial_\phi X^\mu\right) \\ &= -\frac{1}{2}\frac{\eta^4\left(x(\xi)'\right)^2}{\xi^2} \end{aligned} \tag{B.0.18}$$

and similarly

$$-\frac{1}{4}Z_{\mu\nu}Z^{\mu\nu}=-\frac{1}{2}\frac{\eta^4\left(z(\xi)'\right)^2}{\xi^2} \tag{B.0.19}$$

The energy density is:

$$\begin{aligned} \mathcal{E} &= -\mathcal{L} \\ &= \frac{\eta^4(x')^2}{2\xi^2}+\frac{\eta^4(z')^2}{2\xi^2}+\eta^4(h')^2+\frac{\eta^4h^2}{\xi^2}\left([g_z^Hz+g_X^Hx]-n\right)^2 \\ &\quad+\eta^4\left(\frac{\sigma}{\eta}\right)^2(s')^2+\eta^4\left(\frac{\sigma}{\eta}\right)^2\frac{s^2}{\xi^2}\left([g_z^Sz+g_X^Sx]-m\right)^2 \\ &\quad+\eta^4\left[\lambda\left(h^2-1\right)^2+\kappa\left(\frac{\sigma}{\eta}\right)^4\left(s^2-1\right)^2+\alpha\left(\frac{\sigma}{\eta}\right)^2\left(h^2-1\right)\left(s^2-1\right)\right] \end{aligned} \tag{B.0.20}$$

For the special case $\epsilon=0$, $\alpha=0$ the Higgs portal term in the potential goes away, and the coefficients $g_Z^H=1$, $g_X^H=0$, $g_Z^S=0$, $g_X^S=1$. As expected, in the absence of interactions between the SM and dark sectors our energy reduces to the sum of energies of two separate Nielsen–Olesen strings.

If we pull out the factor of η^4 by writing this as $\mathcal{E}\equiv\eta^4\mathcal{E}_0$, then the energy per

unit length (string tension) becomes

$$\begin{aligned}\mu &= \int \mathcal{E} dA \\ &= \eta^4 \int \mathcal{E}_0 \; r \; dr \; d\theta \\ &= \eta^4 \int \mathcal{E}_0 \; \frac{1}{\eta^2} \; \xi \; d\xi \; d\theta \\ &= 2\pi\eta^2 \int \mathcal{E}_0 \; \xi \; d\xi \end{aligned} \tag{B.0.21}$$

We use the profile functions to calculate the string tension in units of $2\pi\eta^2$, which is the result of evaluating the integral

$$\mu = \int_{\xi=0}^{\infty} (\mathcal{E}_X + \mathcal{E}_Z + \mathcal{E}_H + \mathcal{E}_S + u) \; \xi \; d\xi \tag{B.0.22}$$

where (defining $A \equiv \frac{\sigma}{\eta}$)

$$\mathcal{E}_X = \frac{(x')^2}{2\xi^2} \tag{B.0.23}$$

$$\mathcal{E}_Z = \frac{(z')^2}{2\xi^2} \tag{B.0.24}$$

$$\mathcal{E}_H = (h')^2 \; + \; \frac{h^2}{\xi^2} \left([g_z^H z + g_X^H x] - n \right)^2 \tag{B.0.25}$$

$$\mathcal{E}_S = A^2 (s')^2 \; + \; A^2 \frac{s^2}{\xi^2} \left([g_z^S z + g_X^S x] - m \right)^2 \tag{B.0.26}$$

$$u = \lambda \left(h^2 - 1 \right)^2 + \kappa A^4 \left(s^2 - 1 \right)^2 + \alpha A^2 \left(h^2 - 1 \right) \left(s^2 - 1 \right) \tag{B.0.27}$$

APPENDIX C

ELLIPTICITY OF BIPROBABILITY PLOTS IN THE PRESENCE OF A STERILE NEUTRINO

C.1 Four-Flavor Mixing Matrix in Vacuum

Here we present the elements of the four-lepton mixing matrix relevant to the processes $\nu_\mu \to \nu_\mathrm{e}$ and $\overline{\nu}_\mu \to \overline{\nu}_\mathrm{e}$ in vacuum, and point out interesting features. In "Parametrization II" (where we use δ_{24} rather than δ_{14}), the combinations we need for $\nu_\mu \to \nu_\mathrm{e}$ and $\overline{\nu}_\mu \to \overline{\nu}_\mathrm{e}$ can be put into a form where factors of $\sin\delta_{13}$ and $\cos\delta_{13}$

are emphasized:

$$\begin{aligned}
\mathrm{Re}\left[U_{\mu 1}U_{\mathrm{e}1}^{*}U_{\mu 2}^{*}U_{\mathrm{e}2}\right] &= [\frac{1}{16}c_{14}^{2}(-2c_{23}c_{13}^{3}s_{14}\cos\delta_{24}\sin\left(4\theta_{12}\right)\sin\left(2\theta_{24}\right) \\
&\qquad + c_{24}^{2}s_{23}^{2}\sin^{2}\left(2\theta_{12}\right)\sin^{2}\left(2\theta_{13}\right) \\
&\qquad + 16c_{12}^{2}c_{13}^{2}s_{12}^{2}\left(c_{13}^{2}s_{14}^{2}s_{24}^{2}-c_{23}^{2}c_{24}^{2}\right))] \\
&+ \cos\delta_{13}[\frac{1}{8}c_{13}^{2}c_{14}^{2}s_{13}(2c_{13}s_{14}s_{23}\cos\delta_{24}\sin^{2}\left(2\theta_{12}\right)\sin\left(2\theta_{24}\right) \\
&\qquad - c_{24}^{2}\sin\left(4\theta_{12}\right)\sin\left(2\theta_{23}\right))] \\
&+ \sin\delta_{13}[-\frac{1}{4}c_{13}^{3}c_{14}^{2}s_{13}s_{14}s_{23}\sin\delta_{24}\sin^{2}\left(2\theta_{12}\right)\sin\left(2\theta_{24}\right)] \qquad \text{(C.1.1)} \\
\mathrm{Im}\left[U_{\mu 1}U_{\mathrm{e}1}^{*}U_{\mu 2}^{*}U_{\mathrm{e}2}\right] &= c_{12}c_{13}^{3}c_{14}^{2}c_{23}c_{24}s_{12}s_{14}s_{24}\sin\delta_{24}-\sin\delta_{13}[c_{12}c_{13}^{2}c_{14}^{2}c_{23}c_{24}^{2}s_{12}s_{13}s_{23}] \qquad \text{(C.1.2)} \\
\mathrm{Re}\left[U_{\mu 1}U_{\mathrm{e}1}^{*}U_{\mu 3}^{*}U_{\mathrm{e}3}\right] &= [c_{12}c_{13}c_{14}^{2}s_{13}^{2}\left(c_{23}c_{24}s_{12}s_{14}s_{24}\cos\delta_{24}+c_{12}c_{13}\left(s_{14}^{2}s_{24}^{2}-c_{24}^{2}s_{23}^{2}\right)\right)] \\
&+ \sin\delta_{13}[\frac{1}{8}c_{12}^{2}c_{14}^{2}s_{14}s_{23}\sin\delta_{24}\sin\left(4\theta_{13}\right)\sin\left(2\theta_{24}\right)] \\
&+ \cos\delta_{13}[-\frac{1}{8}c_{14}^{2}(c_{12}^{2}s_{14}s_{23}\cos\delta_{24}\sin\left(4\theta_{13}\right)\sin\left(2\theta_{24}\right) \\
&\qquad + 2c_{13}^{2}c_{24}^{2}s_{13}\sin\left(2\theta_{12}\right)\sin\left(2\theta_{23}\right))] \qquad \text{(C.1.3)} \\
\mathrm{Im}\left[U_{\mu 1}U_{\mathrm{e}1}^{*}U_{\mu 3}^{*}U_{\mathrm{e}3}\right] &= \frac{1}{2}c_{12}c_{13}c_{23}c_{14}^{2}s_{12}s_{13}^{2}s_{14}\sin\delta_{24}\sin\left(2\theta_{24}\right) \\
&+ \cos\delta_{13}[\frac{1}{2}c_{12}^{2}c_{13}c_{14}^{2}s_{13}s_{14}s_{23}\sin\delta_{24}\sin\left(2\theta_{24}\right)] \\
&+ \sin\delta_{13}[\frac{1}{2}c_{12}c_{13}c_{14}^{2}s_{13}(c_{12}s_{14}s_{23}\cos\delta_{24}\sin\left(2\theta_{24}\right) \\
&+ c_{13}c_{24}^{2}s_{12}\sin\left(2\theta_{23}\right))] \qquad \text{(C.1.4)} \\
\mathrm{Re}\left[U_{\mu 2}U_{\mathrm{e}2}^{*}U_{\mu 3}^{*}U_{\mathrm{e}3}\right] &= -c_{13}c_{14}^{2}s_{12}s_{13}^{2}\left(c_{12}c_{23}c_{24}s_{14}s_{24}\cos\delta_{24}+c_{13}s_{12}\left(c_{24}^{2}s_{23}^{2}-s_{14}^{2}s_{24}^{2}\right)\right) \\
&\quad + \sin\delta_{13}[\frac{1}{8}c_{14}^{2}s_{12}^{2}s_{14}s_{23}\sin\delta_{24}\sin\left(4\theta_{13}\right)\sin\left(2\theta_{24}\right)] \\
&\quad + \cos\delta_{13}[\frac{1}{2}c_{13}c_{14}^{2}s_{12}s_{13}s_{23}(2c_{12}c_{13}c_{23}c_{24}^{2} \\
&- s_{12}s_{14}\cos\delta_{24}\sin\left(2\theta_{24}\right)\cos\left(2\theta_{13}\right))] \qquad \text{(C.1.5)} \\
\mathrm{Im}\left[U_{\mu 2}U_{\mathrm{e}2}^{*}U_{\mu 3}^{*}U_{\mathrm{e}3}\right] &= -\frac{1}{2}c_{12}c_{13}c_{23}c_{14}^{2}s_{12}s_{13}^{2}s_{14}\sin\delta_{24}\sin\left(2\theta_{24}\right) \\
&+ \cos\delta_{13}[\frac{1}{2}c_{13}c_{14}^{2}s_{12}^{2}s_{13}s_{14}s_{23}\sin\delta_{24}\sin\left(2\theta_{24}\right)] \\
&+ \sin\delta_{13}[\frac{1}{2}c_{13}c_{14}^{2}s_{12}s_{13}(s_{12}s_{14}s_{23}\cos\delta_{24}\sin\left(2\theta_{24}\right) \\
&- c_{12}c_{13}c_{24}^{2}\sin\left(2\theta_{23}\right))] \qquad \text{(C.1.6)} \\
\left|U_{\mu 4}^{*}U_{\mathrm{e}4}\right|^{2} &= \frac{1}{4}s_{24}^{2}\sin^{2}\left(2\theta_{14}\right) \qquad \text{(C.1.7)}
\end{aligned}$$

where $c_{ij} \equiv \cos\theta_{ij}$ and $s_{ij} \equiv \sin\theta_{ij}$. We have written them in this form, singling out $\sin\delta_{13}$ and $\cos\delta_{13}$, for a specific reason. Comparison with Eq. (4.2.23) and Eq. (4.2.25) shows that we can always write the $\nu_\mu \to \nu_\mathrm{e}$ probability P and the $\overline{\nu}_\mu \to \overline{\nu}_\mathrm{e}$ probability $\overline{P}$ in the form

$$P = A + B\cos\delta_{13} + C\sin\delta_{13}, \quad \overline{P} = \overline{A} + \overline{B}\cos\delta_{13} + \overline{C}\sin\delta_{13}, \tag{C.1.8}$$

where the coefficients A, B, C, $\overline{A}$, $\overline{B}$, $\overline{C}$ are independent of δ_{13} but complicated functions of the other mixing parameters θ_{ij}, δ_{ij}, the mass-squared splittings δm^2_{ij}, and the ratio L/E of baseline length to neutrino energy. In Appendix C.2, we will put this form to use towards understanding the effect of new parameters.

C.2 Generalized Proof of Ellipticity in $(P, \overline{P})$ Space, and Parametric Dependence

Here we present a proof that even in the presence of mixing with a fourth "sterile" state, the trajectory in $(P, \overline{P})$ space is elliptical. This is directly analogous to the proof given in [133] for the case of three-neutrino mixing. This will allow us to characterize the deviation from the standard model case in terms of the new parameters.

As shown in Appendix C.1, the $\nu_\mu \to \nu_\mathrm{e}$ probability P and the $\overline{\nu}_\mu \to \overline{\nu}_\mathrm{e}$ probability $\overline{P}$ can always be written in the form

$$P = A + B\cos\delta_{13} + C\sin\delta_{13}, \quad \overline{P} = \overline{A} + \overline{B}\cos\delta_{13} + \overline{C}\sin\delta_{13}, \tag{C.2.1}$$

where the coefficients A, B, C, $\overline{A}$, $\overline{B}$, $\overline{C}$ are independent of δ_{13} but complicated functions of the other mixing parameters θ_{ij}, δ_{ij}, the mass-squared splittings δm^2_{ij}, and the ratio L/E of baseline length to neutrino energy.

Now we can eliminate $\cos\delta_{13}$ and $\sin\delta_{13}$ to get a parametric equation relating P and $\overline{P}$:

$$\begin{aligned} 1 &= \cos^2\delta_{13} + \sin^2\delta_{13} \\ &= \left(\frac{C\overline{P} - \overline{C}P + \overline{C}A - C\overline{A}}{C\overline{B} - \overline{C}B}\right)^2 + \left(\frac{B\overline{P} - \overline{B}P + \overline{B}A - B\overline{A}}{B\overline{C} - \overline{B}C}\right)^2 \end{aligned} \tag{C.2.2}$$

In the limit of no hidden sector, $\theta_{i4} = 0$, and in vacuum, we will have $A = \overline{A}$, $B = \overline{B}$, $C = -\overline{C}$ and we have

$$1 = \left(\frac{P + \overline{P} - 2A}{2B}\right)^2 + \left(\frac{P - \overline{P}}{2C}\right)^2 \tag{C.2.3}$$

This is also appeared in [133], and in coordinates $P_\pm \equiv \frac{1}{\sqrt{2}}\left(P \pm \overline{P}\right)$ it describes an ellipse centered at $P_- = 0$ and $P_+ = A/\sqrt{2}$. Since P_- is the CP asymmetry $A_{\mu\mathrm{e}}$ defined in Eq. (4.2.26) (up to a multiplying factor), we can see from Eq. (C.2.3) that this provides a fuller picture of the probabilities in $(P, \overline{P})$ space.

Is Eq. (C.2.2) also an ellipse in $(P, \overline{P})$ space? By inspection is not obvious that coordinates (x, y), analogous to $P_\pm$, can be chosen so that Eq. (C.2.2) can be put into the form $1 = (x/\alpha)^2 + (y/\beta)^2$. However, it turns out that we can always find a

principal axis transformation that does this. We will shift the coordinates to eliminate the linear terms, and then apply a principal axis transformation. In terms of the $(P, \overline{P})$ plane, this corresponds to first centering the ellipse on the origin, and then rotating it.

To see this, we expand Eq. (C.2.2) as:

$$R^2 = \overline{S}\,\overline{P} + SP + C_1\overline{P}^2 + C_2 P\overline{P} + C_3 P^2 \tag{C.2.4}$$

where we have defined

$$\begin{aligned}
R^2 &= B^2\overline{C}^2 - 2B\overline{C}\overline{B}C + \overline{B}^2C^2 - A^2\overline{B}^2 - A^2\overline{C}^2 \\
&\quad + 2A\overline{A}B\overline{B} + 2A\overline{A}\overline{C}C - \overline{A}^2B^2 - \overline{A}^2C^2 && \text{(C.2.5)}\\
\overline{S} &= 2AB\overline{B} + 2A\overline{C}C - 2\overline{A}B^2 - 2\overline{A}C^2 && \text{(C.2.6)}\\
S &= -2A\overline{B}^2 - 2A\overline{C}^2 + 2\overline{A}B\overline{B} + 2\overline{A}\overline{C}C && \text{(C.2.7)}\\
C_1 &= B^2 + C^2 && \text{(C.2.8)}\\
C_2 &= -2B\overline{B} - 2\overline{C}C && \text{(C.2.9)}\\
C_3 &= \overline{B}^2 + \overline{C}^2 && \text{(C.2.10)}
\end{aligned}$$

Defining new coordinates

$$u \equiv P + \frac{\overline{S} - 2C_1 S}{4C_1C_3 - C_2} \tag{C.2.11}$$

$$v \equiv \overline{P} + S - \frac{2C_3\overline{S} - 4C_1C_3S}{4C_1C_3 - C_2} \tag{C.2.12}$$

allows this to be written as a quadratic form:

$$\begin{aligned}
R^2 - \alpha^2 \equiv r^2 &= \begin{pmatrix} u & v \end{pmatrix} \begin{pmatrix} C_3 & C_2/2 \\ C_2/2 & C_1 \end{pmatrix} \begin{pmatrix} u \\ v \end{pmatrix} \\
&\equiv \sum_{i,j=1}^{2} V_i W_{ij} V_j = V^{\mathrm{T}} \cdot W \cdot V && \text{(C.2.13)}
\end{aligned}$$

where

$$\begin{aligned}
\alpha^2 \equiv [&C_1\left(3C_2^2S^2 + 4C_3\overline{S}\left(C_3\overline{S}^2(\overline{S}+2) - 2S\right) - 2C_2S\left(S - 2C_3\overline{S}(4\overline{S}+3)\right)\right) \\
&+ 16C_3^2C_1^3S^2(\overline{S}+1)^2 + \overline{S}\left(C_2\left(-2C_2S - 4C_3\overline{S}^2 + S\right) + C_3\overline{S}\right) \\
&- 4C_3C_1^2S\left(S\left(4C_2(\overline{S}+1) - 3\right) + 4C_3\overline{S}(\overline{S}+1)^2\right)]/((C_2 - 4C_1C_3)^{\,2}) && \text{(C.2.14)}
\end{aligned}$$

Now the principal axis transformation that we want is the one that diagonalizes the matrix W, i.e. we want to find the coordinates (eigenvectors) (x, y) in which W is

diagonal. If Z is the matrix of normalized eigenvectors of W, then

$$\begin{aligned} r^2 &= V^{\mathrm{T}} \cdot (Z^{\mathrm{T}} Z) \cdot W \cdot (Z^{\mathrm{T}} Z) \cdot V \\ &= (Z \cdot V)^{\mathrm{T}} \cdot (Z \cdot W \cdot Z^{\mathrm{T}}) \cdot (Z \cdot V) \\ &= (x \quad y) \begin{pmatrix} \lambda_1 & 0 \\ 0 & \lambda_2 \end{pmatrix} \begin{pmatrix} x \\ y \end{pmatrix} \end{aligned} \tag{C.2.15}$$

This finally is in the form of an ellipse,

$$1 = \lambda_1 \left(\frac{x}{r}\right)^2 + \lambda_2 \left(\frac{y}{r}\right)^2, \tag{C.2.16}$$

which has principal axes along x and y, of length $L_x = r/\sqrt{\lambda_1}$, $L_y = r/\sqrt{\lambda_2}$ respectively. Now we can say how these properties depend on the new parameters in the theory.

APPENDIX D

PREVIOUSLY PUBLISHED WORK

Some of the work presented here has been previously published. Chapter 2, "Dark Strings and their Couplings to the Standard Model," was published in Physical Review D [141], and was coauthored by Tanmay Vachaspati and Andrew Long. They have given their permission for this work to appear in this dissertation. Chapter 3, "Sensitivity of Gravitational Waves from Preheating to a Scalar Field's Interactions," was published in Physical Review D [143], and has no coauthors. Chapter 4, "Effect of Sterile Neutrino Parameters on CP Violation Measurements," has not been published but will be submitted for publication in collaboration with Cecilia Lunardini.